Università degli Studi di Catania
Scuola Superiore di Catania

International PhD

in

ENERGY

XXIII cycle

Adsorption Machine & Desiccant Wheel based SOLAR COOLING in a Second Law perspective

Santo Bivona

Coordinator of PhD
Prof. Alfio Consoli

Tutor
Prof. Luigi Marletta

a.a. 2007/2010

FOREWARD

The energy demand for summer conditioning is rising year by year due to new massive installation of small/medium size electrical chiller for commercial and residential buildings. Electrical chillers are characterized by low price, easy and quick installation and can provide both cooling and heating if used as heat pumps. On the other hand they need relevant amount of electrical power to operate. This leads to high consumption of fossil fuels for power production, which results in high emission of greenhouses gasses and risk of electricity grid overload.

To find new solutions for air conditioning, research activities are focused on exploiting solar energy for cooling purposes. Fig. (I) shows the cooling and heating loads and the course of the solar radiation during the 12 months of the year. The maximum of the solar radiation occurs in the peak of the cooling load. Therefore, it appears obvious that, using a thermally driven machine and suitable solar collectors, it is possible to take advantage of the solar system for cooling purposes.

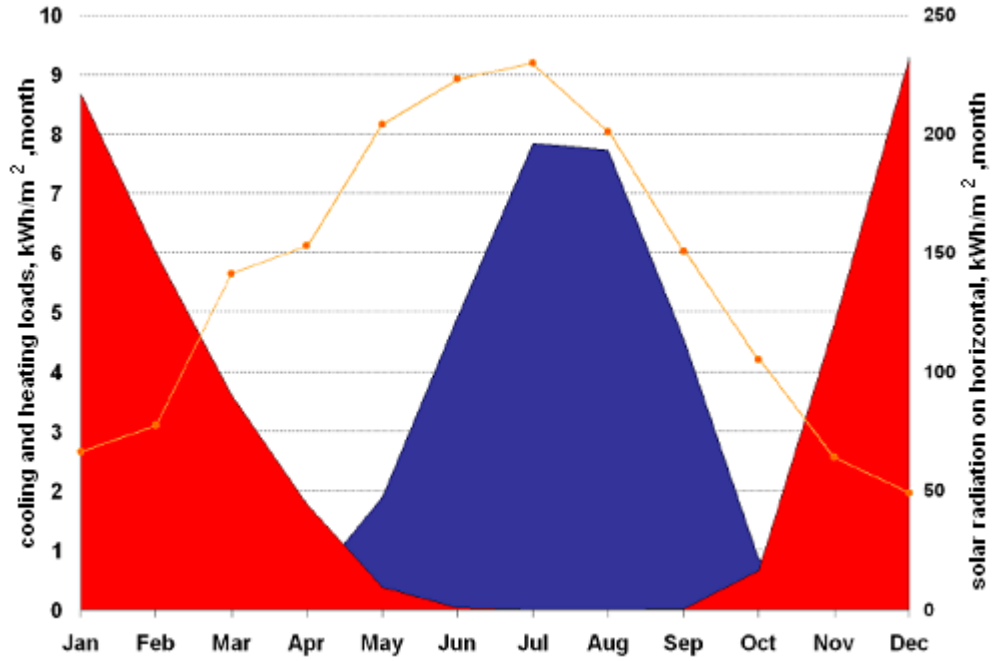

Fig. (I) Cooling (in blue) and heating (in red) loads.

Solar cooling plants are supposed to be able to:

- Reduce summer electrical consumption and risk of grid overload and black-out.
- Reduce greenhouse gas emission and air pollution due to fossil fuel utilization.
- Provide domestic hot water taking advantage of the solar field throughout the year.

This thesis investigates on exploiting solar energy to provide air conditioning for a small office room. Two different systems based on sorption materials will be analyzed from the First and Second Law point of view, in order to be compared in terms of main features, performance and limits of use.

Plant layout design parameters will be assessed after a number of simulations in dynamic condition, involving solar collectors type and area, heat storage and different system control strategies. Results can be compared in terms of energy performance to find the best compromise between performance and predicted cost. Thus, by means of the First and Second Law analysis, the main figures of merit will be assessed.

A rather new HVAC plant layout, based on a desiccant rotary wheel (solar DEC), will be also analyzed. A mathematical model will be developed and implemented in a computer code in the MathCAD environment, to predict the thermodynamic conditions of air streams at the outlet of a desiccant wheel.
This will allow the simulation of the solar DEC and its analysis in a First and Second Law perspective.

The sensitivity theory will be also applied in order to investigate the systems response to deviations of some state variables from their nominal values. In this context a number of sensitivity coefficients will be determined in relation to the most relevant design parameters. That provides useful information for control strategies in dynamic regime and hints for systems design and optimization.

.

1. SOLAR COOLING SYSTEM: AN OVERVIEW

1.1.Introduction

The most recent surveys ascertain that the demand for building cooling has been increasing in the past few years and will continue to do so dramatically in the near future. The AUDITAC study showed that in 1990 about 10,000 GWh of primary energy were consumed in Europe by small Room Air Conditioners (RAC) (<12 kW) with 540 Mm^2 (million square meters) of cooled floor area and that in 2020 this value is expected to increase by a factor of four to about 44,000 GWh, with a cooled area of 2,400 Mm^2. Although high, this value does not include centralized systems, generally installed in large commercial buildings.

The reasons for such a forecast in the cooling demand are several, but mostly due to the more and more popular tendency of modern architecture to use glass façade surface areas, higher demand for comfort, quantitative increase of office and service buildings, increasing number of electric appliances and, in one word, expected economic growth.

All that implies energy, economic and environmental consequences. The technologies currently available are those based on electrically driven compression chillers and thermally driven sorption chillers. Actually, with electric chillers being dominant, the concern is about electricity consumption and, more importantly, black-out risks which may occur in large urban areas, when several thousands of small and large size air-conditioning units are likely to be activated almost simultaneously during the hottest hours of the day in the summer season.

Solar cooling systems may help alleviate this problem, considered that the peak cooling demand in summer is synchronous with solar radiation availability.

But there are also different kind and perhaps more substantial reasons which should encourage the shift to new technologies, such as those based on thermodynamic considerations.

1.2.Conventional cooling technology in a Second Law perspective

Air conditioning for the summer season mostly relies on cooling and cooling is mostly based on either electrically-driven or thermally-driven chillers. The energy indicator for both is the

well known Coefficient of Performance (COP) which, for the two technologies, is defined respectively as:

$$COP_{el} = \frac{Q}{P_{el}} \qquad COP_{th} = \frac{Q}{Q_g}$$

being Q the cooling power (useful effect), P_{el} the electricity required to drive the chiller and Q_g the thermal power offered to the generator of the thermal (or sorption) chiller. Actual values for the COP lay in the following range: $COP_{el} = 2 \div 4$; $COP_{th} = 0.6 \div 1.2$.
On the basis of these numbers one should not conclude that electric chillers are better than thermal chillers, because such a comparison is not properly stated. Indeed the two definitions of COP refer to energy of different quality: heat (Q_g) for the sorption machine and electricity (P_{el}) for the compression machine. A more rational basis for comparison is the Primary Energy Ratio, defined as the ratio of the delivered useful cold (Q) to the Primary Energy (PE) consumption to drive the machine:

$$PER = \frac{Q}{PE}$$

The PE in the currently accepted definition is energy that has not been subjected to any conversion or transformation process, therefore one may consider fossil fuels as sources of PE. As a result, the PER may be assessed by combining the previous equations, such as:

$$PER_{el} = COP_{el}\,\eta_{el} \qquad PER_{th} = COP_{th}\,\eta_g$$

being $\eta_{el} = P_{el} / EP$ the efficiency of the electric system (nationwide efficiency) and $\eta_g = Q_g / EP$ the efficiency of the boiler driving the sorption chiller. Rough numbers may be as follows: h_{el} = 0.40 (recommended value for Europe); h_g=0.90, thus: PER_{el}=(2÷4)·0.4=0.8÷1.6 and $PER_{th} = (0.7 \div 1.2) \cdot 0.9 = 0.63 \div 1.08$.

Looking at these results one may conclude that current technologies for cooling are quite acceptable, and in certain cases (for $PER > 1$), apparently able to provide the user with a cooling energy even greater than the exploited PE. Of course there is no violation of the

physics laws, since COPs do not include, by definition, the energy taken from the environment.

A quite different picture appears when one looks at the problem from a second law perspective. In this case we have to judge the technologies on the basis of the exergy efficiency, defined as the ratio of the exergy required by the end-use to that exploited to drive the system. Now the purpose is to extract from the building the heat Q in order to maintain the interior spaces at temperature T
(e.g., T = 26 °C = 299 K) against an outdoor (environment) temperature T_o (e.g., T_o = 33 °C = 306 K).

For an electric chiller the exploited exergy is P_{el} (electric energy is pure exergy). For a sorption chiller, the thermodynamic potential which drives the machine may be assessed as Q_g (1– T_o/T_g). The maximum temperature T_g of the energy source, for a chiller powered by a conventional gas boiler, may be assumed equal to the flame temperature (e.g., T_g = 1,500 K).

In formulas:

$$\zeta_{el} = \frac{-Q(1-\frac{T_o}{T_a})}{P_{el}} = COP_{el}(\frac{T_o}{T_a}-1) = 3(\frac{306}{299}-1) = 7\%$$

$$\zeta_{th} = \frac{-Q(1-\frac{T_o}{T_a})}{Q_g(1-\frac{T_o}{T_g})} = COP_{th}\frac{(\frac{T_o}{T_a}-1)}{(1-\frac{T_o}{T_g})} = 0.7\frac{(\frac{306}{299}-1)}{(1-\frac{306}{1500})} = 2\%$$

The results reveal that, under the light of the 2nd Law, the current technologies for cooling are not as good as described, via COP and REP, by the first law. The poor exergy efficiencies tell us something about the improper use we make of the energy sources in this field. The sad thing is that these technologies are also the most widespread in the world and involve both the civil and the industrial sectors.

In conclusion it is of interest to investigate if solar technologies are suitable to this aim.

1.3.Solar technologies for cooling

The system under consideration are generally divided into two main categories: close and open cycles.

1.3.1. Closed-cycle systems

These types of systems are based mainly on the absorption cycle. In its simplest, single-effect configuration, an absorption system employs a refrigerant expanding from a condenser to an evaporator through a throttle. A second working fluid is the absorbent. When heat is supplied to the desorber, it absorbs refrigerant vapor from the evaporator at low pressure, and desorbs into the condenser at high pressure. The absorption system is hence a heat-driven heat pump; the heat may come from a variety of sources, including solar. The system operates between two pressure levels, and interacts with three heat reservoirs at various temperature levels: at low temperature in the evaporator; at the intermediate temperature (ambient conditions) in the absorber and condenser. Currently the most common absorbent-refrigerant pairs are LiBr-water and water-ammonia.

Single-effect absorption systems have a limited COP: about 0.7 for LiBr-water and 0.6 for ammonia-water, with consequences in terms of solar collector area. Better performance can be achieved by using a higher temperature heat source and a double stage design. In this case high temperature collectors, such as evacuated tube or concentrating collectors must be used. The higher cost of the cooling machine and the solar collector should hence be considered.

Double stage absorption chiller may have COP as high as 1.0-1.2, while triple-effect, although still under development, may achieve COP of about 1.7. These systems may be adapted to and employed in a solar-powered installation with high temperature solar collectors. The single stage system requires temperature in the range 80-100°C; for a higher supply temperature, it is worth switching to a double stage system, up to about 160°C, and then to a triple-effect. As to the cooling power, only very few systems are commercially available in the in the range of small capacities (< 100 kW), whereas much more manufacturers offer products for large capacities up to several thousands kilowatts.

Adsorption chillers working with solid sorption materials are also available. For a continuous operation it is necessary to work with two or more adsorbers, in such a way that when the first is the desorption the other in the adsorption phase. Adsorption systems allow for somewhat lower driving temperatures but have a somewhat lower COP compared to absorption systems under the same conditions. Silica gel or zeolite adsorption machines with cooling capacities of about 75 kW to several hundreds kilowatt are now available but with very limited application on the field. The noiseless operation and the use of environmentally friendly working fluids (mostly water) are further advantages of this technology.

1.3.2. Open-cycle systems

Open-cycle systems are based on the use of desiccant materials which may be liquid or solids. The cycle is "open" in the sense that the refrigerant is discarded from the system after providing the cooling effect and new refrigerant is supplied in its place in an open-ended loop. In this type of systems air cooling and dehumidification is not obtained by means of chilled water, but by specific treatments to the supply (or process) air streams. The solid or liquid sorbent is regenerated with ambient or exhaust air heated to the required temperature by the solar heat source.

For systems using solid sorption material such as silica gel, it is usual to employ a rotary bed carrying the sorbent material, referred to as a 'desiccant wheel', to allow continuous operation. Systems employing liquid sorption materials are less widespread but also available on the market. An interesting feature of desiccant materials is that they have the possibility of energy storage by means of concentrated hygroscopic solutions, as well as bacteriostatic qualities.

2. INTRODUCTION TO EXERGY ANALYSIS

In this chapter the main differences between First and Second Law analysis will be assessed. The concept of *exergy*, which leads to a different perspective in developing a system performances evaluation, will be shown. At the same time the equation needed to proceed with the air conditioned system analysis will be pointed out.

2.1.The First Law of Thermodynamics

When dealing with energy balances, the First Law of Thermodynamics is usually taken into account. It states that energy is a conservative property; this means that during any real steady-state process the overall energy flow leaving a system equals the overall energy flow entering the system.

Actually, the different forms of energy (thermal, mechanical, internal, potential, kinetic) may individually undergo quantitative changes, but the overall amount of energy is conserved. The energy balance equation, which quantifies the energy conservation law for a stationary process observed through a control volume, may be stated as follows:

$$\dot{Q} - P = \sum_{uscita} \dot{m}_k \cdot \left(h + g \cdot z + \frac{w^2}{2} \right)_k - \sum_{entrata} \dot{m}_k \cdot \left(h + g \cdot z + \frac{w^2}{2} \right)_k \tag{2.1}$$

Where:

- $\dot{Q}$ = thermal energy flow crossing the system boundaries [W]
- P = mechanical power crossing the system boundaries [W]
- $\dot{m}$ = mass flow rate entering / leaving the system [kg/s]
- z = height of the system above a reference level [m]
- w = mass flow velocity [m/s]
- h = specific enthalpy measured at the system inlet and outlet [kJ/kg]

The index of performance derived from such an approach compares the amount of energy required by the final user (either electric, or mechanical, or thermal) to the total amount of energy exploited by the system, expressed as:

$$\eta = \frac{Energy\ release\ to\ the\ user}{Energy\ \ provided\ to\ the\ system}$$

One must realize that such a definition compares different forms of energy. As an example, in the case of a power plant for the production of electric energy, the energy efficiency (η_{el}) is defined as:

$$\eta_{el} = \frac{P_{el}}{\dot{Q}_{th}}$$

where P_{el} is the electric power, and Q_{th} the thermal energy to drive the system.

But, as a matter of fact, different forms of energy have different potentials to produce useful work. So the definition of efficiency stated above is a comparison between quantities which are metrically homogeneous but not conceptually equivalent.

2.2.The Second Law of Thermodynamics

The Second Law of Thermodynamics may help overcome this drawback, on the basis of a rather different approach to system analysis.
The starting point is that real processes are not reversible and give rise to entropy production: friction, hysteresis, molecular or thermal diffusion are the most common examples of irreversibilities occurring in a real process. The mathematical form of the Second Law most suitable for our purposes is the Clausius equation:

$$\sum_{Inlet}(\dot{m}\cdot s)_k - \sum_{Outlet}(\dot{m}\cdot s)_k = \sum_j \left(\frac{\dot{Q}}{T}\right)_j - \sigma \tag{2.2}$$

where:

- $\dot{m}$ = mass flow rate [*kg/s*]
- s = specific entropy content [*kJ/(kgK)*];
- $\dot{Q}$ = heat transfer occurring through the system boundaries [*W*]
- T = temperature of the environment being involved in the heat transfer [*K*]
- σ = overall entropy production due to irreversibility [*W/K*]

As stated by the Second Law, $\sigma \geq 0$, being $\sigma = 0$ only for ideal (reversible) processes. This relationship is precious, as it allows the assessment of entropy production σ, which is always the unknown of the problem. It is intuitive that when dealing with complex systems, it is possible to decompose them into several, more simple subsystems; by evaluating σ for each one of them, it is possible to detect the ones most responsible for thermodynamic drawbacks and thus provide corrective measures.

2.2.1. The Gouy-Stodola equation

The first law contains a term for work, but no term for irreversibility, whereas the second law contains a term for irreversibility but not for work. Combining the first and the second law statements allows to state a more general equation than the previous ones. Before doing this it is appropriate to adopt the following expressions:

$$Q = Q_0 + \sum_j Q_j \qquad \frac{Q}{T} = \frac{Q_0}{T_0} + \sum_j \frac{Q_j}{T_j} \tag{2.3}$$

Being Q_o the heat transfer to the environment and T_o its temperature.
By combining equations (2.1) and (2.2) and taking into account eq. (1.3), one obtains the Gouy-Stodola equation:

$$P = \sum_n \dot{Q}_n \cdot \left(1 - \frac{T_0}{T_n}\right) + \sum_{inlet} \dot{m}_k \cdot \left(h - T_0 s + \frac{w^2}{2} + gz\right)_k - \sum_{outlet} \dot{m}_k \cdot \left(h - T_0 s + \frac{w^2}{2} + gz\right)_k - T_0 \sigma \tag{2.4}$$

For an ideal reversible process (σ = 0), the Gouy-Stodola equation yields:

$$P_{id} = \sum_n \dot{Q}_n \cdot \left(1 - \frac{T_0}{T_n}\right) + \sum_{inlet} \dot{m}_k \cdot \left(h - T_0 s + \frac{w^2}{2} + gz\right)_k - \sum_{outlet} \dot{m}_k \cdot \left(h - T_0 s + \frac{w^2}{2} + gz\right)_k \tag{2.5}$$

For all real processes σ > 0, thus $P_{id} > P$, in other terms

$$P_{id} - P = \sigma T_0 > 0 \tag{2.6}$$

This means that irreversibilities erode the thermodynamic potential of the energy flows; in other words, at the end of the process or at the system outlet, the energy flows have a lower potential to produce work, and this reduction is measured by the entropy production σT_o. This term is also referred to as “Irreversibility”:

$$I = \sigma T_0 \tag{2.7}$$

2.2.2. The dead state

The work potential of a system at a given state may be assessed by letting the system proceed towards and actually reach a stable equilibrium with the environment. In fact, when the system and the environment are in equilibrium, no further change of state can occur spontaneously and hence no further work can be produced.

When such a situation occurs, the system is said to be in the *dead state*. Specifically the dead state is characterized by conventional values for pressure p_o and temperature T_o. Additional requirements for the dead state are that the velocity of the fluid stream is zero ($w_o = 0$) and the gravitational potential energy is zero ($z_o = 0$). These restrictions of pressure, temperature, velocity and elevation characterize the *restricted dead state*, associated with the thermomechanical equilibrium with the environment. It is restricted in the sense that the chemical equilibrium with the environment is not considered, that is the control mass is not allowed to pass into or react chemically with the environment.

The problem of the chemical equilibrium with the environment will be dealt with later on.

2.3.The concept of exergy

Exergy is defined as the work potential of a system relative to its dead state. Following this definition, for each term appearing in eq. (2.5), it is possible to derive an expression for exergy.

Exergy of (mechanical. or electrical) work:

$$E_P = P \tag{2.8}$$

Exergy of heat Q available at temperature T:

$$E_Q = Q \cdot \left(1 - \frac{T_0}{T}\right) \tag{2.9}$$

Exergy of a mass flow:

$$E_m = \dot{m}\left[(h-h_0) - T_0 \cdot (s-s_0) + \frac{w^2 - w_0^2}{2} + g \cdot (z-z_0)\right] \tag{2.10}$$

So for a control volume, eq. (2.4) may be rewritten in terms of exergy, as follows:

$$(E_P)_{outlet} - (E_p)_{inlet} = (E_Q)_{inlet} - (E_Q)_{outlet} + (E_m)_{inlet} - (E_m)_{outlet} - \sigma T_o \tag{2.11}$$

And rearranging the terms:

$$(E_P + E_Q + E_m)_{inlet} = (E_P + E_Q + E_m)_{outlet} + \sigma T_0 \tag{2.12}$$

Therefore:

$$\sigma T_0 = \sum_{inlet} E_j - \sum_{outlet} E_k \tag{2.13}$$

The irreversibility can then be quantified as the difference in exergy measured at the inlet and outlet of the control volume.

2.3.1. Exergy and Anergy

Considering a given amount of thermal energy Q available at the temperature T allows to state that:

$$E_Q = Q \cdot \left(1 - \frac{T_0}{T}\right) \tag{2.14}$$

E_Q can be thought of as the maximum work which can be extracted from a Carnot cycle, receiving the heat Q and working between the temperatures T and T_o . By rewriting the equation in the form:

$$E_Q = Q - Q \cdot \frac{T_0}{T} \tag{2.15}$$

it is easy to recognize Q as the amount of energy available at the beginning, and $Q \cdot \frac{T_0}{T}$ as the amount of energy rejected to the environment as thermal waste; at these conditions, energy is no longer recoverable for technical purposes. Some Authors refer to this quantity as "not available energy" or Anergy.

Similar considerations can be made in relation to the mass flow, where:

The exergy content is: $(h - h_0) - T_0 \cdot (s - s_0) + \frac{w^2 - w_0^2}{2} + g \cdot (z - z_0)$

The energy content is: $(h - h_0) + \frac{w^2 - w_0^2}{2} + g \cdot (z - z_0)$

The anergy content is: $T_0 \cdot (s - s_0)$

All forms of energy at the dead state are anergy. The natural environment is an infinite reservoir of anergy. Distinction should be made between anergy and irreversibility. The former has always existed, the latter results while a process is occurring. Irreversibility is anergy which arises whenever a physical event takes place.

Anergy may enter the control volume and then grow by addition of the irreversibilities. Eventually the anergy flow will join the irreversibility flow, so that at the system outlet the anergy results higher than it was at the inlet.

To summarize the previous results, the following relationship can be stated between energy, exergy and anergy :

$$Energy = Exergy + Anergy$$

A pictorial view of the concepts outlined so far is provided in Fig. 2-1. Its message is clear: going through the physical system, the exergy flow is lowered by the entropy production, the anergy flow increases by the same quantity, while the energy flow remains constant.

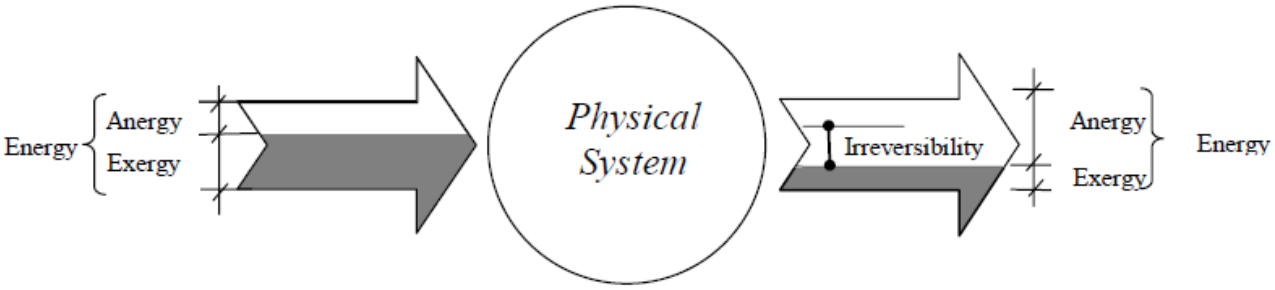

Fig. 2-1Exergy and anergy flows across a physical system.

In conclusion, by using the exergy and anergy concepts, the first and second law of thermodynamics may be reformulated as follows:

- in any process the sum of exergy and anergy remains constant;
- in any real process the exergy decreases and the anergy increases by the same quantity as the entropy production;
- the anergy cannot be converted into exergy.

2.3.2. Exergy efficiency

According to this approach, the thermodynamic figure of merit for a process in a second law perspective is the exergy efficiency, defined as:

$$\zeta = \frac{Exergy\ output}{Exergy\ input}$$

In formulas:

$$\zeta = \frac{E_{outlet}}{E_{inlet}} = \frac{E_{outlet} - \sigma T_0}{E_{inlet}} = 1 - \frac{\sigma T_0}{E_{inlet}} \tag{2.16}$$

The exergy efficiency is thus a ratio between quantities that now are both metrically and conceptually homogeneous. The numerical values of ζ never exceed unity. The maximum exergy efficiency ($\zeta = 1$) is only achievable by ideal systems ($\sigma = 0$).

2.3.3. Exergy of humid air

The availability of a mixture of substances at a given temperature and pressure (*T, p*) is the maximum work obtainable by bringing the stream to the thermo-mechanical equilibrium with the environment.

Some common energy engineering processes have a mass interaction with the environment, in the sense that the mass may be released to the environment and/or have chemical reactions with it.

In the realm of the HVAC, a relevant case of chemical interaction with the environment is the diffusion process. This process occurs, for example, when the exhaust air is released to the outside from conditioned rooms or when the condensed water is dripping out from a cooling coil.

On the other hand, humid air is a binary mixture of dry air and water vapour; of course everyone of these components has its own thermal, mechanical and chemical interaction with the environment. In order to analyze these processes in a second law perspective, it is necessary to take into account the chemical potential of the constituents, since it is different from that of the environment.

After reaching the mechanical, thermal and chemical equilibrium with the environment, the system is said to be in the ultimate dead state.

The concept of chemical equilibrium involves the calculation of the chemical potential of substances and an extensive theoretical treatment, which is not the case to go through here: the interested reader is referred to the specialized literature.

Actually, the problem of psychrometric processes in terms of "available energy" was first stated and solved by Wepfer, Gaggioli and Obert in a fundamental article published in 1979 [2]. They derived the basic equation for the humid-air streams availability by re-writing the Gouy-Stodola equation, in a proper way for HVAC applications, stating that the global availability is obtained by summing up the thermomechanical and the chemical availability. By doing this, one obtains the following relationship for the evaluation of the exergy of a humid air stream, as a function of pressure *p*, temperature *T*, and absolute humidity *x*:

$$e_a\left(T,x,p\right)=\left(c_{pa}+x\cdot c_{pv}\right)\left(T-T_0-T_0\ln\frac{T}{T_0}\right)+\left(1+\bar{x}\right)R_aT_0\ln\frac{p}{p_0}+R_aT_0\left[\left(1+\bar{x}\right)\ln\frac{1+\bar{x}_0}{1+\bar{x}}+\bar{x}\ln\frac{\bar{x}}{\bar{x}_0}\right] \tag{2.17}$$

where:

- $\bar{x} = x / 0{,}622$;
- C_{pa} is the dry air specific heat;
- C_{pv} is the water vapour specific heat;
- R_a is the gas constant for the dry air;

The reference condition (ultimate dead state), denoted with the subscript "$_0$" is usually assumed to be that of outdoors; therefore: $x_o = x_E$; $T_o = T_E$; $p_o = p_E$; $e_E = e_o = 0$. The exergy of a water flow rate, when kinetic and potential terms can be disregarded, reduces to:

$$e_w = c_{pw}(T - T_0) - T_0 c_{pw} \ln \frac{T}{T_0} - R_v T_o \ln \phi_0 \qquad (2.18)$$

where c_{pw} is the specific heat for liquid water, R_v the water vapour constant and ϕ_o the relative humidity for the reference state ($\phi_o \doteq \phi_E$) . The exergy of the condensate produced by saturating the vapour contained in the humid air can be expressed as a function of the relative humidity ϕ_o of the outdoor air:

$$e_c = -R_v T_o \ln \phi_0 \qquad (2.19)$$

By using these formulas and the Gouy-Stodola equation, it is possible to study the basic processes of the air conditioning under a second law perspective.

3. SOLAR COOLING SYSTEM DESIGN AND ANALYSIS

This chapter is intended to present the design of a solar cooling system and its energy performance. On the basis of the results coming from the First Law analysis, the system will be analyzed from a Second Law point of view, pointing out its exergy inefficiencies.

3.1.System overview and main components description

The system under investigation in this report (shown in Fig. 3-1) is made up of a thermally driven adsorption machine connected to a water storage tank at the temperature of 85 °C. The

storage tank is fed with water heated by a solar panel field and a back up boiler. The adsorption machine is connected to a dry-cooler transferring the heat rejection to the external environment. The chiller provides cold water for the fan-coil, which produces the cooling effect.

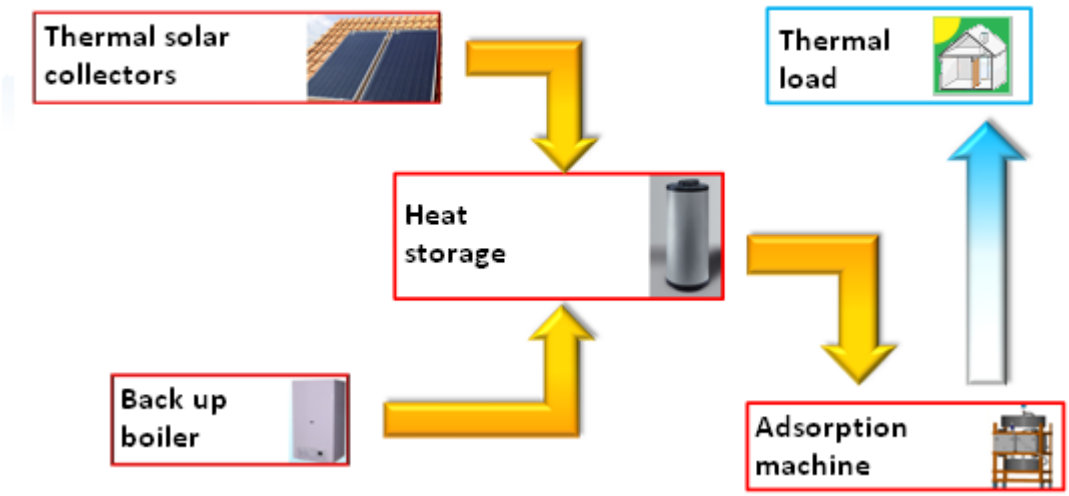

Fig. 3-1System plant layout.

The system dynamic model was built in order to find the optimum values for solar panel field (type, surface and technical specification) and for heat storage volume.
Solar collector used to collect heat for solar cooling application or domestic hot water production can be divided in two main groups: flat plate and evacuated tube collectors.

Flat plate collectors (see Fig. 3-2) consist of an insulated metal box (glass wool is mainly used) to minimize heat losses, a dark-colored absorber plate, to absorb most of the solar radiation and a low iron content glass cover, to obtain high transparency to solar radiation. Solar radiation is absorbed by the plate and transferred to the fluid that circulates through tubes, which are placed between the absorber plate and the glass cover.

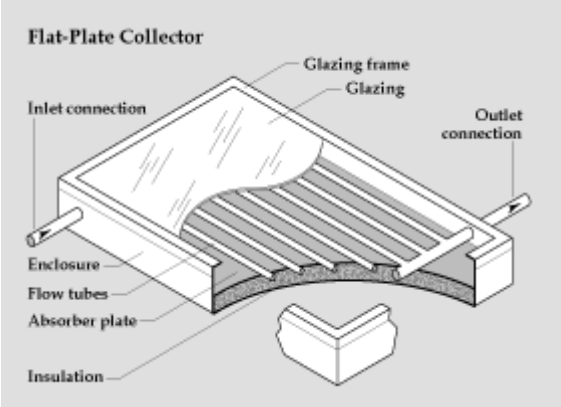

Fig. 3-2 Flat plate collector.

Evacuated tube collectors (Fig. 3-3) consist of evacuated borosilicate glass tubes which heat up solar absorbers and, ultimately, solar working fluid (water or propylene glycol). The vacuum within the evacuated tubes reduces convection and conduction heat losses, allowing them to reach considerably higher temperatures than flat-plate collectors.

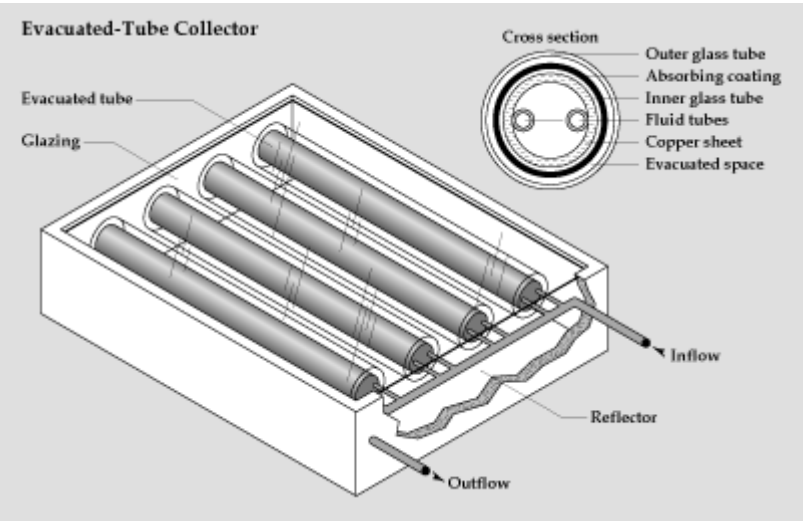

Fig. 3-3 Evacuated tube collector.

The main differences between solar plate and evacuated tube collectors are as follows:

- Cost: evacuated tube collectors are more expensive than flat plate collectors due to their high tech level
- Required temperature: evacuated tube collectors can achieve higher temperature than flat plate
- Available surface for installation: evacuated tube collector requires less surface than flat plate to meet the system's power requirements.

Fig. 3-4 shows how a heat storage tank with two heat exchanger works.

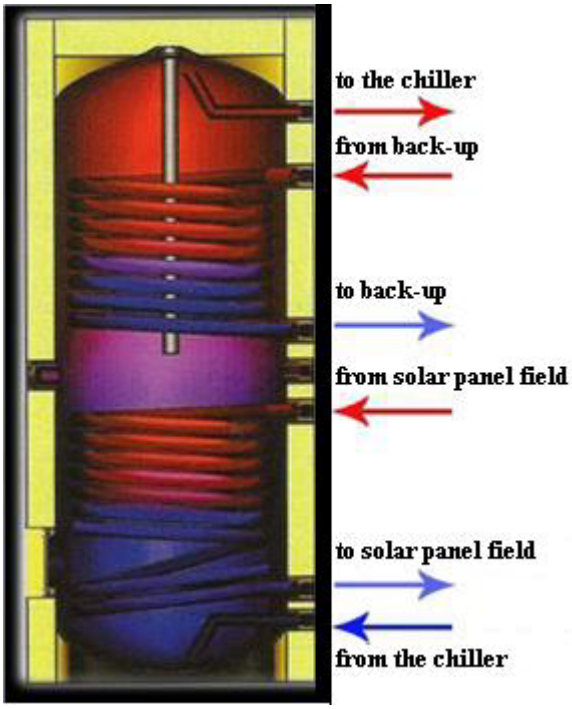

Fig. 3-4 Vertical heat storage tank connection.

The hot water stream feeding the adsorption chiller flows inside the storage leaving from top and entering from bottom. The lower heat exchanger is connected to the solar panel field, while through the higher one flows the water heated by the auxiliary boiler to prevent from using auxiliary power to heat all the storage volume.

3.2.Dynamic model and simulations

The model was built using TRNSYS software. TRNSYS is a simulation program mainly used in the fields of renewable energy engineering and building simulation for passive as well as active solar design. TRNSYS is a commercial software package developed at the University of Wisconsin.

The components of the model are called “types”. The software comes with a wide set of types used in this kind of installation: solar collector (flat plate and evacuated tubes), heat storage tank, chiller and adsorption machine. The software also allows user to create custom types when needed by using FORTRAN subroutines.

The adsorption machine and the type able to simulate its behavior were developed by the CNR-ITAE in Messina on the basis of experimental data, obtained by ITAE [3] and shown in Fig. 3-5 and Fig. 3-6:

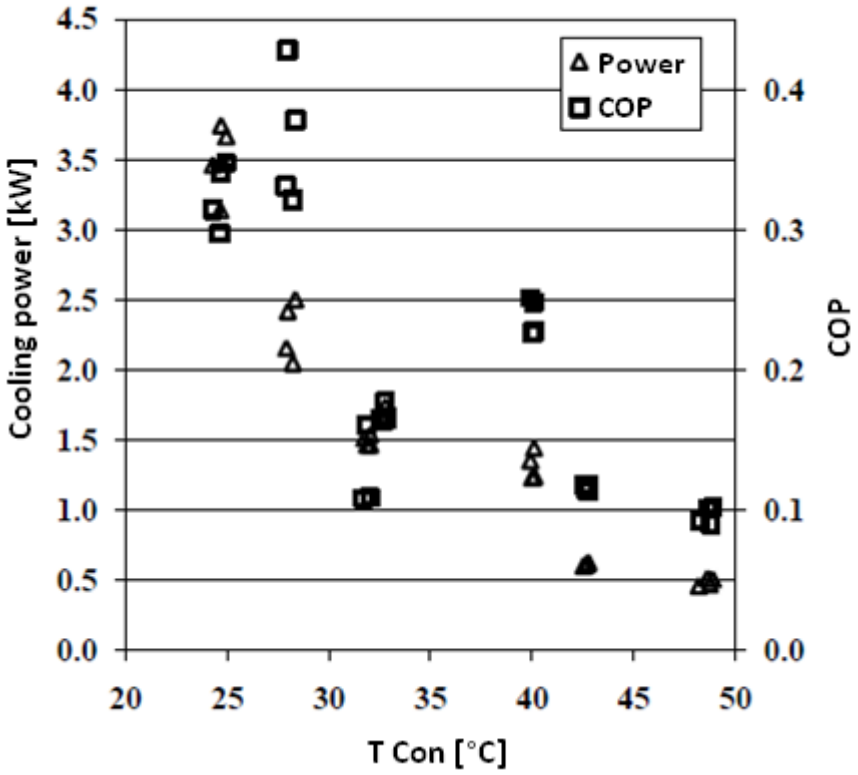

Fig. 3-5 Power and COP referred to the temperature at condenser.

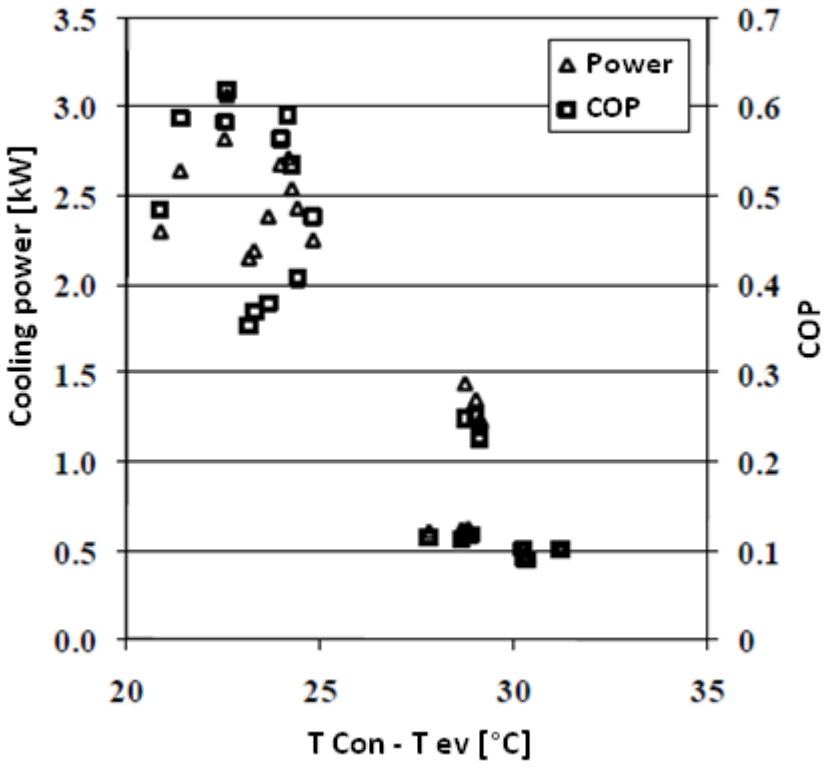

Fig. 3-6 Power and COP referred to condenser – evaporator temperature difference.

The type operates on input data (see Fig. 3-7) using parametric functions, which are obtained by linear interpolation of experimental measurements.

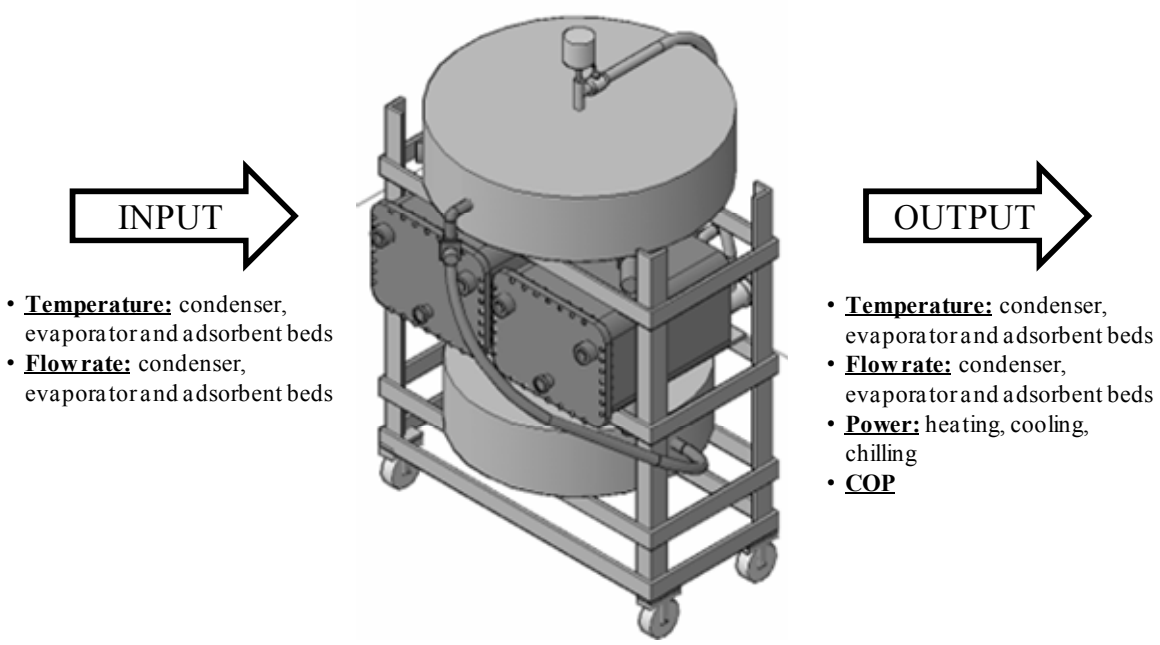

Fig. 3-7 Chiller type input and output

The solar cooling system considered in this study is intended to provide comfort conditions in an office room located in Messina (Sicily) in summer. Table 3-1 summarizes the main features of the design.

Room description	
West wall surface	7.5 m^2
East wall surface	7.5 m^2
Nord wall surface	12 m^2
South wall surface	12 m^2
West window surface	1 m^2
East window surface	1 m^2
Nord window surface	1 m^2
Room surface	10 m^2
Room Volume	30 m^3
Internal load	
Occupancy (time)	2 (8-18)
Personal computer	2
Artificial lighting	10 W/m^2

Table 3-1 Room and loads description.

The simulations for the determination of the thermal load were performed with TRNSYS The typical input data scheme is shown in Fig. 3-8:

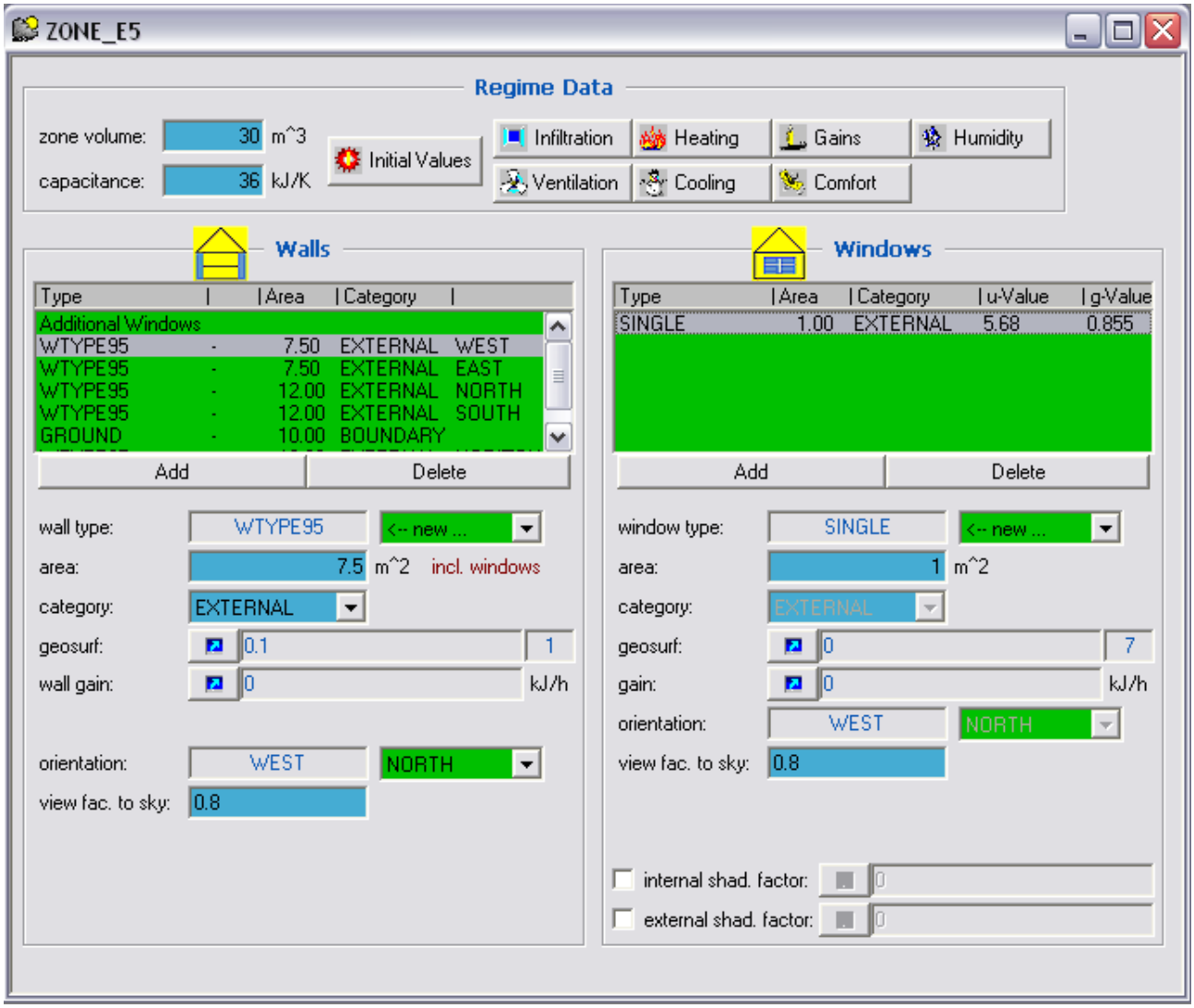

Fig. 3-8 Zone input panel

Results for the warmest summer week are shown in Fig. 3-9. Set point conditions were as follows: 26 °C and 50% relative humidity.

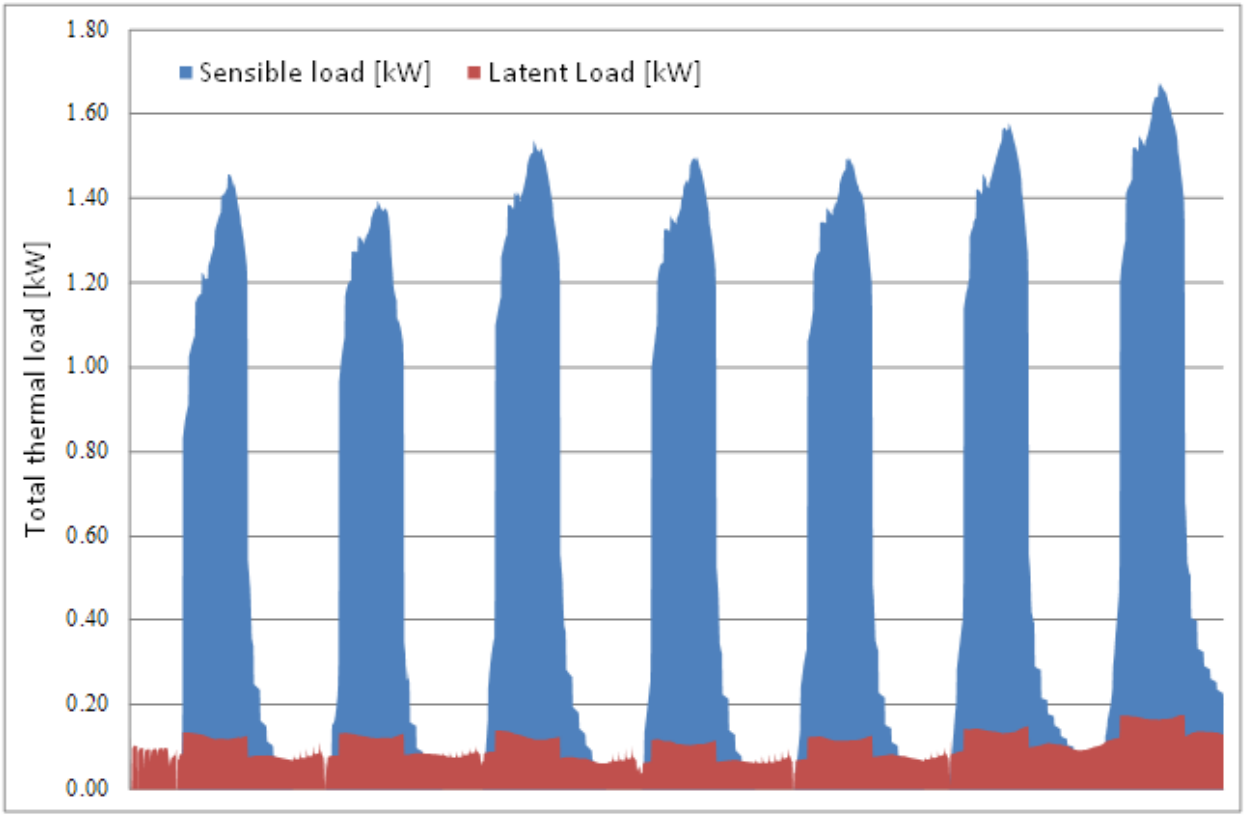

Fig. 3-9 Room thermal loads.

Since the peak load is considerably below 2 kW the adsorption chiller would be capable to meet system requirements.

The system model has been developed with TRNSYS Studio with the components (types) summarized below. They all came with TRNSYS software with the exception of the adsorption chiller built by CRN – ITAE.

- Type 109, Data Reader and Radiation Processor. This component serves the main purpose of reading weather data at regular time intervals from a data file, converting it to a desired system of units and processing the solar radiation data to obtain tilted surface radiation and angle of incidence for an arbitrary number of surfaces. In this mode, Type 109 reads a weather data file in the standard TMY2 format. The TMY2 format is used by the National Solar Radiation Data Base (USA) but TMY2 files can be generated from many programs, such as Meteonorm.
- Type 538, Evacuated Tube Solar Collector. This component models the thermal performance of a evacuated tube solar collector. The solar collector array may consist of collectors connected in series and in parallel. The thermal performance of the collector

array is determined by the number of modules in series and the characteristics of each module.

- Type 540, Flat Plate Solar Collector. This component models the thermal performance of a flat-plate solar collector. The solar collector array may consist of collectors connected in series and in parallel. The thermal performance of the collector array is determined by the number of modules in series and the characteristics of each module. The user has to provide results from standard tests of collector efficiency versus a ratio of fluid average temperature minus ambient temperature to solar radiation.
- Type 700, Boiler. This component models the boiler (auxiliary heater). This model will attempt to meet the user-specified outlet temperature taking into account the boiler efficiency and the combustion efficiency, which have to be defined by the user.
- Type 60, Vertical Storage Tank. This component models a stratified liquid storage tank. It includes numerous features such as allowing for multiple heat exchangers within the tank and allowing for unmatched numbers of inlet and outlet flows. Users may define between 0 and 3 (inclusive) internal heat exchangers.
- Type 508, Cooling Coil Using Bypass Fraction Approach. The cooling coil is modeled using a bypass approach in which the user specifies a fraction of the air stream that bypasses the coil. The remainder of the air stream is assumed to exit the coil at the average temperature of the fluid in the coil and at saturated conditions. The model is alternatively able to internally bypass fluid around the coil so as to maintain the outlet air dry bulb temperature above a user specified minimum.
- Type 753, Heating Coil Using Bypass Fraction Approach. This component models a simple heating coil where the air is heated as it passes across a coil containing a hotter fluid (typically water). It uses the bypass fraction approach for heating coils to solve for the outlet air and water conditions. This model has been used to simulate how the dry cooler behaves.
- Type 56, Multi-Zone Building. This component models the thermal behavior of the building previously generated by running the preprocessor program TRNBuild.

Types simulating pumps, flow diverters, flow mixers and fans were also used to obtain the whole system layout, as shown in Fig. 3-10.

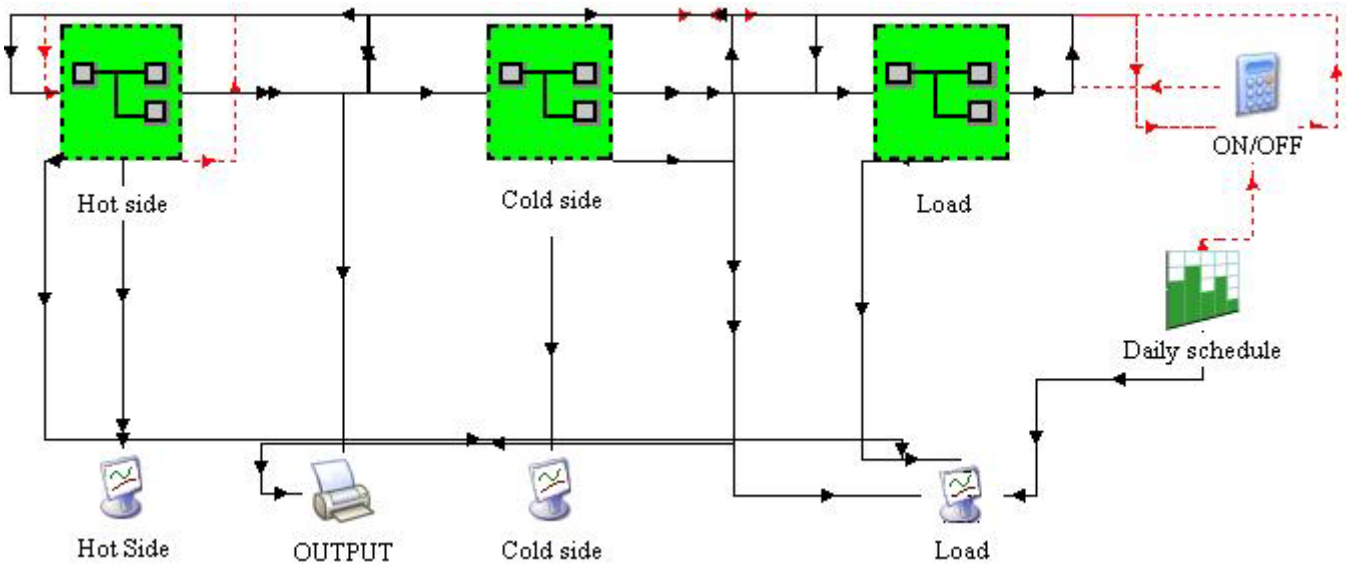

Fig. 3-10 TRNSYS system layout.

As appears in Fig. 3-10, the system is split in three subsystem referring to the hot side, the cold side and the load. There are also components that display the system output data or controlling the on/off timing. The three subsystems are shown and described below.

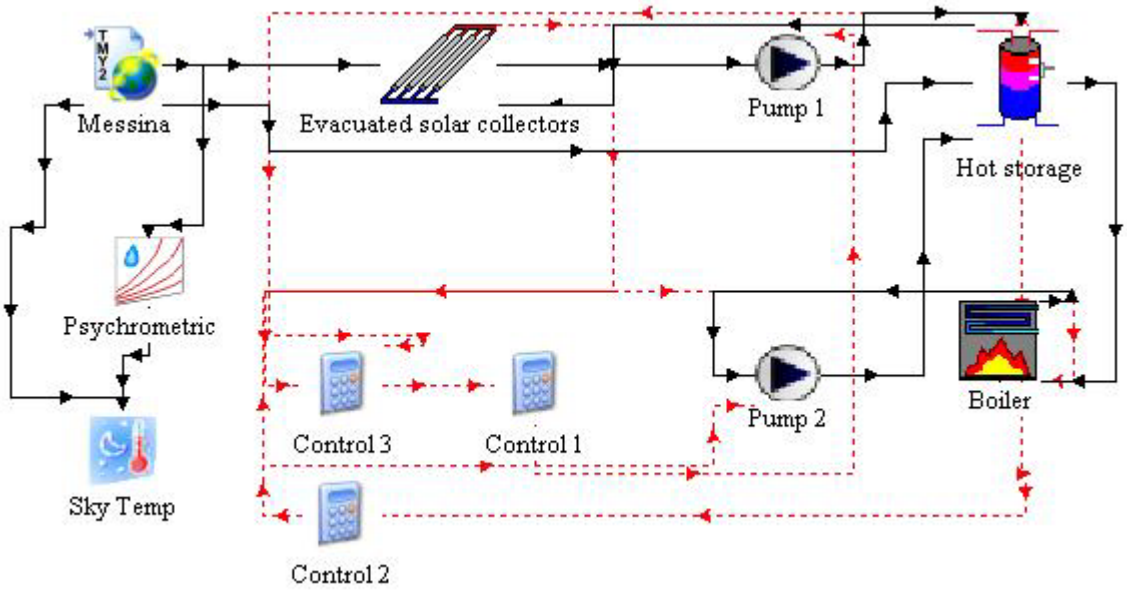

Fig. 3-11 Hot side subsystem.

Fig. 3-11 shows the "hot side" subsystem, whose components provide hot water for the adsorption machine. It is possible to recognize the solar collectors and the boiler connected to the heat storage. The two pumps, controlled by additional types, make the fluid flow go across the storage heat exchangers.

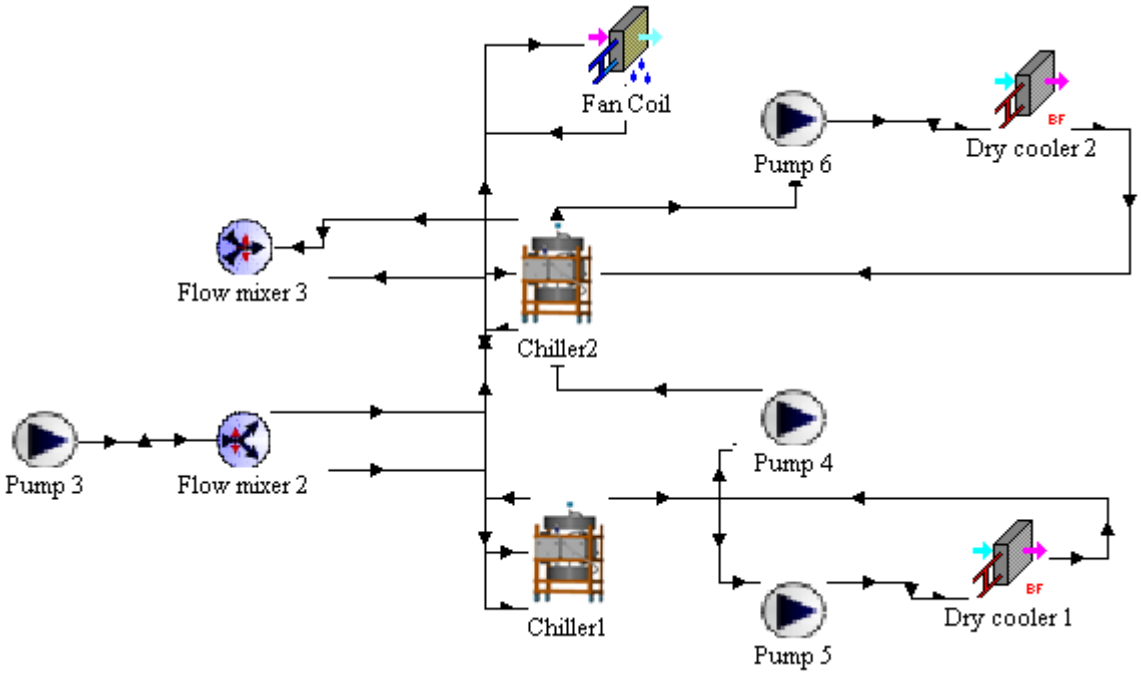

Fig. 3-12 Cold side subsystem.

Fig. 3-12 shows the "cold side" subsystem. There are two types simulating two adsorption machines in series, in order to match all the cooling load. Simulation results show that the second chiller provides only 1% of the total cooling power, and is in idle for the majority of the time. Two heating coils simulate the dry cooler, which removes the machines thermal waste, while the cooling coil simulates the fan coil, which reduces the room air temperature.

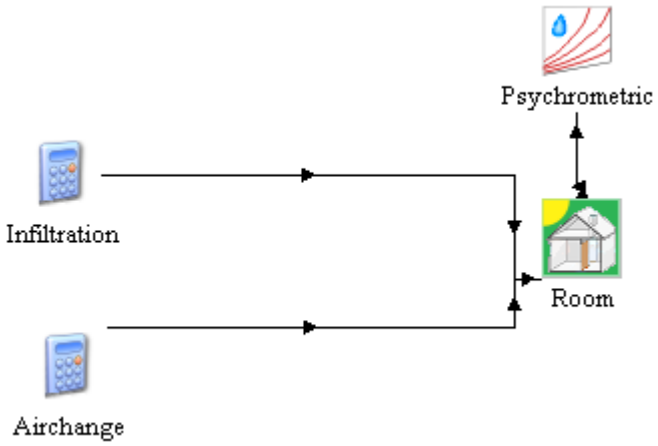

Fig. 3-13 Load subsystem.

Fig. 3-13 shows the "load subsystem". The room type was created, as described above, with the TRNBUILD feature. Two additional types are used to control infiltration and air change flow rates during the course of the day.

The collectors and boiler pumps control system was made up in order to achieve the highest efficiency. The main points taken into account while developing the control were:

- The office is occupied by the two persons from 8.00 a.m. to 6.00 p.m., so the adsorption machine would work only during this time.
- The pump connecting the solar collector to the heat storage makes the fluid flow circulate only if the outlet collector fluid temperature is higher than the stored water temperature. This is to avoid stored water being cooled by the collector fluid flow.
- The boiler is turned on when the heat storage temperature falls below 80 °C, to prevent the adsorption machine from working with water at low temperature.
- The whole system is off during night, when no solar radiation can be gathered by solar collectors.

3.3.Simulation results

The TRNSYS model has been used to perform different parametric analysis. The simulation time starts on June the 15th and ends on September the 15th. Simulations were run to find the optimum for the system referring to:

- Solar collectors tilt angle
- Heat storage tank volume
- Total collectors surface.

The technical specification for the solar collectors, heat storages and boiler types were taken from real components available in the market. The flat plate and evacuated tube collectors are from the same manufacturer, and the same is for three different heat storage models.
Fig. 3-14 shows the technical specification for the collectors adopted for the simulation:

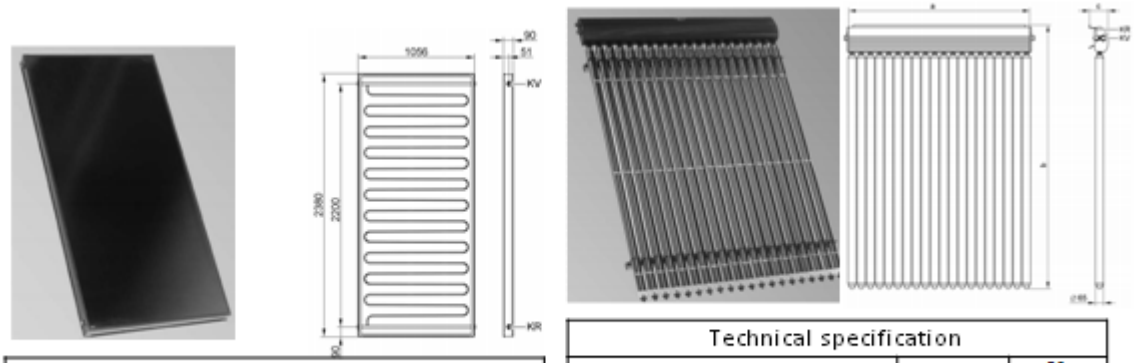

Technical specification		
Gross collector area	m²	2.51
Absorber area	m²	2.32
Size: Lenght Height Widht	 mm mm mm	 1056 2380 90
Zero Loss Coll. efficiency	%	79.3
Heat Loss Coefficient k1	W/(m²K)	3.95
Heat Loss Coefficient k2	W/(m²K²)	0.0122
Thermal capacity	kJ/(m²K)	6.4
Weight	kg	52
Liquid content	l	1.83
Max operationg pressure	bar	6
Stagnation temperature	°C	221

Technical specification		
Number of heat pipes		20
Gross collector area	m²	2.88
Absorber area	m²	2.05
Size: Lenght Height Widht	 mm mm mm	 1418 2031 143
Zero Loss Coll. efficiency	%	81.5
Heat Loss Coefficient k1	W/(m²K)	1.43
Heat Loss Coefficient k2	W/(m²K²)	0.076
Thermal capacity	kJ/(m²K)	5.4
Weight	kg	51
Liquid content	l	1.2
Max operationg pressure	bar	6
Stagnation temperature	°C	150

Fig. 3-14 Solar collector chosen for the simulation.

Fig. 3-15, 16 and 17 show the technical specification of the three heat storage tanks chosen. The main difference is the volume, which is equal to 300, 500 and 750 dm^3:

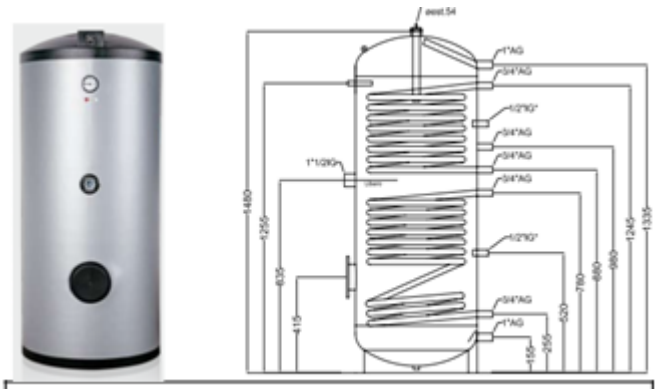

Technical specification		
Capacity	l	300
Shell width	mm	50
Weight	kg	118
Upper heat exchanger: Surface Flow rate Losses	 m² m³/h mbar	 0.9 2.5 75
Lower heat exchanger Surface Flow rate Losses	 m² m³/h mbar	 1.3 2.5 85
Heat transfer coefficient	W/(mK)	0.023

Fig. 3-15 300 dm^3 storage.

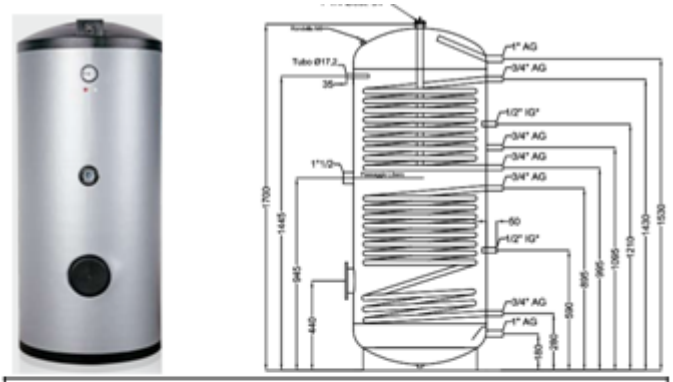

Technical specification		
Capacity	l	500
Shell width	mm	50
Weight	kg	156
Upper heat exchanger: Surface Flow rate Losses	 m² m³/h mbar	 1.2 3 90
Lower heat exchanger Surface Flow rate Losses	 m² m³/h mbar	 1.7 3 140
Heat transfer coefficient	W/(mK)	0.023

Fig. 3-16 500 dm^3 storage.

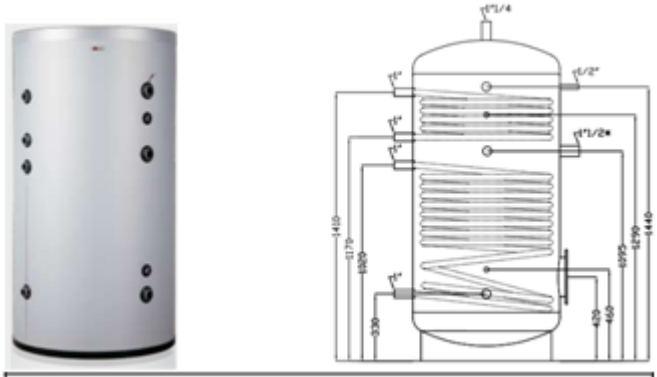

Technical specification		
Capacity	l	750
Shell width	mm	85
Weight	kg	189
Upper heat exchanger: Surface Flow rate Losses	 m² m³/h mbar	 1.5 4 140
Lower heat exchanger Surface Flow rate Losses	 m² m³/h mbar	 2.5 4 220
Heat transfer coefficient	W/(mK)	0.023

Fig. 3-17 750 dm^3 storage.

To evaluate and compare the system performance two different parameters were taken into account:

- The Solar Fraction, which is defined as the ratio of the solar power to the total thermal load which, in turn, is the sum of the thermal power provided to the system by both the solar collectors and the boiler:

$$SF = \frac{\dot{Q}_{coll}}{\dot{Q}_{coll} + \dot{Q}_{boiler}} \tag{3.1}$$

Where:

SF is the Solar Fraction

$\dot{Q}_{coll}$ is the thermal power provided by the solar collectors

$\dot{Q}_{boil}$ is the thermal power provided by back-up boiler

- The Primary Energy Ratio, which is defined as the ratio of the enthalpy difference between the inlet flow rate air and room inside air to the total Primary Energy provided form outside to the whole system (gas boiler and auxiliary devices):

$$PER = \frac{\Delta h}{\dot{Q}_{gas} + P_{aux} / 0.37} \tag{3.2}$$

Where:

PER is the Primary Energy Ratio

Δh is the enthalpy difference between inlet flow rate and room air

$\dot{Q}_{gas}$ is the boiler Primary Energy consumption

P_{aux} is the auxiliary devices electrical consumption, which is converted to Primary Energy consumption by means of the Italian electrical power production efficiency (0,37)

The auxiliary devices consumption data were taken from the manufacturer technical specifications, and were assumed to be equal to 800 W.

The first set of simulations investigates about the optimal solar field tilt angle. The solar collectors field is due to south (only the tilt angle was changing).

Fig. 3-18 refers to simulations for evacuated tube collectors, while Fig. 3-19 refers to simulation related to flat plate collectors. Both of them show how the SF reacts to the tilt angle.

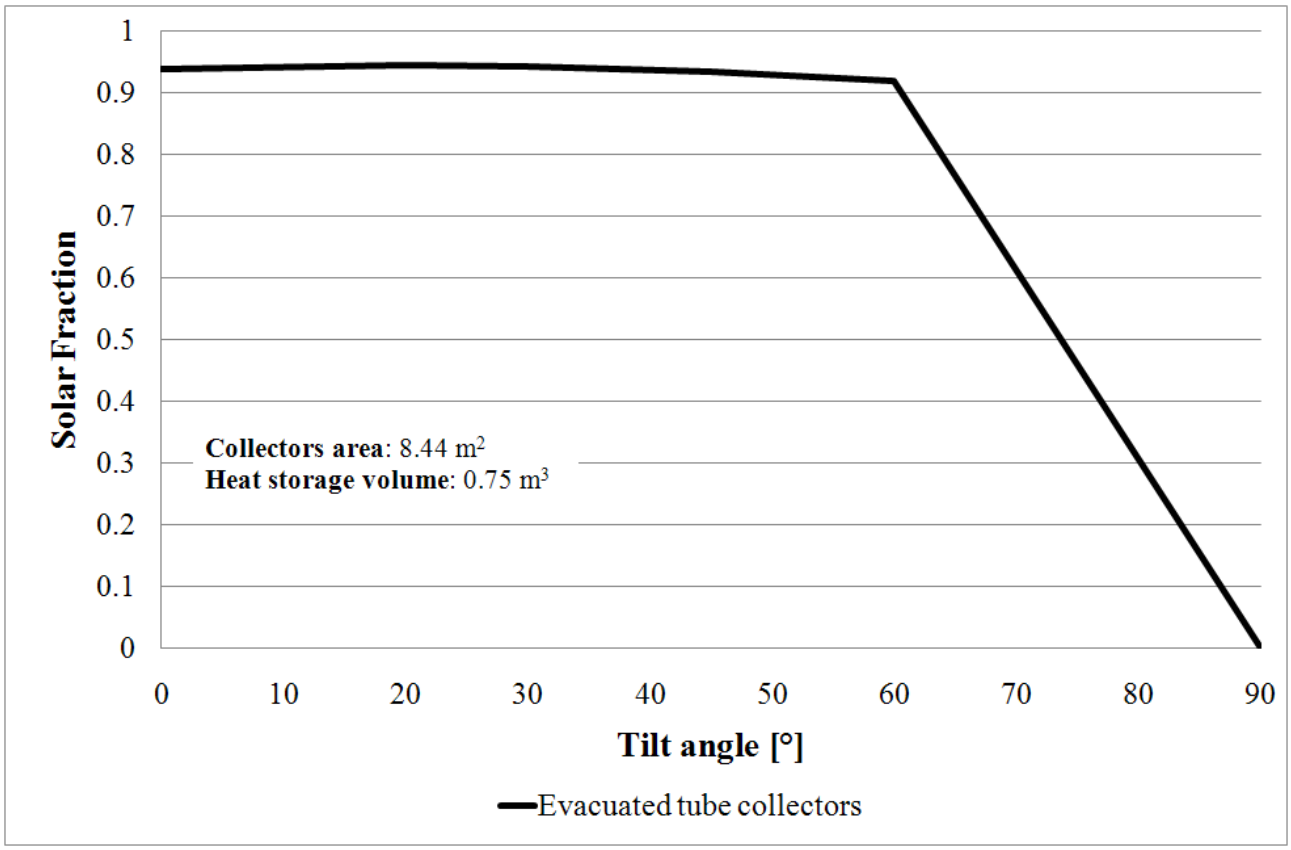

Fig. 3-18 SF vs. Evacuated tube collector field tilt angle.

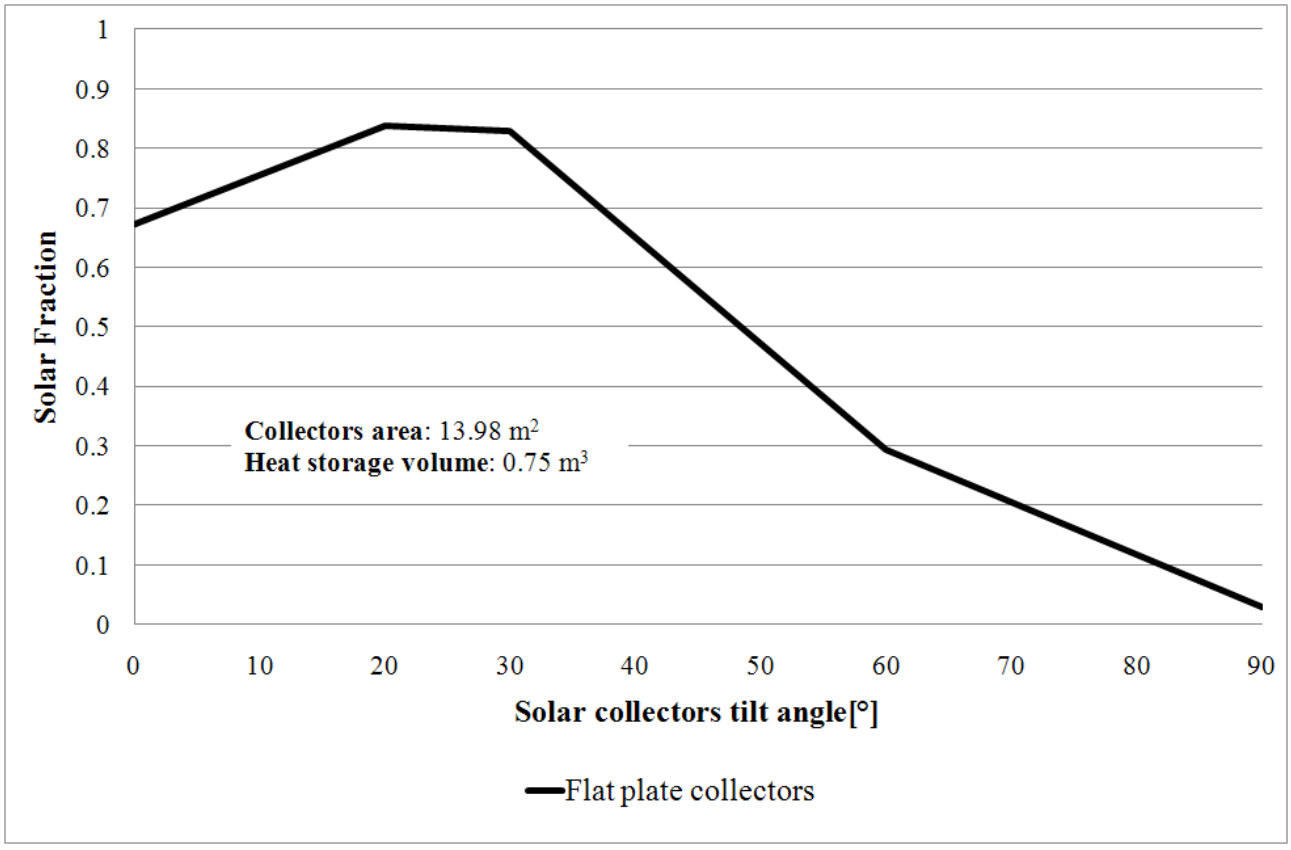

Fig. 3-19 SF vs. Flat plate tube collector field tilt angle.

Fig. 3-18 shows that the evacuated tube collectors allow to achieve high values of SF into a wide range of tilt angle values. This is due to the cylindrical concentrating surfaces, located inside the collector, which can gather energy from the solar radiation even if it is not perpendicular to the plate surface. On the other hand, flat plate collectors work at their best only in a little range of tilt angle, because they absorb the solar radiation only if it is perpendicular to the plate surface (see Fig. 3-19).

Fig. 3-20 and 21 show the results obtained in terms of PER. They refer to the same set of simulations done for the SF analysis.

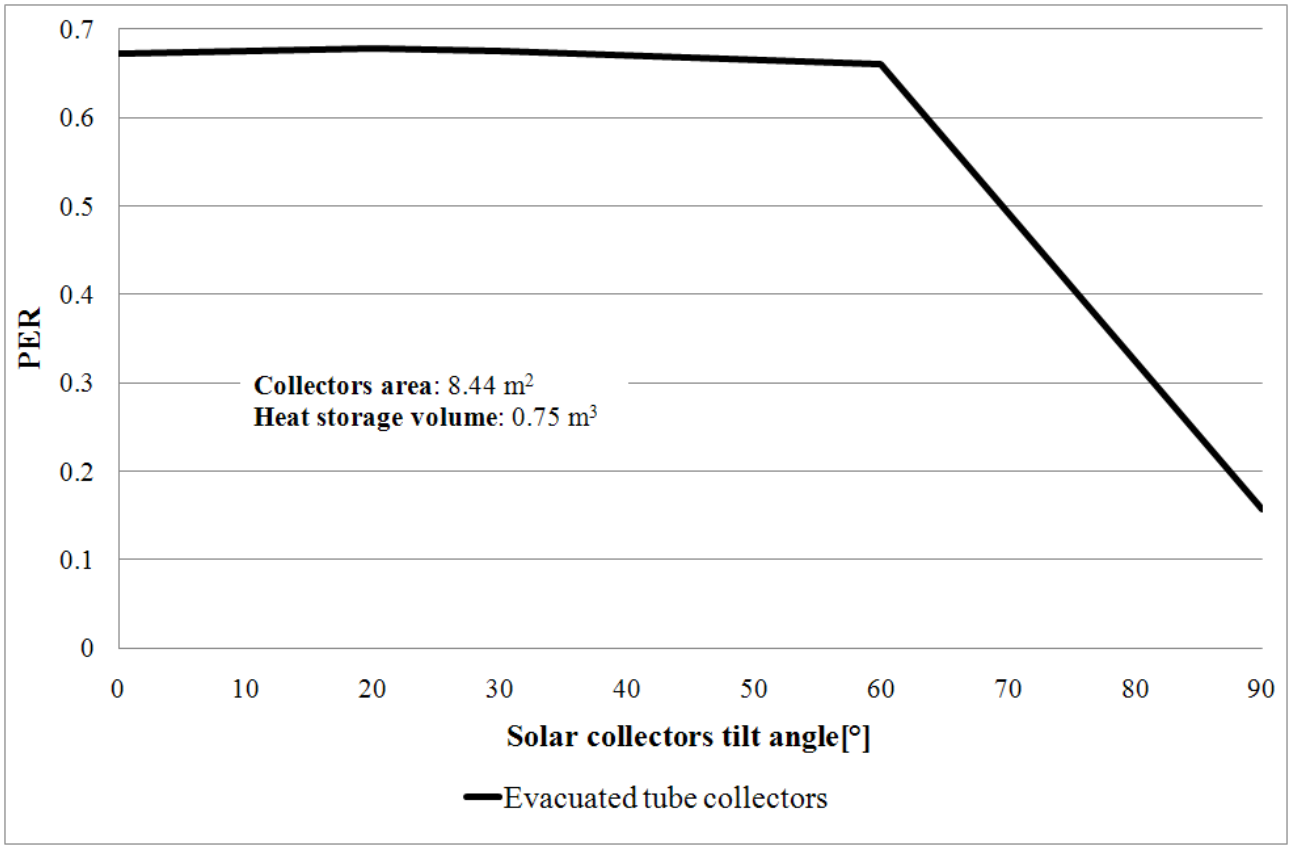

Fig. 3-20 PER vs. Evacuated tube collector field tilt angle.

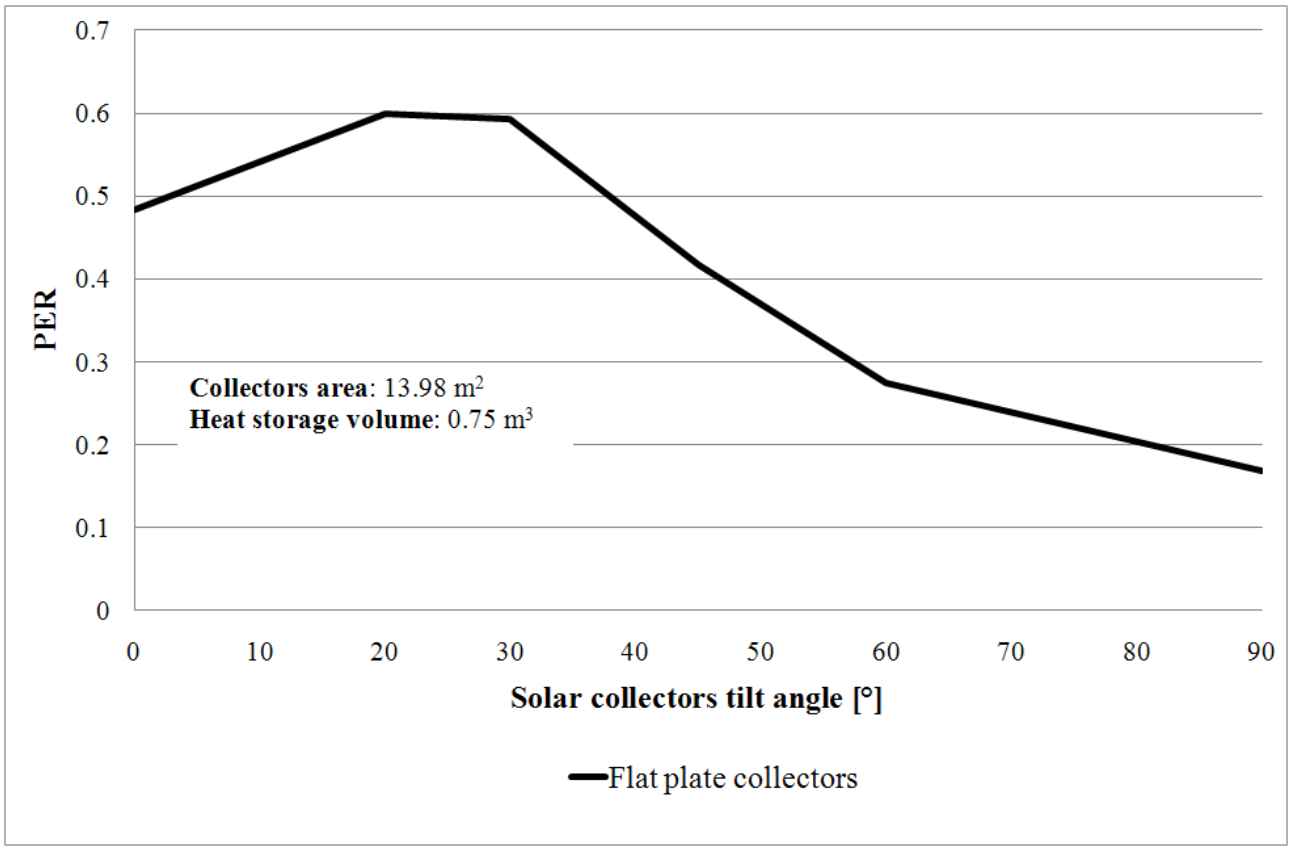

Fig. 3-21 PER vs. Flat plate tube collector field tilt angle.

These graphs show that even from the PER point of view the evacuated tube collector field works better than the flat plate tube collector field, being less influenced by the tilt angle.

Taking into account these results, the tilt angle for all of the further simulations performed has been set equal to 20° for both the evacuated and the flat plate collectors fields.

A second set of simulations was aimed at finding the best values for both the total solar collectors area and the volume of heat storage. Simulations related to the optimum for the solar collectors area per unit of nominal solar power installed (A) were performed according to the formula provided by H. M. Henning [4].

$$A = \frac{1}{G \cdot COP \cdot \eta_{coll}} \tag{3.3}$$

The average solar radiation value (G) has been set equal to 0.8 kW/m^2 and the machine COP can be assumed equal to 0.35. For the evacuated solar collectors, whose thermal efficiency (η_{coll}) is equal to 0.55, the result is 6.5 m^2/kW, while, for the flat plate collectors, whose

thermal efficiency is equal to 0.4, the result is 18.5 m^2/kW. As the system has to be capable of providing a cooling peak power equal to 2 kW, simulations have been run considering a maximum area of 13 m^2 for the evacuated tube collectors and 19 m^2 for the flat plate collectors.

Results are shown in Fig. 3-22:

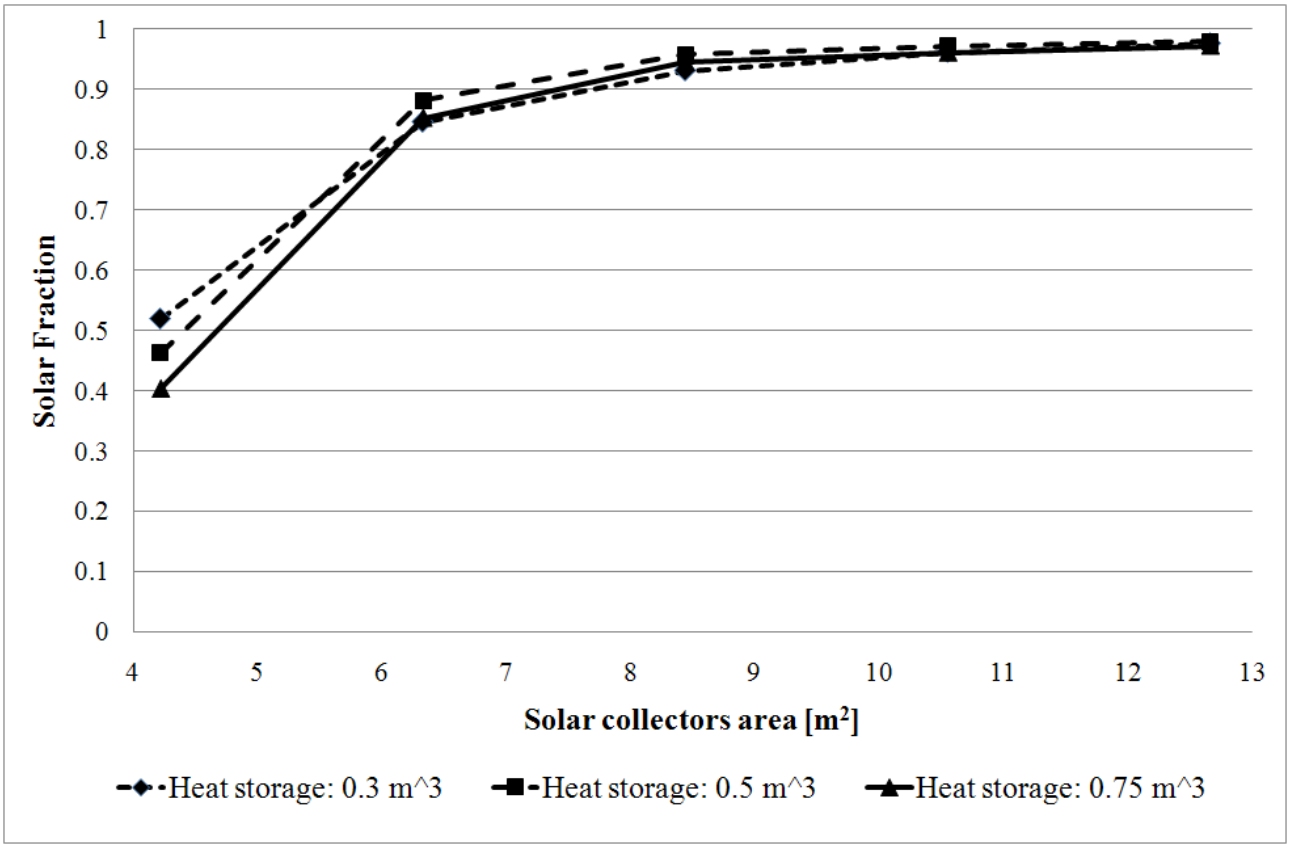

Fig. 3-22 Solar Fraction vs. Evacuated solar collectors area for different values of heat storage volume.

Fig. 3-22 shows how the SF value changes using different values for the evacuated solar collectors area and for the heat storage volume. SF does not seem to be affected by changing in the heat storage and it reaches a very high level (95 %) with just 8.5 m^2 of solar collectors.

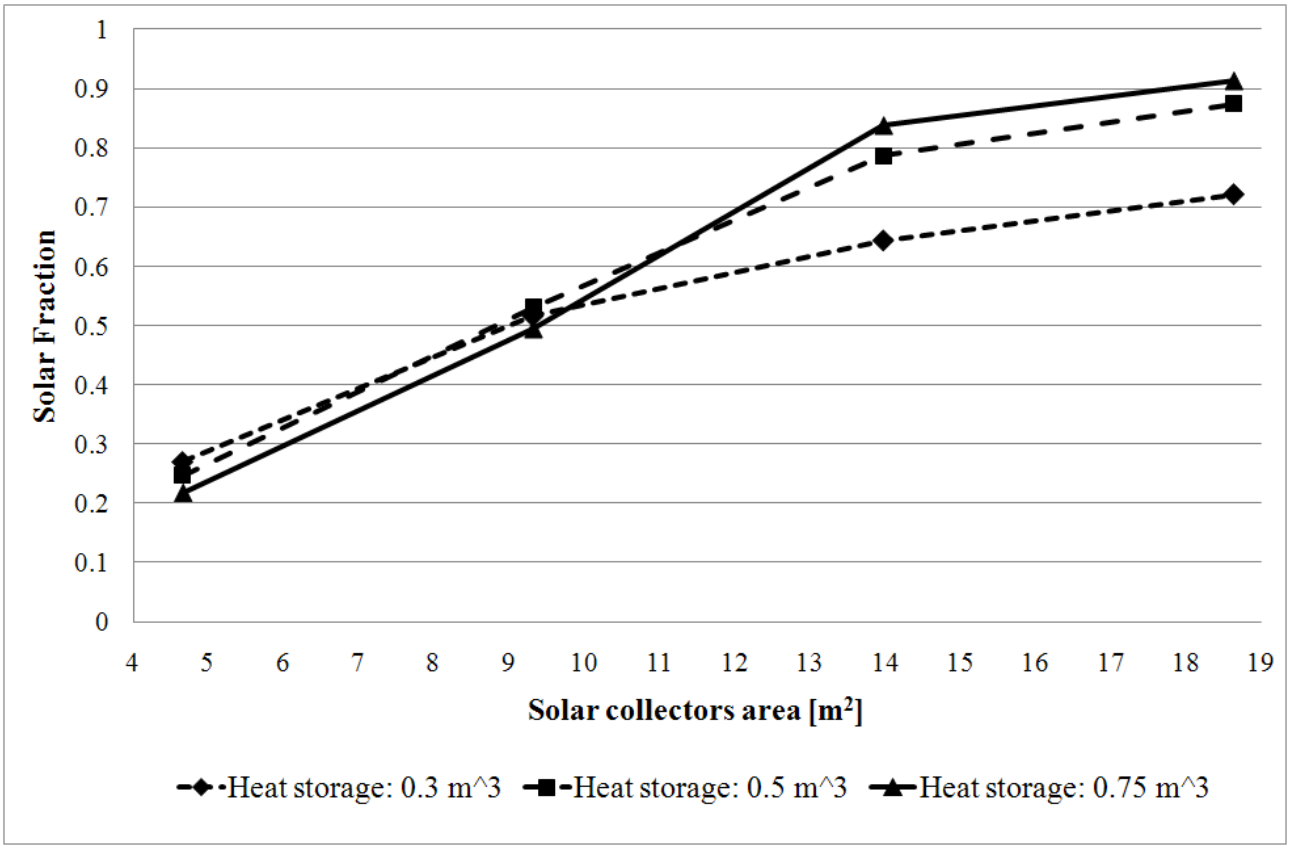

Fig. 3-23 Solar Fraction vs. Flat plate solar collectors area for different values of heat storage volume.

Fig. 3-23 shows how the SF depends on the total flat plate collectors area and on the heat storage volume. Using flat plate collectors, high level of SF can be achieved only with high surface of solar panels and the heat storage has a relevant impact on the system performance. This happens because the flat plate collectors work at their best only a few hours a day and the system has to be able to store the thermal power needed during the low efficiency hours. The highest SF value (0,90 %) can be reached by using 18.5 m^2 of flat plate solar collectors and a heat storage volume equal to 0.75 m^3.

Fig. 3-24 and 25 show the results in terms of PER.

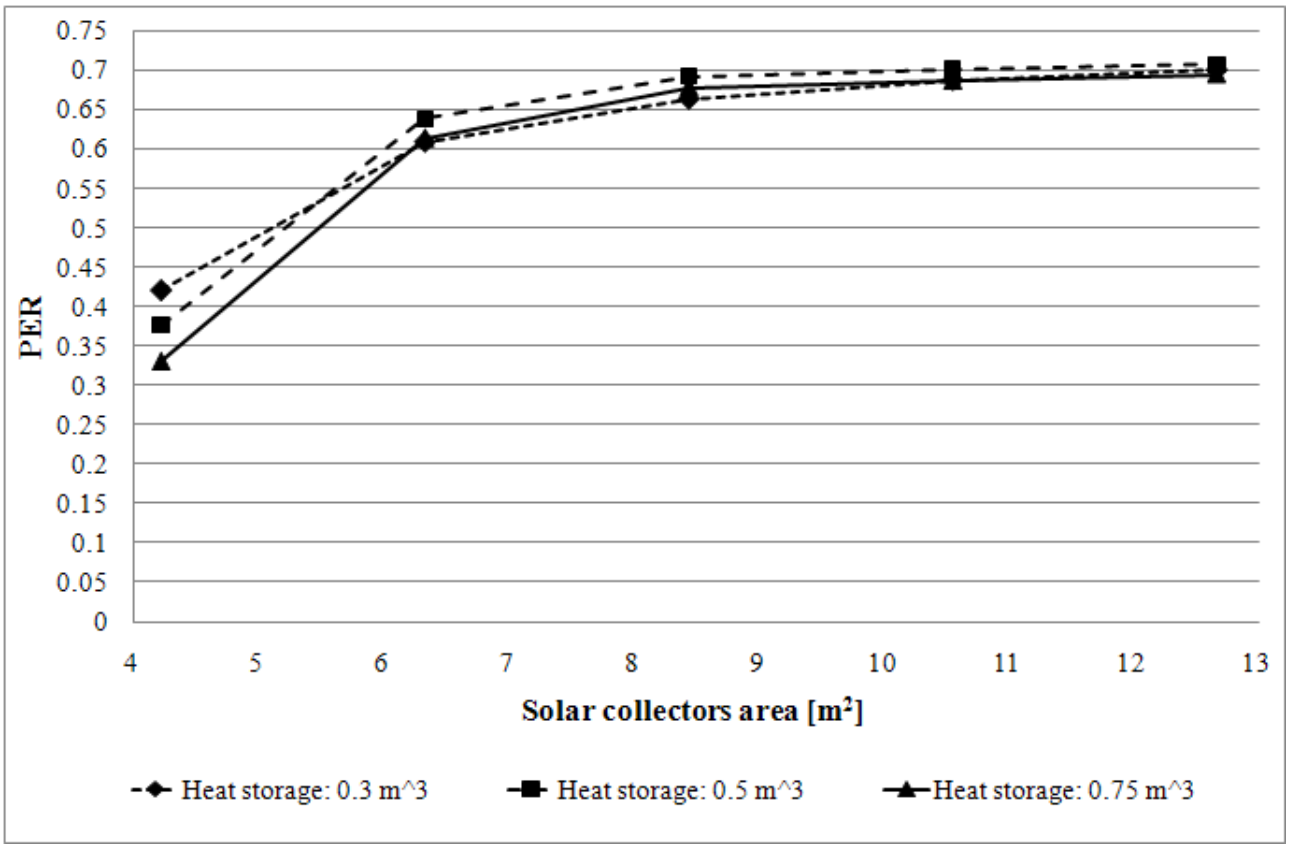

Fig. 3-24 PER vs. Evacuated solar collectors area for different values of heat storage volume.

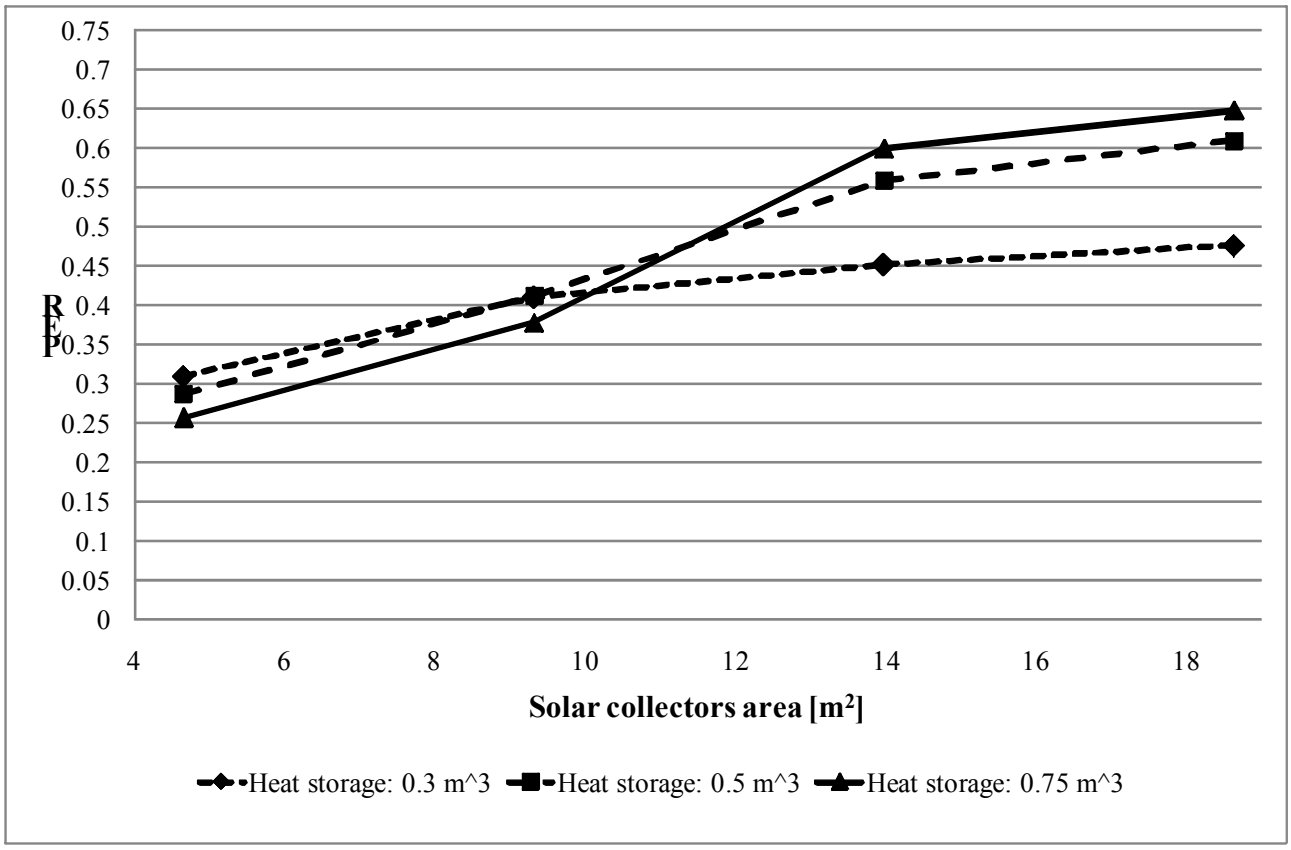

Fig. 3-25 PER vs. Flat plate solar collectors area for different values of heat storage volume.

PER results are very similar to SF results as they depend on the same conditions. Using evacuated tube allows to gather more solar thermal energy than using flat plate collectors and make the system less depending on the heat storage volume. Using evacuated solar collectors also allows to reach higher SF values than using flat plate collectors with lower collecting area.

In conclusion the solar cooling system was finally designed withn the following specifications:

- series of 4 evacuated tube solar collectors;
- solar collectors area equal to 8.44 m^2;
- gross solar collectors area equal to 11.52 m^2;
- solar field tilt angle equal to 20°;
- heat storage volume equal to 0.3 m^2;

The simulation performed according to these values ensures that this system can grant the required comfort level to the room inhabitants, even during the warmest observed summer week. The week starts on July the 17th and ends on 23th. Fig. 3-26 shows that the inside temperature would not rise over 26 °C, while the outside temperature reaches 34 °C.

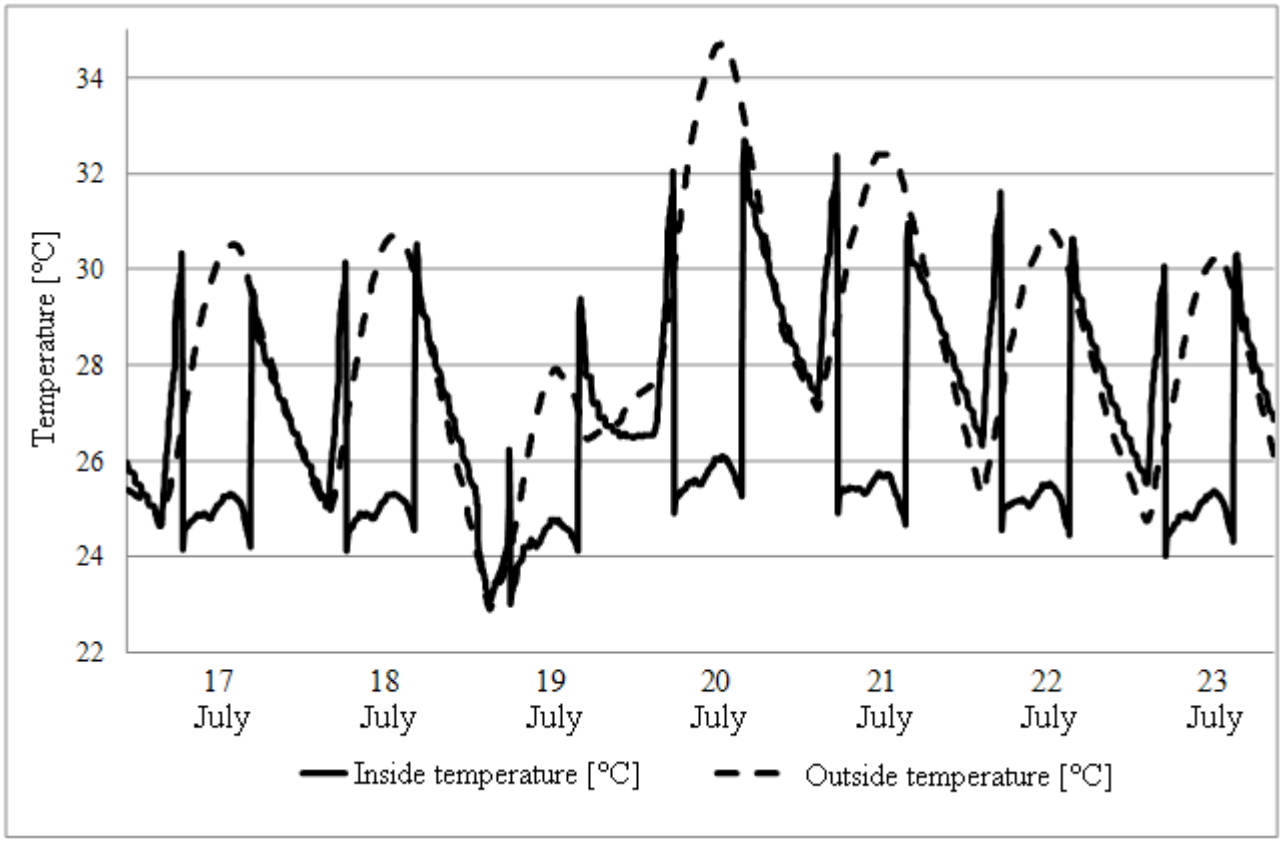

Fig. 3-26 Inside and outside temperature during the warmest summer week.

3.4.Energy analysis and plant sizing

Since the system is able to control the air temperature, but it cannot operate any regulation on air relative humidity, only the sensible cooling load will be taken into account for a deeper thermal analysis.

3.4.1. Thermal loads

The total thermal load (Q_{sens}) is given by the sum of external ($Q_{sens,est}$) and internal ($Q_{sens,int}$) thermal loads. The result is provided by TRNSYS simulation.

$$\dot{Q}_{sens} = \dot{Q}_{sens,est} + \dot{Q}_{sens,int} = 1{,}4\ kW$$

Since the room is occupied by two persons, the system has to provide fresh air from outside according to the Italian regulation (Norma UNI 10339) the fresh air flow rate depends on people occupancy and is set to $40\ \frac{m^3}{h\ pers}$

Outside fresh air enters at external temperature (t_E = *30 °C*) and, after an adiabatic mixing with ambient air, its temperature decreases to 26 °C. The corresponding cooling load has to be taken into account:

$$\dot{m}_{fresh} = 40 \frac{m^3}{h\ pers} \cdot 2 \cdot 1{,}22 \frac{kg}{m^3} \cdot \frac{1}{3600} \cong 0.03 \frac{kg}{s}$$

$$\dot{Q}_{fresh} = \dot{m}_{fresh} \cdot cp_a \cdot \left(t_E - t_A\right) \cong 0.1\ kW$$

Where cp_a stands for air specific heat capacity $\left(1{,}004 \frac{kJ}{kg \cdot K}\right)$

The total sensible load is equal to:

$$\dot{Q}_{sens,tot} = \dot{Q}_{sens} + \dot{Q}_{fresh} = 1{,}5\ kW$$

Now it is possible to go on with the thermohygrometric analysis of the system.

3.4.2. Fan coil

The fan coil removes heat from the ambient air. The unit gets cold water at the temperature of 13 °C ($t_{ch,out}$) from the adsorption chiller. The cold water flow rate circulating through the cold piping system, which connects the fan coil to the cooling machine, is given by the energy balance on the component. The outlet water temperature is supposed to be 18 °C, so that the difference between fan coil water inlet and outlet (Δt_{fc}) is equal to 5 °C.

$$\dot{Q}_{sens,tot} = \dot{m}_{w,fc} \cdot cp_w \cdot \Delta t_{fc} \qquad \Rightarrow \qquad \dot{m}_{w,fc} \cong 0{,}07 \frac{kg}{s}$$

Where cp_w stands for water specific heat capacity $\left(4{,}186 \frac{kJ}{kg \cdot K}\right)$

The air flow rate handled by the fan coil is known from its technical specification:

$$\dot{m}_{a,fc} = 600 \frac{m^3}{h}$$

Fan coil outlet air thermohygrometric conditions are:

$$t_I = t_A - \frac{\dot{m}_{w,fc} \cdot c_{pw} \cdot \Delta t_{fc}}{\dot{m}_{a,fc} \cdot c_{pa}} = 18.5\ °C \qquad h_I = 45.14 \frac{kJ}{kg} \qquad x_I = 10.5 \frac{g}{kg}$$

Where h_i stands for outlet air specific enthalpy, while x_i stands for outlet air humidity ratio.

3.4.3. Adsorption machine

The adsorption machine has to provide all the cooling power required for air conditioning. The thermal power (Q_{hot}) needed to produce the cooling effect can be calculated on the basis of the estimated COP value.

$$\dot{Q}_{hot} = \frac{\dot{Q}_{sens,tot}}{COP} \cong 5\ kW$$

The chiller receives hot water from the storage at a temperature ($T_{hot,in}$) of 85 °C. The hot water flow rate circulating through the hot piping system, which connects the adsorption chiller to the hot water storage, is given by the energy balance on the component. The outlet water temperature is supposed to be 80 °C, so that the difference between fan coil water inlet and outlet (Δt_{hot}) is equal to 5 °C.

$$\dot{Q}_{hot} = \dot{m}_{w,hot} \cdot cp_w \cdot \Delta t_{hot} \qquad \Rightarrow \qquad \dot{m}_{w,hot} \cong 0{,}24\ \frac{kg}{s}$$

The total thermal power entering the adsorption machine is the sum of $\dot{Q}_{hot} + \dot{Q}_{sens,tot}$

$$\dot{Q}_{hot} + \dot{Q}_{sens,tot} = 6{,}5\ kW$$

The same quantity leaves the adsorption machine moving towards the dry cooler

3.4.4. Dry cooler

Thermal waste production ($\dot{Q}_{sens,tot} + \dot{Q}_{hot}$) belonging to the adsorption machine is transferred to the environment by the dry cooler. The inlet water temperature (t_{dc_in}) is 35 °C, the outlet water temperature (t_{dc_out}) is 30 °C, so the temperature difference (Δt_{dc}) is equal to 5 °C. By means of the energy balance the dry cooler flow rate results equal to:

$$\dot{m}_{dc} = \frac{\dot{Q}_{sens,tot} + \dot{Q}_{hot}}{c_{pw} \cdot \Delta t_{dc}} = 0{,}31\ \frac{kg}{s}$$

The total power entering the dry cooler is the sum of thermal power belonging to the adsorption machine ($\dot{Q}_{hot} + \dot{Q}_{sens,tot}$) plus the required grid electrical power (P_{el} = 700 W).

$$\dot{Q}_{hot} + \dot{Q}_{sens,tot} + P_{el} = 7{,}2\ kW$$

3.4.5. Thermal solar collectors and gas boiler

The optimum for thermal solar collector, according to dynamic simulation, is a 11,5 m^2 evacuated tube field. The related SF value has been set to 80%:

$$SF = \frac{Q_{coll}}{Q_{coll} + Q_{boiler}} = 0{,}8$$

Thermal power provided by heating devices (solar collectors (Q_{coll}) and boiler (Q_{boiler})) are:

$$\dot{Q}_{coll} = \dot{Q}_{hot} \cdot SF = 4\ kW \qquad \dot{Q}_{boiler} = \dot{Q}_{hot} \cdot (1 - SF) = 1\ kW$$

Referring to the technical specification provided by the manufacturer, the solar collector circulating water flow rate (m_{coll}) is 0,08 kg/s. The water temperature difference (Δt_{coll}) between collector inlet and outlet is:

$$\Delta t_{coll} = \frac{\dot{Q}_{coll}}{cp_w \cdot \dot{m}_{coll}} = 12{,}1\ °C$$

The solar collector energy efficiency is also provided by the manufacturer:

$$\eta_{sc} = 54{,}8\ \%$$

The thermal power delivered with the incident solar radiation ($\dot{Q}_{sun}$) is:

$$\dot{Q}_{sun} = \frac{\dot{Q}_{coll}}{\eta_{sc}} = 7{,}3\ kW$$

The water flow rate circulating inside the boiler ($\dot{m}_{boiler}$) can be calculated by means of the energy balance on the component. The temperature difference between water inlet and outlet (Δt_{boiler}) has been set to 5 °C

$$\dot{m}_{boiler} = \frac{\dot{Q}_{boiler}}{cp_w \cdot \Delta t_{boiler}} = 0{,}05\ \frac{kg}{s}$$

The thermal power provided by the fuel ($\dot{Q}_{fuel}$),assuming $\eta_{boiler} = 0{,}9$, is

$$\dot{Q}_{fuel} = \frac{\dot{Q}_{boiler}}{0{,}9} = 1{,}1\ kW$$

The thermal power produced by both solar collector and boiler is delivered to the heat storage tank by means of two heat exchangers. The temperature of the water, feeding the adsorption machine, inside the storage is equal to 85 °C.

3.4.6. Results of energy analysis

The global system thermal performance will be now calculated. Two different index will be used: the COP_{global} and the COP_{rnw}. Both of them are ratios between thermal energy entering into the system and the provided cooling effect but the former involves all the thermal energy (solar collector + boiler) while the latter (COP_{rnw}) is calculated without taking into account the thermal energy gathered from the sun, which is a renewable energy source.

$$COP_{rnw} = \frac{\dot{Q}_{sens,tot}}{\dot{Q}_{boiler}} = 1{,}5 \qquad COP_{global} = \frac{\dot{Q}_{sens,tot}}{\dot{Q}_{boiler} + \dot{Q}_{coll}} = 0{,}3$$

Results are summarized in Table 3-2 Energy analysis resultswhile Fig. 3-27 provides a graphic representation of the global energy balance.

Component	**Q_{in} [W]**	**Q_{out} [W]**	**Loss [W]**	**Loss [%]**	**Efficiency [%]**
Solar collectors	*7300*	*4000*	*3300*	*97*	*54,8*
Boiler	*1100*	*1000*	*100*	*3*	*90,0*
Heat storage	*5000*	*5000*	*0*	*0*	*100*
Dry cooler	*6500 + 700*	*7200*	*0*	*0*	*N.d.*
Adsorption machine	*1500*	*6500*	*0*	*0*	*COP = 0,3*
Fan coil	*1500*	*1500*	*0*	*0*	*100*
Total			*3400*	*100*	

Table 3-2 Energy analysis results

The fan coil and the hot storage have efficiency index equal to maximum achievable (100%) and the boiler a very high one (90%). From a *First Law* point of view it seems that the main inefficiencies in the system belong to the adsorption machine and to the solar collector.

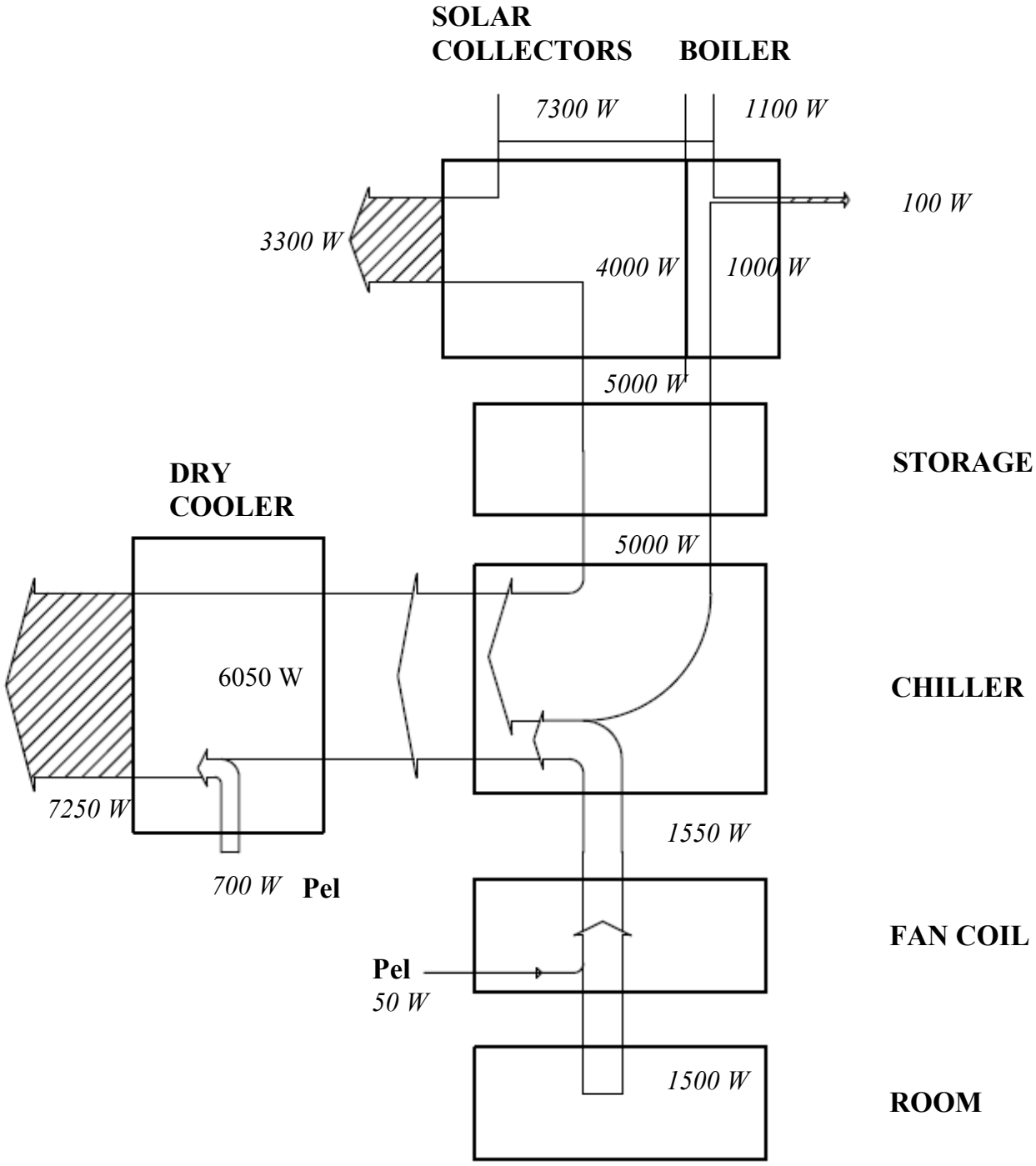

Fig. 3-27 Energy flow chart.

In the energy flow chart only two components are responsible of considerable losses (solar collector and dry cooler), while the others are apparently "ideal" (like the storage or the fan coil).

3.5.Exergy analysis

Now, the exergy analysis of the system will be carried out to point out the efficiency in exploiting the thermodynamic potential of energy sources referring to the final use. For each

component the irreversibility production will be calculated as the difference between the entering and exiting exergy flows, as stated by the Gouy - Stodola Theorem. The ratio between the same values gives the index of exergy efficiency.

3.5.1. Solar collectors

The exergy flow entering into this component is provided by the solar radiation and can be calculated by using the eq. (2.9):

$$E_{in\_SUN} = \frac{\dot{Q}_{coll}}{\eta_{SC}} \cdot \left(1 - \frac{T_E}{T_{plate}}\right) = 1{,}69\ kW$$

where T_{plate} is the average collector temperature and η_{SC} is the collector energy efficiency. The simulation results give T_{plate} = 393 K and η_{SC} = 0,55.

The inlet/outlet water flow rate exergy gain, which depends on the temperature difference, can be now calculated by using the eq. (2.18)

$$e_{coll\_in} = 96{,}9\ \frac{kJ}{kg} \qquad e_{coll\_out} = 106{,}6\ \frac{kJ}{kg}$$

The total exergy gain ($E_{out,coll}$) provided by the solar panel field is:

$$E_{out,coll} = \dot{m}_{coll} \cdot \left(e_{coll\_out} - e_{coll\_in}\right) = 0{,}77\ kW$$

The irreversibility production (I_{coll}) can be calculated as the difference between the inlet (E_{in_sun}) and the outlet ($E_{out,coll}$) exergy flow:

$$I_{coll} = E_{in\_SUN} - E_{out,coll} = 0{,}92\ kW$$

The exergy efficiency index ζ_{coll} is (see eq.2.16)

$$\zeta_{coll} = \frac{E_{out,coll}}{E_{in\_SUN}} = 45{,}5\ \%$$

3.5.2. Boiler

The exergy flow rate entering the boiler can be calculated by means of the eq. (2.9) but now the highest temperature is the flame temperature (T_F = *1500 K*) and the energy efficiency index is η_{BL} = *0,9*.

$$E_{in\_BL} = \frac{\dot{Q}_{boiler}}{\eta_{BL}} \cdot \left(1 - \frac{T_E}{T_F}\right) = 0{,}89\ kW$$

The inlet/outlet water flow rate exergy gain, which depends on the temperature difference, can be now calculated by means of eq. (2.18).

$$e_{boiler\_in} = 91{,}4\ \frac{kJ}{kg} \qquad e_{coiler\_out} = 96{,}9\ \frac{kJ}{kg}$$

The total exergy gain provided by the solar panel field is:

$$E_{out,BL} = \dot{m}_{boiler} \cdot \left(e_{boiler\_out} - e_{boiler\_in}\right) = 0{,}17\ kW$$

The irreversibility production (I_{boiler}) can be calculated as the difference between the inlet (E_{in_BL}) and the outlet (E_{out_BL}) exergy flow:

$$I_{boiler} = E_{in\_BL} - E_{out\_BL} = 0{,}72\ kW$$

The exergy efficiency index ζ_{boier} is see (2.16):

$$\zeta_{boiler} = \frac{E_{out\_BL}}{E_{in\_BL}} = 19{,}1\ \%$$

3.5.3. Heat storage

The heat storage does not play any role in the energy balance (from a First Principle point of view) under the steady state hypothesis: the entering energy flow equals the exiting one. But from a Second Principle point of view the thermal energy storing leads to inefficiency production related to the heat exchange.

The entering exergy flow ($E_{in,store}$) rate can be calculated as the sum of the exergy flows exiting from the solar panel field ($E_{out,coll}$) and from the boiler ($E_{out,BL}$):

$$E_{in,store} = E_{out,coll} + E_{out,BL} = 0{,}94\ kW$$

The exiting exergy flow rate feeds the adsorption machine and is related to the difference between the inlet and outlet chiller hot water temperature ($T_{hot,in}$ = 358 K e $T_{hot,out}$ = 353 K).

$$e_{ads\_in} = 90\ \frac{kJ}{kg} \qquad e_{ads\_out} = 87\ \frac{kJ}{kg}$$

The heat storage outlet exergy flow rate ($E_{out,store}$) is:

$$E_{out,store} = \dot{m}_{w,hot} \cdot \left(e_{ads\_in} - e_{ads\_out}\right) = 748\ W$$

The irreversibility production (I_{store}) is:

$$I_{store} = E_{out,store} - E_{in,store} = 197\ W$$

Now it is possible to calculate the storage exergy efficiency index (ζ_{store}):

$$\zeta_{acc} = \frac{E_{out,acc}}{E_{in,acc}} = 79{,}6\ \%$$

There isn't any transformation taking place inside the heat storage. All the irreversibility production is given by the heat transfer (that implies temperature difference) between the fluid circulating through the two heat exchangers and the hot water stored.

3.5.4. Dry cooler

The dry cooler transfers the heat rejection coming from the adsorption machine condenser to the external environment. The specific exergy flow exiting from this component can be calculated knowing inlet and outlet temperature (T_{dc_in} = *308 K,* T_{dc_out} = *303 K*):

$$e_{dc\_in} = 71{,}6\ \frac{kJ}{kg} \qquad e_{dc\_out} = 71{,}4\ \frac{kJ}{kg}$$

The total oulet exergy flow is:

$$E_{out,dc} = \dot{m}_{w,dc} \cdot \left(e_{dc\_in} - e_{dc\_out}\right) = 54\ W$$

This component uses electrical energy, which is pure exergy, to operate; so the total inlet exergy flow equals the electrical power consumption:

$$E_{in\_dc} = P_{el,dc} = 0{,}7\ kW$$

The irreversibility production is:

$$I_{dc} = E_{out,dc} - E_{in,dc} = 646\ W$$

The dry cooler exergy efficiency index (ζ_{dc}) is:

$$\zeta_{dc} = \frac{E_{out,dc}}{E_{in,dc}} = 7{,}7\ \%$$

The irreversibility production belonging to this component is very high due to the high quantity of electrical energy (= pure exergy) needed to operate.

3.5.5. Fan coil

The Fan Coil operates the heat exchange between the cold water flow rate $\dot{m}_{w,fc}$, which has been cooled down at the temperature $t_{fc,in}$ = 13 °C by the adsorption machine, and the room air, whose temperature is equal to 26°C. The outlet temperature of the water exiting from the

fan coil is $t_{fc,out}$ = 18°C, and this temperature gap is one of the two exergy flows which fuel this component. The other one is the electric power needed to operate ($P_{el,fc}$ = *50 W*).
The inlet and outlet water specific exergy contents are:

$$e_{fc\_in} = 73{,}4\ \frac{kJ}{kg} \qquad e_{fc\_out} = 72{,}4\ \frac{kJ}{kg}$$

The total inlet exergy flow is:

$$E_{in\_FC} = \dot{m}_{w,fc} \cdot \left(e_{fc\_in} - e_{fc\_out}\right) + P_{el,fc} = 76 + 50 = 126\ W$$

The outlet exergy flow can be calculated taking into account the fan coil inlet and outlet air temperature difference and the air flow rate. These data allow to calculate the sensible thermal load covered, which is the exergy flow rate exiting from the fan coil. The room air and the fan coil outlet air specific exergy contents can be calculated by using the eq. (2.17) referring to these quantities:
Room air temperaure (t_A) = *26 °C,* fan coil outlet air temperature *(t_I) = 17,4 °C,* Room air and fan coil outlet air humidity ratio *($x_A = x_I$) = 10,5 g/kg.*

$$e_A = 0{,}5\ \frac{kJ}{kg} \qquad e_I = 0{,}87\ \frac{kJ}{kg}$$

$$E_{out\_FC} = \dot{m}_{a,fc} \cdot \left(e_I - e_A\right) = 74\ W$$

Where:

- e_A is the room air specific exergy content;
- e_I is the fan coil outlet air specific exergy content;
- $\dot{m}_{a,fc}$ is the air flow rate;
- E_{out_FC} is the fan coil outlet exergy flow rate.

The irreversibility production is:

$$I_{FC} = E_{in\_FC} - E_{out\_FC} = 52\ W$$

The fan coil exergy efficiency index (ζ_{fc}) is:

$$\zeta_{Fan\ Coil} = \frac{E_{out\_FC}}{E_{in\_FC}} = 58{,}7\ \%$$

3.5.6. Adsorption machine

The adsorption machine is fuelled by two different exergy flows. The first one is the hot water flow rate exiting from the heat storage, which is equal to:

$$E_{out,store} = \dot{m}_{w,hot} \cdot \left(e_{ads\_in} - e_{ads\_out}\right) = 748\ W$$

The second one is the exergy flow rate exiting from the dry cooler.

$$E_{out,dc} = 54\ W$$

The total exergy flow rate fuelling the adsorption machine is:

$$E_{in\_ads} = E_{out,store} + E_{out,dc} = 802\ W$$

The exergy outlet flow rate is the cold water which fuels the fan coil. This flow rate has been calculated and is equal to:

$$E_{out,ADS} = E_{in\_FC} = 76\ W$$

The irreversibility production, which can be calculated as the difference between inlet and outlet exergy flow rate, is:

$$I_{ADS} = E_{in\_ADS} - E_{out\_ADS} = 726\ W$$

The adsorption machine exergy efficiency index (ζ_{ADS}) is:

$$\zeta_{ADS} = \frac{E_{out\_ADS}}{E_{in\_ADS}} = 9{,}5\ \%$$

3.5.7. Results of exergy analysis

The results of the exergy analysis are summarized in Table 3-3, while Fig. 3-28 can be used to make a comparison between the system's components exergy consumption.
Fig. 3-29 gives an outlook on irreversibility production.

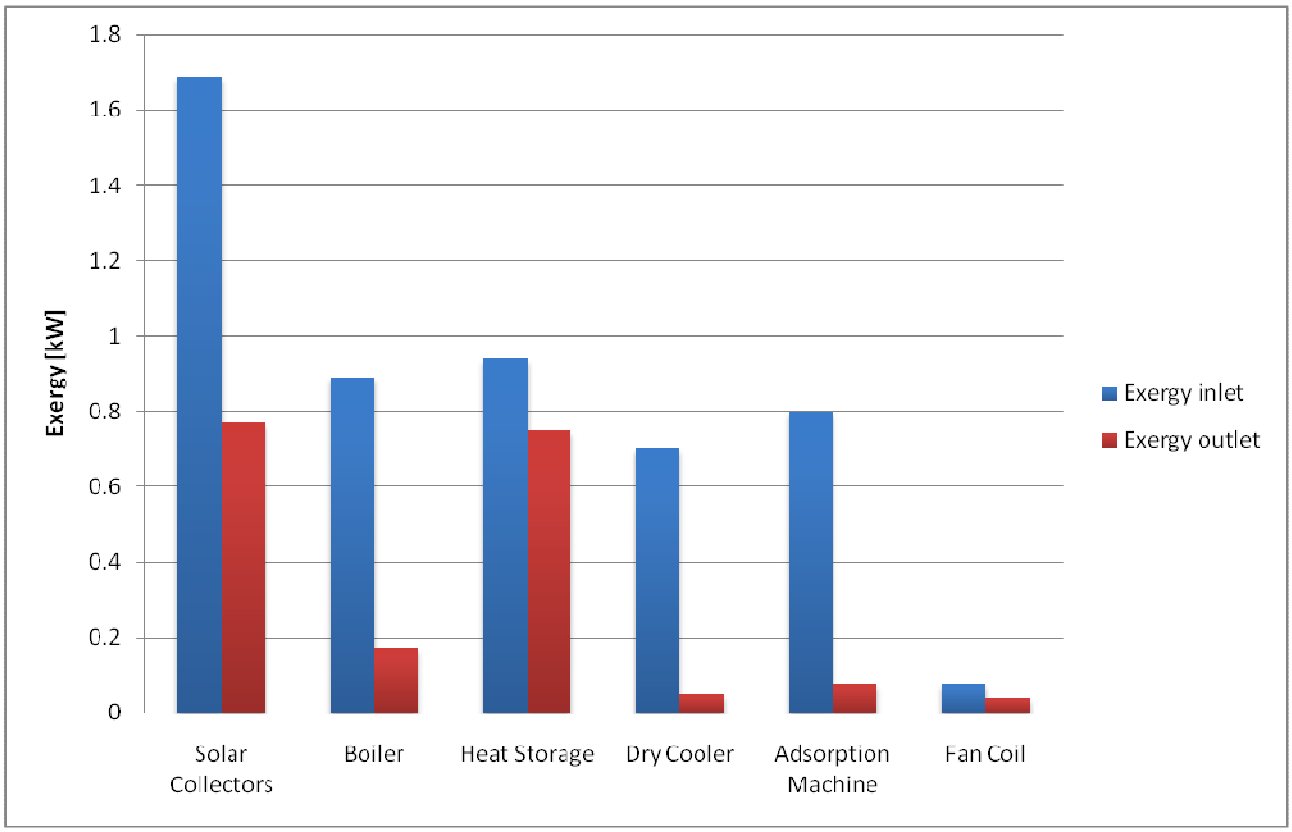

Fig. 3-28 Components inlet and outlet exergy flow rates.

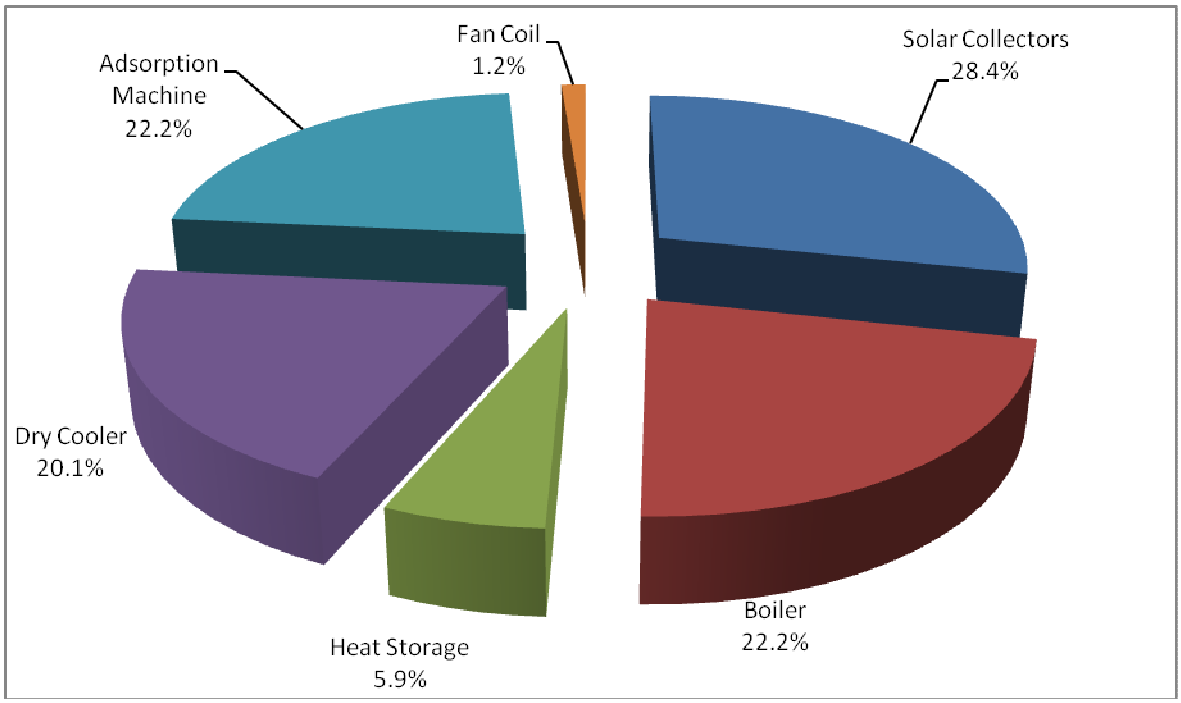

Fig. 3-29 Components irreversibility production.

Component	E_{in} [W]	E_{out} [W]	Irreversibility [W]	Irreversibility [%]	Efficiency [%]
Solar collectors	*1695*	*775*	*920*	*28,21*	*45,72*
Boiler	*890*	*170*	*720*	*22,08*	*19,10*
Heat storage	*945*	*748*	*197*	*6,04*	*79,15*
Dry cooler	*700*	*54*	*646*	*19,81*	*7,71*
Adsorption machine	*748 + 50*	*76*	*726*	*22,26*	*9,5*
Fan coil	*76+50*	*74*	*52*	*1,59*	*58,73*
Total			*3261*	*100*	

Table 3-3 Exergy analysis results.

Looking at the exergy efficiency data, reported in Table 3-3 it is clearly evident that the most critical system components are the dry-cooler, the adsorption machine and the boiler, even if the energy efficiency data is very high for both the hot storage and the boiler (see table 3). For what concerns the dry-cooler, the inefficiency is related to the huge electrical energy (made up of pure exergy) consumption required for lowering the temperature of the cooling water. The losses caused by the adsorption machine are related to its low energy efficiency (COP = 0,3) and to the relatively high water temperature fueling the machine (85 °C). The gas boiler behaves similarly to the adsorption chiller: the maximum temperature reached inside this component is 1200 °C (flame temperature), but is used to produce hot water at only 85 °C. The big gap between these two temperatures leads to a low exergy efficiency value.

Main suggestions to raise the global exergy efficiency are:

- An adsorption chiller able to work with water temperature as low as possible and with a better energy efficiency (higher COP)
- The dry-cooler needs huge amounts of electrical energy to work. An evaporative cooler could reduce electrical consumption.
- The Solar Fraction could be increased to reduce the request of hot water from the boiler. If possible thermal energy waste (generally at low temperature) should be used.

The following figure provides a graphic representation of the global exergy balance:

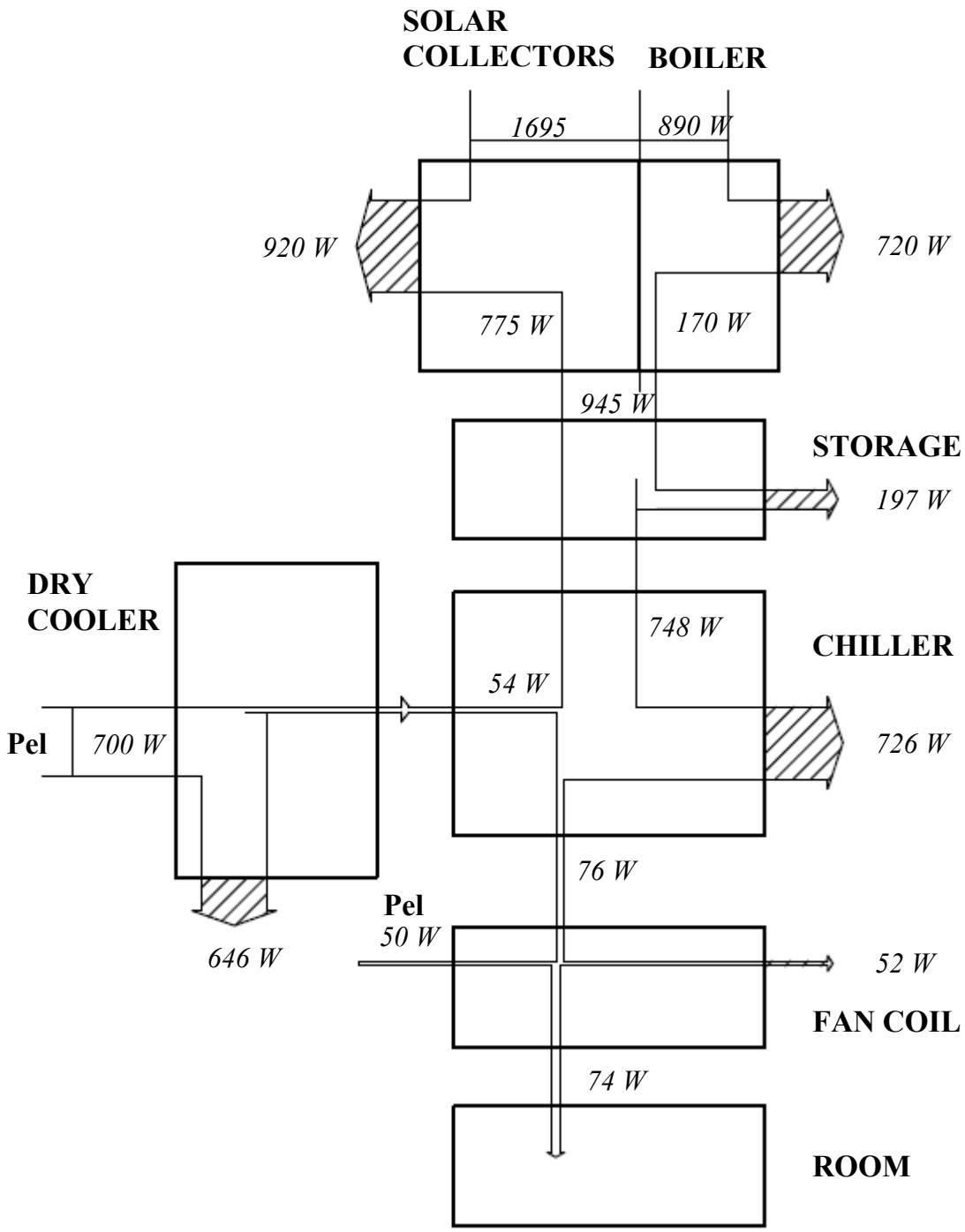

Fig. 3-30 Exergy flow chart.

In the energy flow chart (see Fig. 3-30) there are only two components producing considerable losses (solar collector and dry cooler), while the others are not responsible or even "ideal" (like the storage or the fan coil). In the exergy flow chart all components are responsible of entropy production (which means exergy losses) and the exergy flows proceed from top (solar collector and boiler) to bottom (room) highlighting the different role of "fuel" and "product" for everyone of them.

3.5.8. Global exergy efficiency indexes

The global efficiency indexes of the whole system will now be assessed. These are as follows

- the system exergy efficiency (ζ_{SC});
- the system exergy efficiency without taking into account the solar energy contribution (ζ'_{SC});
- the Primary Energy Ratio (*PER*);
- the Specific Irreversibility Production (*SPIR*).

Looking at the whole system, it is possible to assess the global exergy efficiency referring to the following entering exergy flow rates:

- E_{in_SUN}: the exergy flow rate related to the solar energy;
- E_{in_BL}: the exergy flow rate related to the boiler fuel consumption;
- E_{in_DC}: the exergy flow rate related to the dry cooler electric power consumption;

The system has only one outlet exergy flow, which is related to the thermal sensible load covered:

$$E_{out\_FC} = 74\ W$$

The whole system exergy efficiency index is:

$$\zeta_{SC} = \frac{E_{out\_FC}}{E_{in\_SUN} + E_{in\_BL} + E_{in\_DC}} = 1{,}2\ \%$$

While the whole system exergy efficiency, without taking into account the solar energy contribution is:

$$\zeta'_{SC} = \frac{E_{out\_FC}}{E_{in\_BL} + E_{in\_DC}} = 2{,}5\ \%$$

To assess the *PER* index the boiler and the electrical Primary Energy consumptions are needed.

The boiler Primary Energy consumption (PE_{BL}) is related to the thermal power ($\dot{Q}_{boiler}$) and to the boiler energy efficiency index (η_{BL}):

$$PE_{BL} = \frac{\dot{Q}_{boiler}}{\eta_{BL}} = 1{,}1\ kW$$

The electrical Primary Energy consumption (PE_{Pel}) can be assessed referring to the system electrical power consumption and to the electrical power grid efficiency index ($\eta_{EL} = 0{,}37$):

$$PE_{Pel} = \frac{P_{el}}{\eta_{EL}} = 1{,}9\ kW$$

So the total Primary Energy entering into the system is:

$$PE_{in} = PE_{BL} + PE_{Pel} = 3\ kW$$

The *PER* is equal to the ratio of the sensible thermal load covered, which is the system goal, to the PE_{in}:

$$PER = \frac{\dot{Q}_{sens,tot}}{PE_{in}} = 50\ \%$$

The Specific Irreversibility Production, which can be used to make a comparison between different HVAC system, can be assessed as the ratio of the total system irreversibility production to the thermal load covered:

$$SPIR = \frac{I_{coll} + I_{boiler} + I_{store} + I_{FC} + I_{ADS}}{\dot{Q}_{sens,tot}} = 2{,}13$$

3.6.Comparison with a conventional HVAC system

It is useful to compare the solar cooling design considered so far with a conventional HVAC system in a Second Law perspective. Fig. 3-31 shows the system and the psychrometric process:

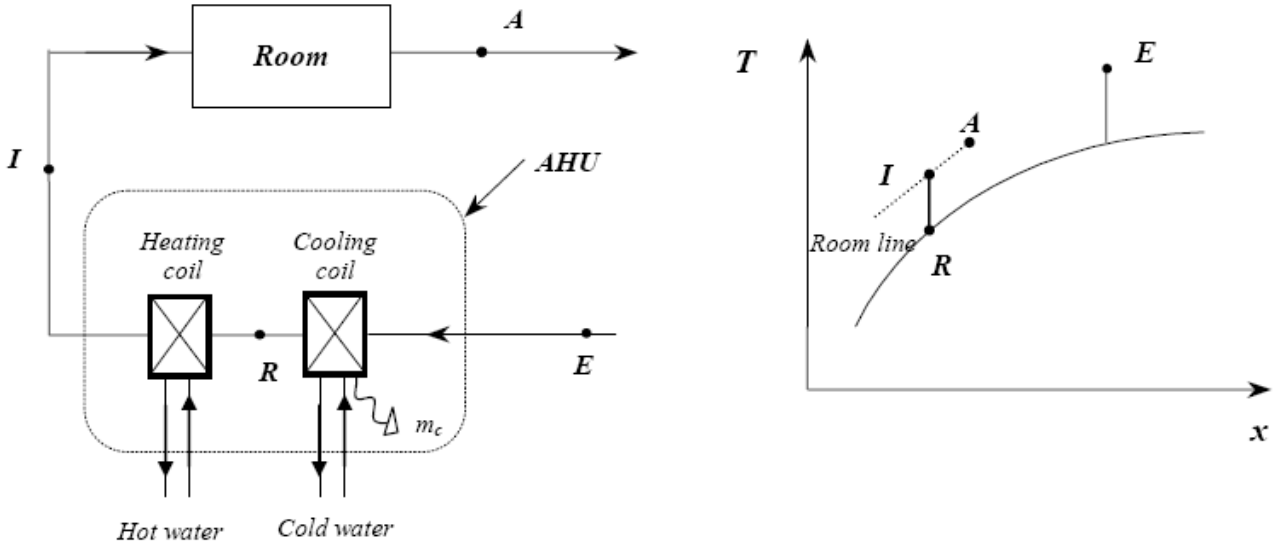

Fig. 3-31 System layout and psychrometric process.

It is an all air system (i.e. without air recirculation), where the sensible (*QS*) to total load (*QT*) ratio is taken to be *R*=*Qs*/*QT*= 0.75. Under this assumption, suitable inlet conditions are those

of state (I). The air mass flow rate is assumed to be m_a=1 kg/s. The cold water feeding the heating coil is produced by a boiler while the cold water feeding the cooling coil is produced by a conventional electric heat pump.

Referring to the psychrometric chart in Fig. 3-31 the air temperature, humidity, and specific exergy content are summarized in the following table:

	t [°C]	x [g/kg]	e [kJ/kg]
A	*26*	*10,5*	*0,61*
E	*35*	*21,4*	*0*
I	*18,5*	*9,5*	*1,05*
R	*13,3*	*9,5*	*1,4*

Table 3-4 Psychrometric air condition.

The PER can be assessed taking into account the total PE consumption and the thermal load covered by the system.

The total PE consumption is given by the sum of the PE fuelling the cooling machine (EP_{CL} = *50,79 kW*) and the PE fuelling the boiler (EP_{BL} = *5,88 kW*):

$$EP_{in} = EP_{CL} + EP_{BL} = 56{,}67\ kW$$

The thermal load covered is equal to:

$$\dot{Q}_{tot} = 10{,}2\ kW$$

The PER can now be assessed:

$$PER = \frac{\dot{Q}_{tot}}{PE_{in}} = 17{,}9\ \%$$

To evaluate the system exergy performance, the global exergy efficiency index has been calculated.

The exergy inlet flow rate (E_{in}) is given by the sum of the exergy flow rate entering the chiller (E_{in_CL} = *53.83 kW*) and the exergy flow rate entering the boiler (E_{in_BL} = *6.47 kW*).

The total exergy flow rate entering the system is:

$$E_i = E_{in\_CL} + E_{in\_BL} = 60{,}3\ kW$$

The exergy outlet flow rate (E_{out}) refers to the air psychrometric process. It can be assessed taking into account the outside air (e_E) and the inlet room air specific exergy contents (e_I)

$$E_{out} = \dot{m}_a \cdot (e_I - e_E) = 1{,}05\ kW$$

The conventional system exergy efficiency index can now be calculated:

$$\zeta_{conv} = \frac{E_{out}}{E_{in}} = 1{,}74\ \%$$

Table 3-5 summarizes the system irreversibility production. These data are needed to calculate the SPIR.

Component	Irreversibility [kW]	Irreversibility [%]
Boiler	*6,15*	*10*
Chiller	*49,29*	*82*
Cooling coil	*2,25*	*4*
Heating coil	*0,67*	*1*
Condensate	*0,9*	*2*
Air discharge	*0,61*	*1*
Total	*59,87*	*100*

Table 3-5 System irreversibility production.

The conventional system SPIR can now be assessed:

$$SPIR_{conv} = \frac{I_{tot}}{\dot{Q}_{tot}} = \frac{59{,}87}{10{,}2} = 5{,}87$$

Table 3-6 gives an outlook on the results of the comparison:

	Solar cooling system	Conventional system
PER	*50 %*	*17,9 %*
ζ	*2,5 %*	*1,74 %*
SPIR	*2,13*	*5,87*

Table 3-6 Solar cooling system vs. Conventional system..

The Solar cooling system can achieve better performance than the Conventional system, whose exergy efficiency index (1,74 %) is affected from the electric heat pump behaviour, responsible for the 82 % of total irreversibility production.

The solar energy contribution reduces the total amount of PE needed to the system to work, and results in a better PER (PER_{SC} = 50 %; PER_{Con} = 17,9 %).

Looking at the two exergy efficiency index (ζ_{Con} = *1,74 %,* ζ_{SC} = *2,5 %*) it is possible to state that the SC system can exploit the thermodynamic potential of the energy sources in a better way than the conventional system.

3.7.Parametric and sensitivity analysis

Starting from the mathematical model of the system, a parametric analysis was made in order to put in evidence how the most significant figures of merit react to deviation of the design parameters from their nominal values. Once again the investigation involved the following data:

- The global exergy efficiency: ζ_{SC}
- The global exergy efficiency excluding thermal power provided by solar collector: ζ'_{SC}
- The Primary Energy Ratio: *PER*
- The Specific Irreversibility Production: *SPIR*

The design parameters chosen as independent variables are the Solar Fraction, which is related to the solar field area, and the machine COP, which is related to the chiller performance.

The SF values range from SF = 0,225 to SF = 0.375.
The COP values range from COP = 0,725 to COP = 0,9.
Results are shown in Fig. 3-32, 3-33, 3-34 and 3-35.

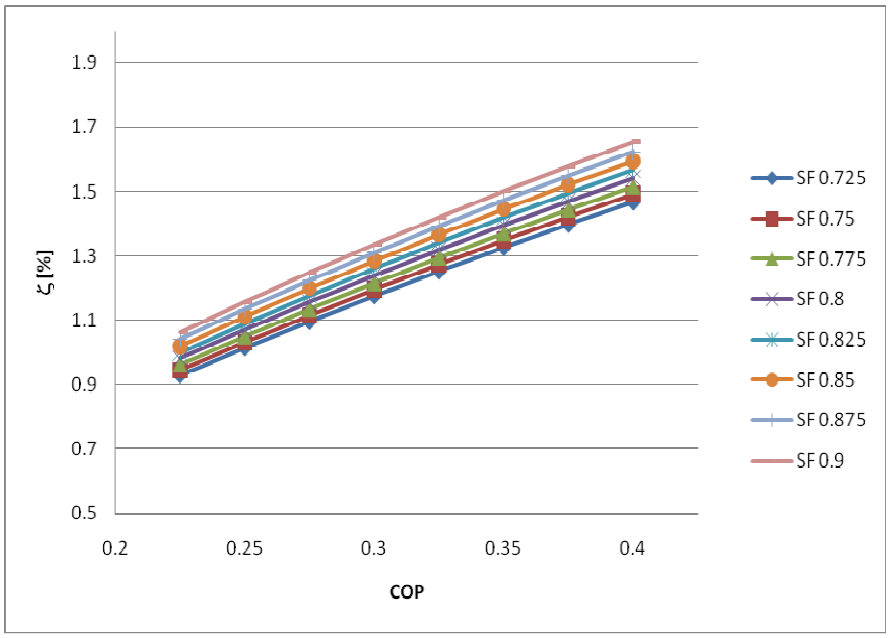

Fig. 3-32 ζ_{SC} vs. COP for different SF values

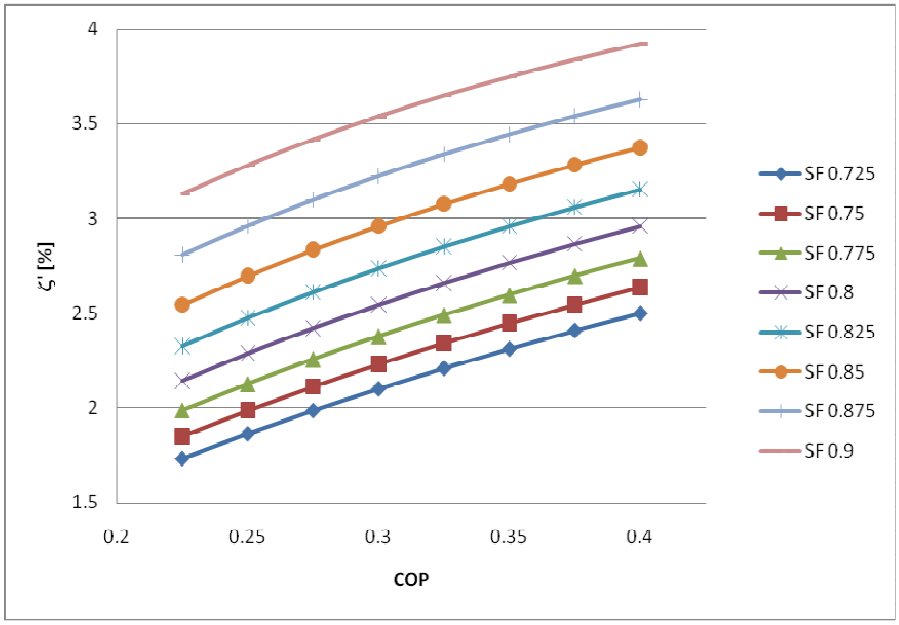

Fig. 3-33 ζ'_{SC} vs. COP for different SF values

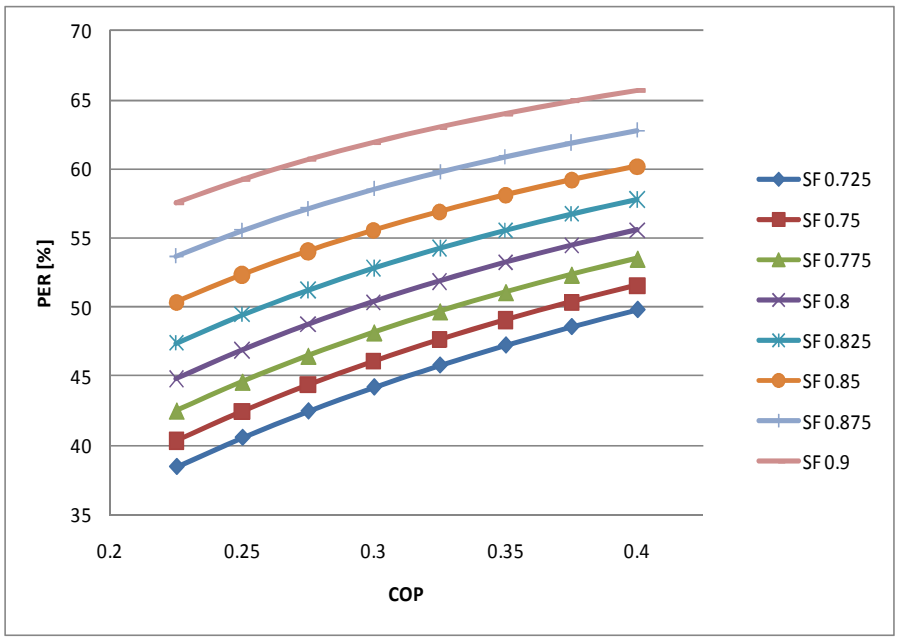

Fig. 3-34 PER vs. COP for different SF values

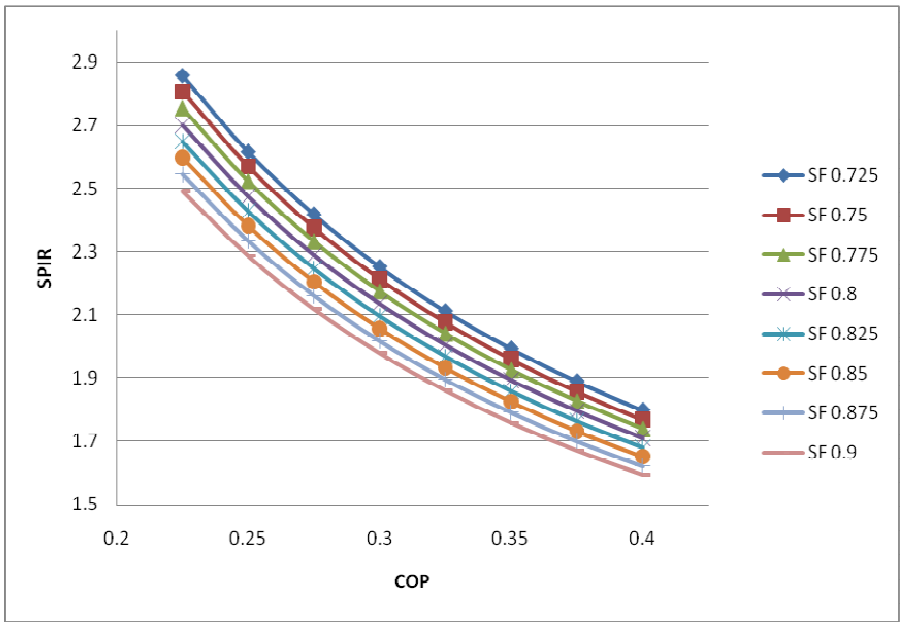

Fig. 3-35 SPIR vs. COP for different SF values.

The graphs show that increasing the COP or the SF improves the system performance and reduces the irreversibility production. Fig. 3-32 shows that rising the SF would result in an improvement of the system exergy efficiency but the same result can be easily achieved by choosing a chiller with an higher COP. The SPIR (which is strictly related to the exergy efficiency) behaviour is very similar to what is shown in Fig. 3-32. The SF has a great impact on the ζ' and on the PER, as can be seen from Fig. 3-33 and Fig. 3-34, while rising the machine COP has a lower effect on PER and SPIR.

Starting from these results, the sensitivity analysis was carried out.

The Sensitivity Analysis is a technique used to determine how different values of an independent variable (x) will impact on a particular dependent (y) variable under a given set of assumptions.

The *sensitivity coefficient* $\sigma_{x,y}$ is defined for each variable of interest, x_0 and y_0 values refer to the nominal system condition:

$$\sigma_{x,y} = \frac{\frac{\Delta y}{y_o}}{\frac{\Delta x}{x_o}} = \frac{x_o}{y_o} \cdot \frac{\Delta y}{\Delta x}$$

This coefficient can assume both positive and negative values. If positive, x and y changes are in the same direction (increasing x would result in a higher y), while with a negative value if x is increased the system will react reducing y. A higher absolute value of the sensitivity coefficient means a higher impact of Δx on Δy. The following figures show how COP and SF modify the main system figures of merit.

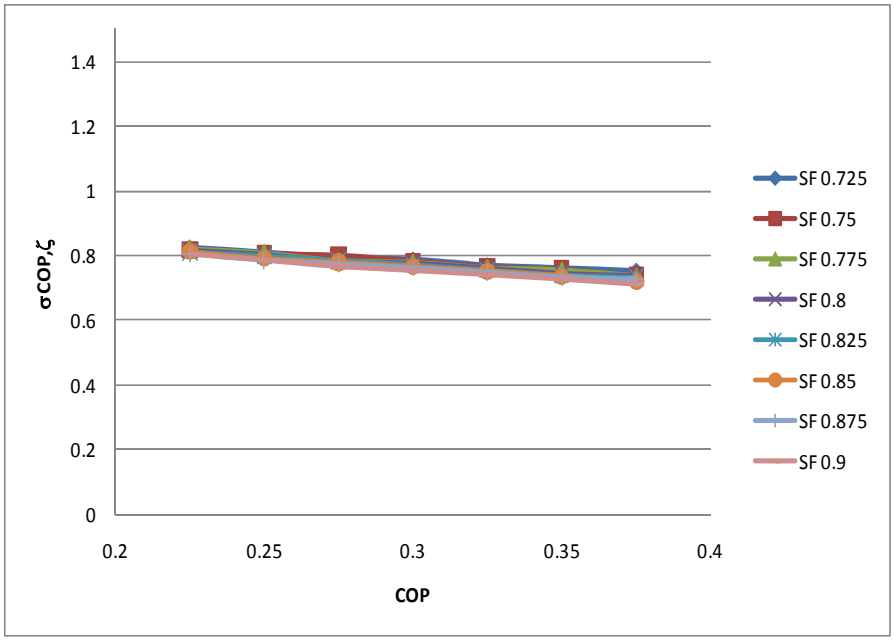

Fig. 3-36 Sensitivity analysis of COP impact on ζ_{SC}

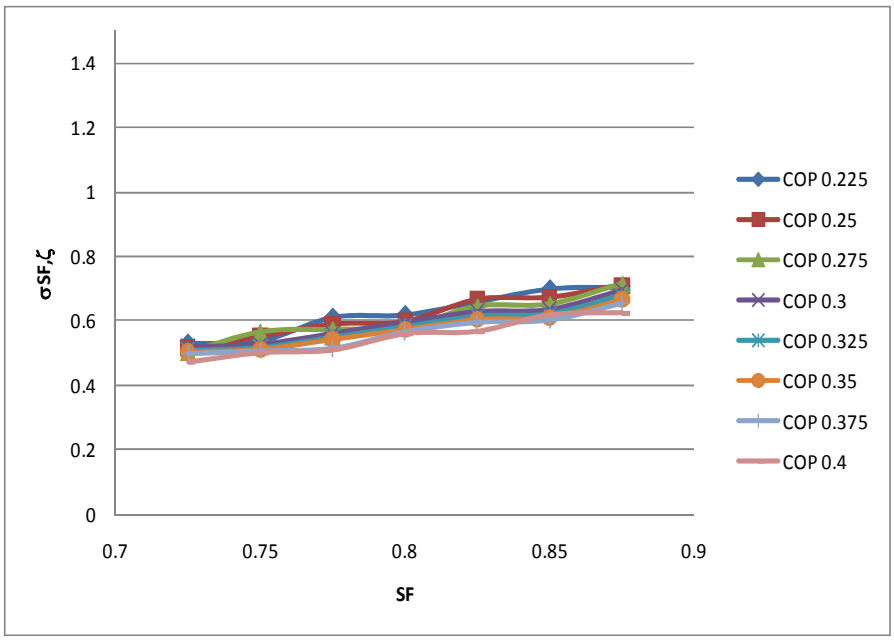

Fig. 3-37 Sensitivity analysis of SF impact on ζ_{SC}

Fig. 3-36 shows that the ζ_{SC} value reacts similarly to changing in COP values for the entire range of variation (0.225 – 0.375). The curve slope is slightly negative and this indicates that changes for higher COP values are less effective than changes for lower values.

For what concerns the SF impact on the system exergy efficiency, the graph in Fig. 3-37 shows an higher curve slope but a maximum value lower than the one reached by the COP curve. Best results, with reference to ζ_{SC} rising, are achieved when improving the SF at higher values (>0.85), while, for system starting whit lower SF values, improving the COP value would be more effective.

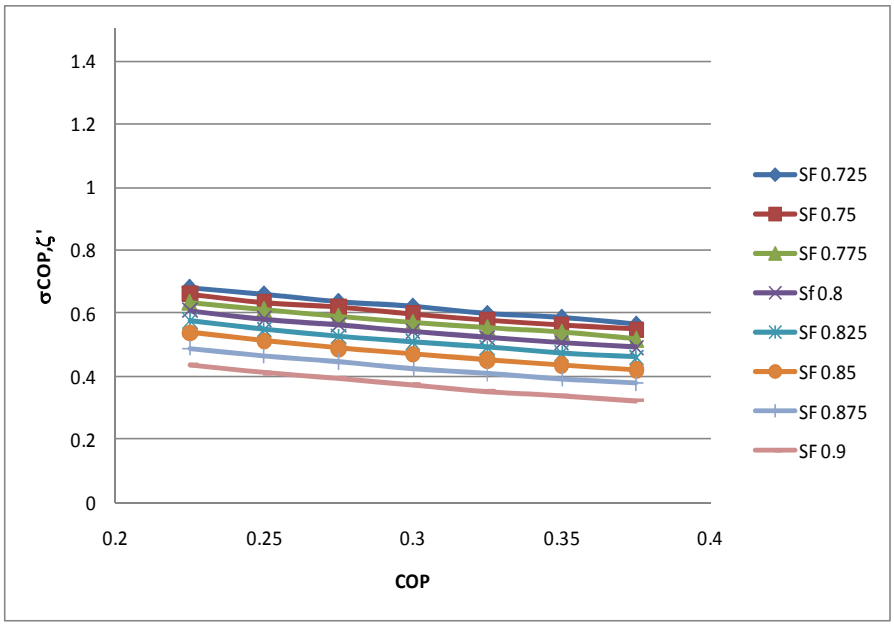

Fig. 3-38 Sensitivity analysis of COP impact on ζ_{SC}'.

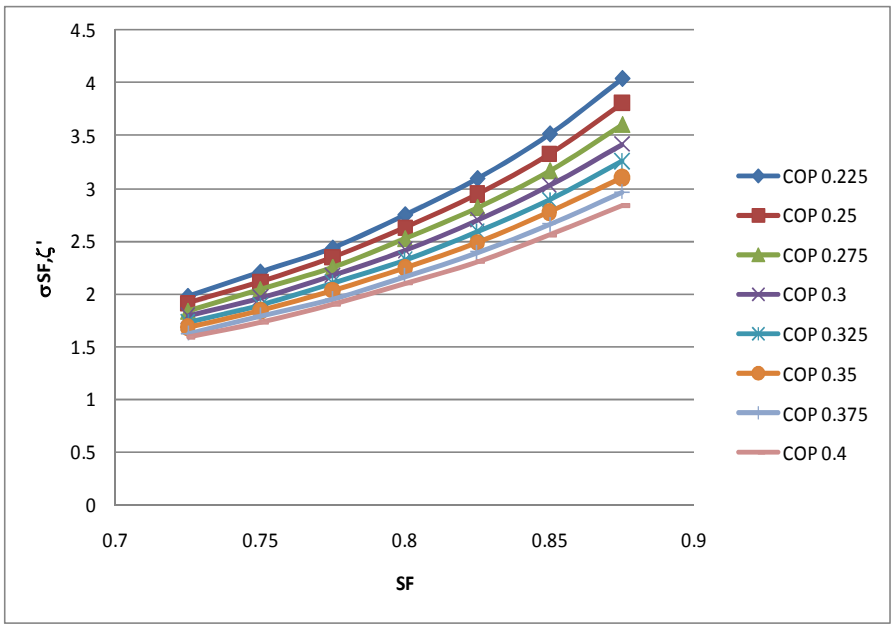

Fig. 3-39 Sensitivity analysis of SF impact on ζ_{SC}'

Fig. 3-38 and Fig. 3-39 show that the ζ_{SC}' index reacts differently to changes in COP and SF values, for what concerns both the curves slope and the maximum values reached. Changing in the COP would be less effective than SF changes, especially when the system is characterized by an high SF value, as the pink curve indicates in the graph on the left. Improvements in the SF would be more effective for any combination of SF and COP, even for the worst one (SF = 0.725; COP = 0.4; $\sigma_{SF,\zeta'}$ = 1.58)

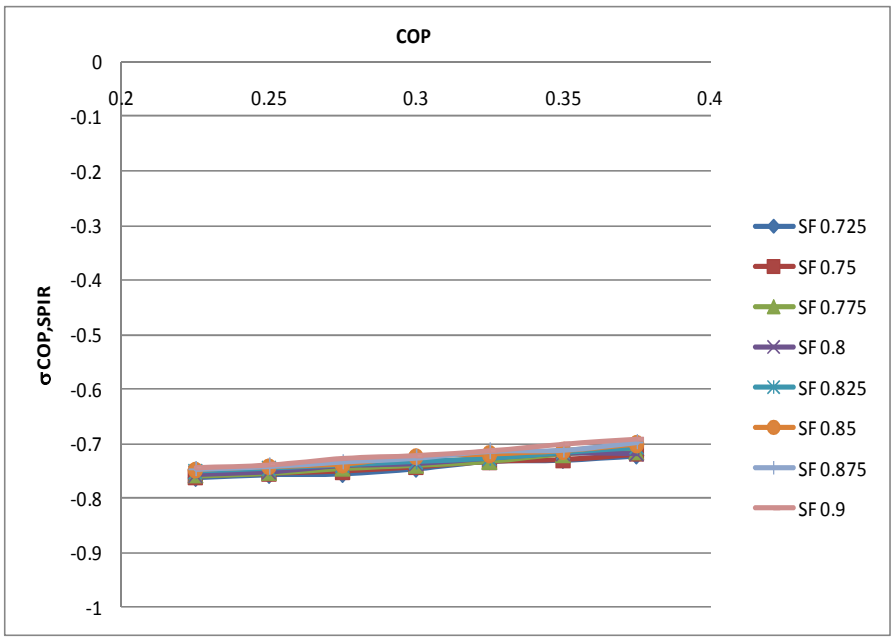

Fig. 3-40 Sensitivity analysis of COP impact on SPIR.

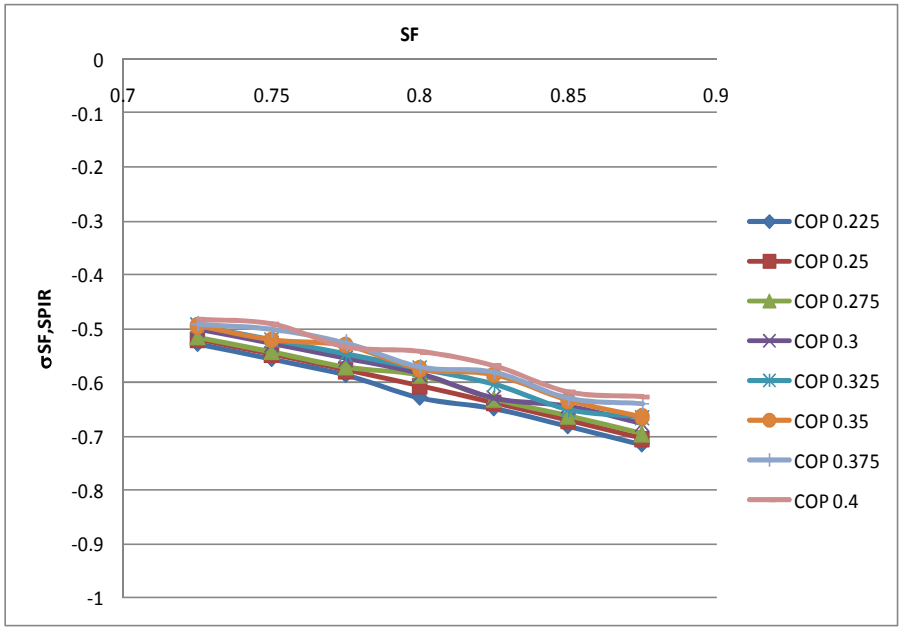

Fig. 3-41 Sensitivity analysis of SF impact on SPIR.

Fig. 3-40 and Fig. 3-41 show the impact of COP and SF changes on SPIR. Rising the COP would be the right choice to lower the irreversibility production for every combination of COP and SF values, while increasing the SF would be effective only if the starting SF value is quite high (>0.8) and if it is combined with a low COP chiller. For the lower starting SF values and high COP values combination (SF = 0.725; COP = 0.4) the absolute value of the SPIR sensitivity to SF change is lower (0.48) than the corresponding one to COP change (COP = 0.372; SF = 0.725; $\sigma_{COP,SPIR} = 0.72$).

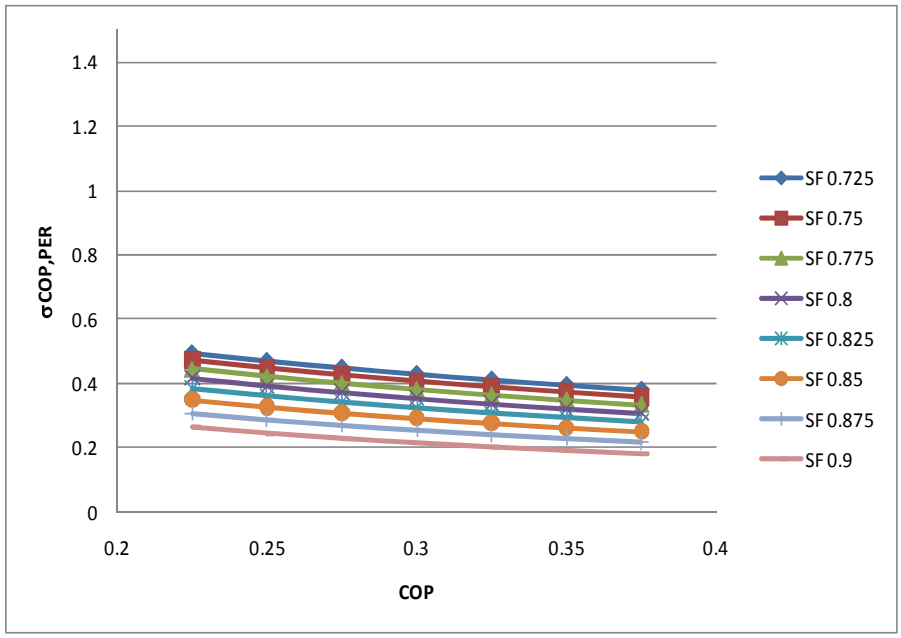

Fig. 3-42 Sensitivity analysis of COP impact on PER.

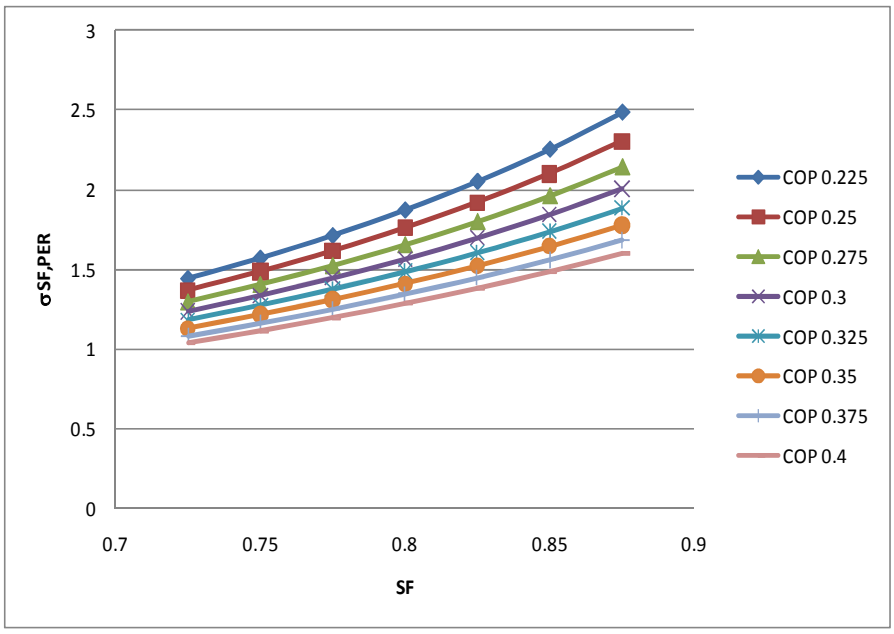

Fig. 3-43 Sensitivity analysis of SF impact on PER.

As shown in Fig. 3-43, the PER and the ζ' sensitivity (see Fig. 3-39) to COP and SF variation are very similar. Both ζ' and the PE consumption (strictly related to the PER) depend firstly on the total solar energy exploiting which is expressed by the SF. Increasing the total solar energy gathered by the collector field would reduce the PE consumption and rise the ζ' and would be more effective than rising the chiller COP even for the worst one (SF = 0.725; COP = 0.4; $\sigma_{SF,PER}$ = 1.04)

4. USE OF A DESICCANT WHEEL IN HVAC SYSTEM

This chapter is intended to present the design and the analysis of an air conditioning system based on a desiccant rotor from a Second Law point of view. Before performing the analysis the wheel performance will be characterized to make MathCAD able to handle it. On the basis of the results coming from the Second Law analysis, the sensitivity analysis will be carried out to investigate how the system reacts to boundary conditions changes.

4.1.Desiccant systems

The current technology makes available many alternatives to the conventional HVAC (Heating, Ventilation and Air Conditioning) plant scheme. In recent times the scientific

community is considering the possibility of integrating desiccant wheels into the air-handling unit for a complete treatment of the humid air streams.

Desiccant dehumidifiers remove moisture from air but so without cooling the air below its dew point. Instead, they rely on the ability of hygroscopic materials (a desiccant such as silica) to adsorb water onto their surfaces. In the process of adsorption, a thin layer of molecules of one substance (usually a liquid or a gas) adheres to the surface of another substance (usually a liquid of a solid). In the case of a desiccant dehumidifier, water vapour from a process stream of moist air adsorbs onto the surface of a desiccant material. Eventually the desiccant material becomes saturated with water and must be regenerated through a drying process. There are two common configurations of desiccant dehumidifier. In the first, process air flows over a bed of desiccant until the desiccant becomes saturated. Periodically, regeneration air is passed across the bed to dry the desiccant, allowing it to then adsorb more water from the process stream. In the other configuration, the process and regeneration air streams operate at the same time and a wheel of desiccant material rotates between the streams. At any given time, a portion of the desiccant is being regenerated while the remainder is adsorbing water from the process stream. Often, the regeneration air comes from the same source as the process air and is heated to lower its relative humidity. Consequently the desiccant dehumidifier requires only a source of heat to dehumidify the process air stream.

For the regeneration process is required an air flow at the temperature of at least 70 °C.

4.2.System layout

A typical DEC system layout is shown in Fig. 4-1, in the desiccant wheel, the external air absolute humidity is reduced by the adsorption materials (1). During this process, the air flow temperature raises before the pre-cooling stage that takes place in a conventional rotary heat exchanger (HEX) (2) without adsorbent material covering. The needed cooling power is supplied by the resumption air that passes on the other side of the recovery wheel (7) after having been cooled by an adiabatic humidification process (6). Now the external air, that has been dehumidificated by the desiccant wheel and pre-cooled by the recovery wheel, is humidified up to the desired value (3) and finally cooled. The resumption air is heated by a heating coil (8) in order to regenerate the desiccant wheel and, after being enriched of water vapour, expelled outside.

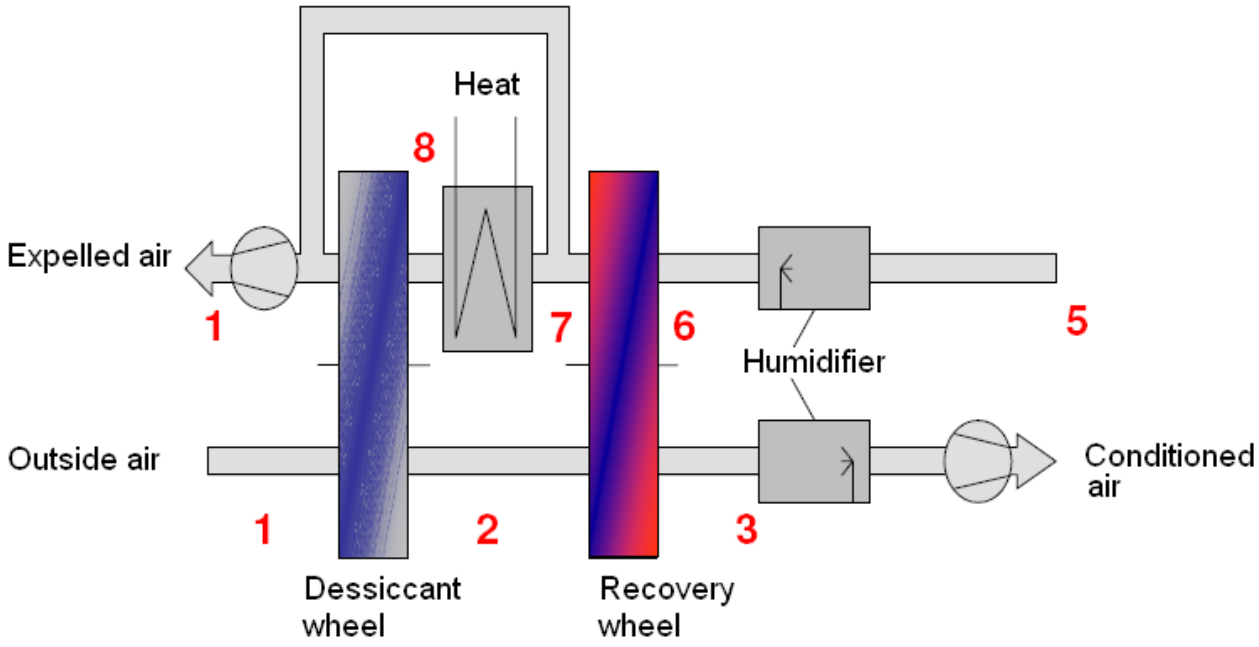

Fig. 4-1 DEC plant layout.

This system plant layout can not be used in warm and humid climates like the mediterranean one. Consequently, the plant scheme has to be modified by adding two cooling coils as shown in Fig. 4-2, while Fig. 4-3 shows transformation on the pshychrometric chart.

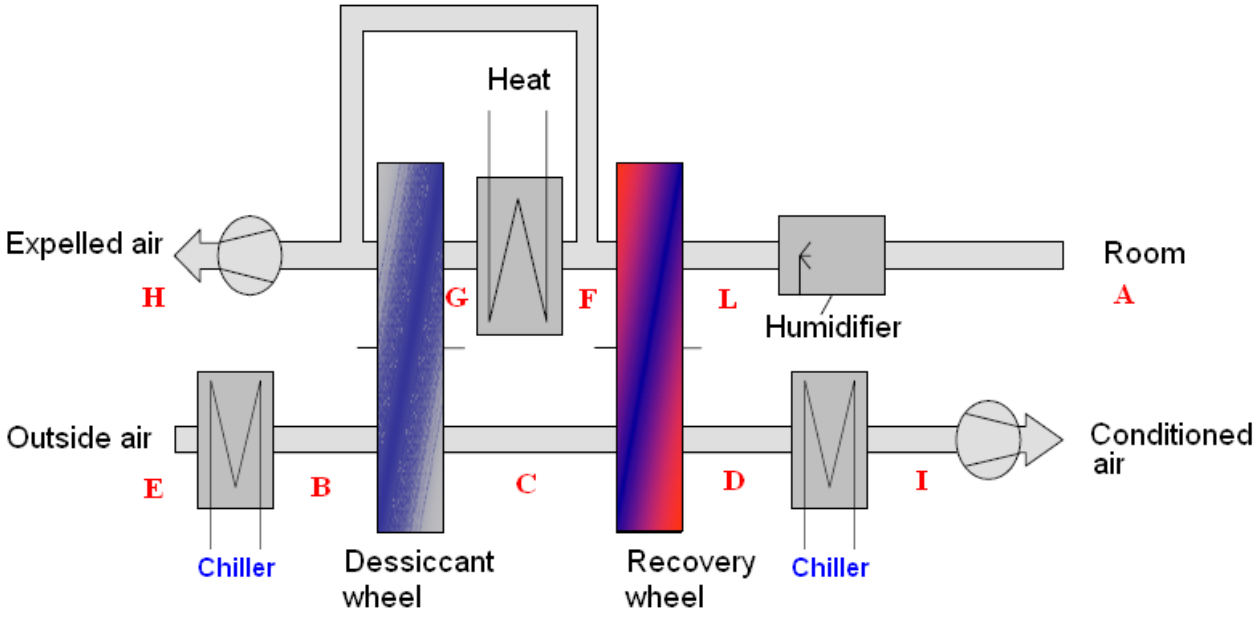

Fig. 4-2 DEC plant layout with pre and post cooling coils.

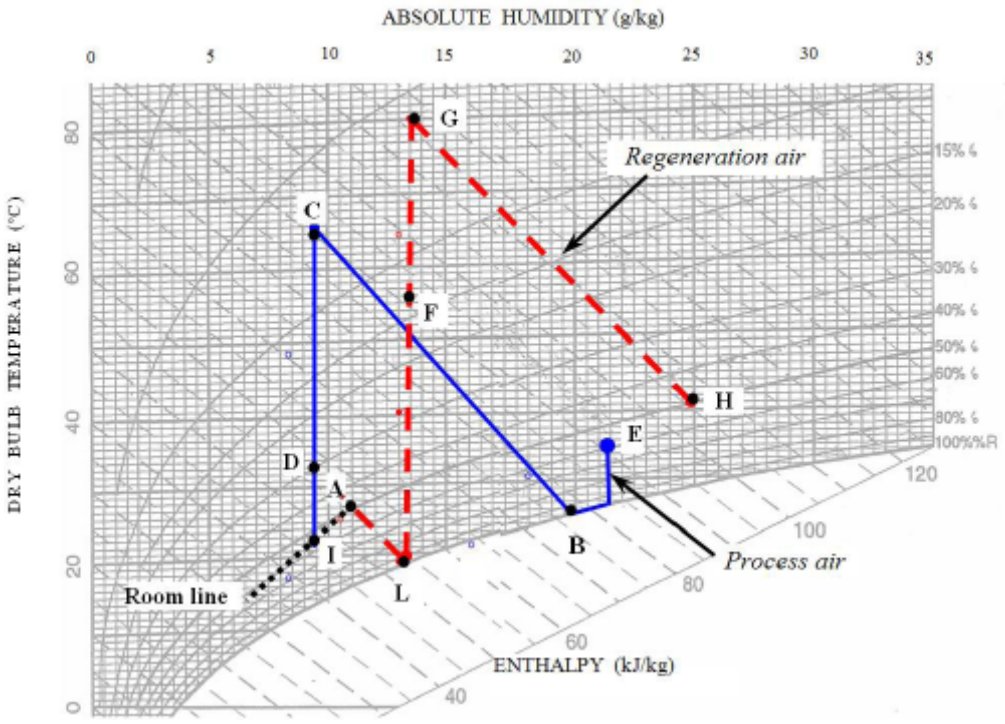

Fig. 4-3 DEC system psychrometric processes.

4.3.Desiccant wheel characterization

A mathematical model of the wheel is needed in order to make MathCAD able to handle this component. The manufacturer provides the rotor performance charts, which allow the user to predict the outlet wheel air condition. A typical chart is shown in Fig. 4-4.

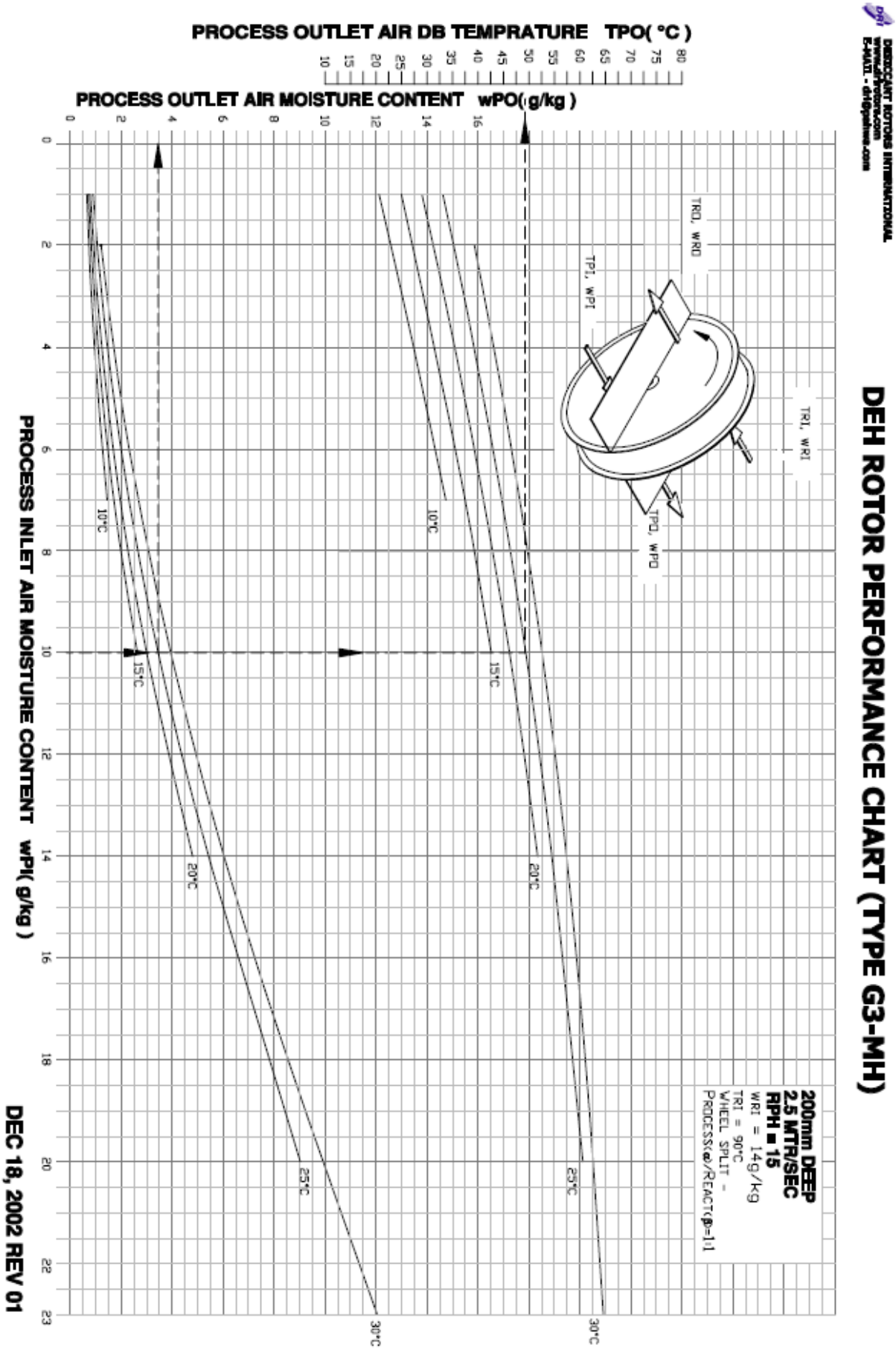

Fig. 4-4 DEC performance chart.

Fig. 4-4 refers to a 200 mm deep wheel, rotating at 2,5 m/s (15 rotations per hour). The regeneration air is supposed to enter the wheel at to 90 °C with a humidity ratio equal to 14 g/kg.

The chart also explains how to find the outlet process air dry bulb temperature and moisture content once the process inlet air dry bulb temperature and moisture content are known.

The others charts provided by the same manufacturer refer to other wheels (with different depth) rotating faster or slower than this one, and regenerated by an air stream in different temperature and humidity condition.

To express the mathematical model of the wheel the Jurinak method [5] was used.

It can be summarised as follows.

The ideal process for adsorption is shown on psychrometric coordinates in Fig. 4-5 below as the line drawn from state P_{in} (process air inlet) to P_{out} (process air outlet)

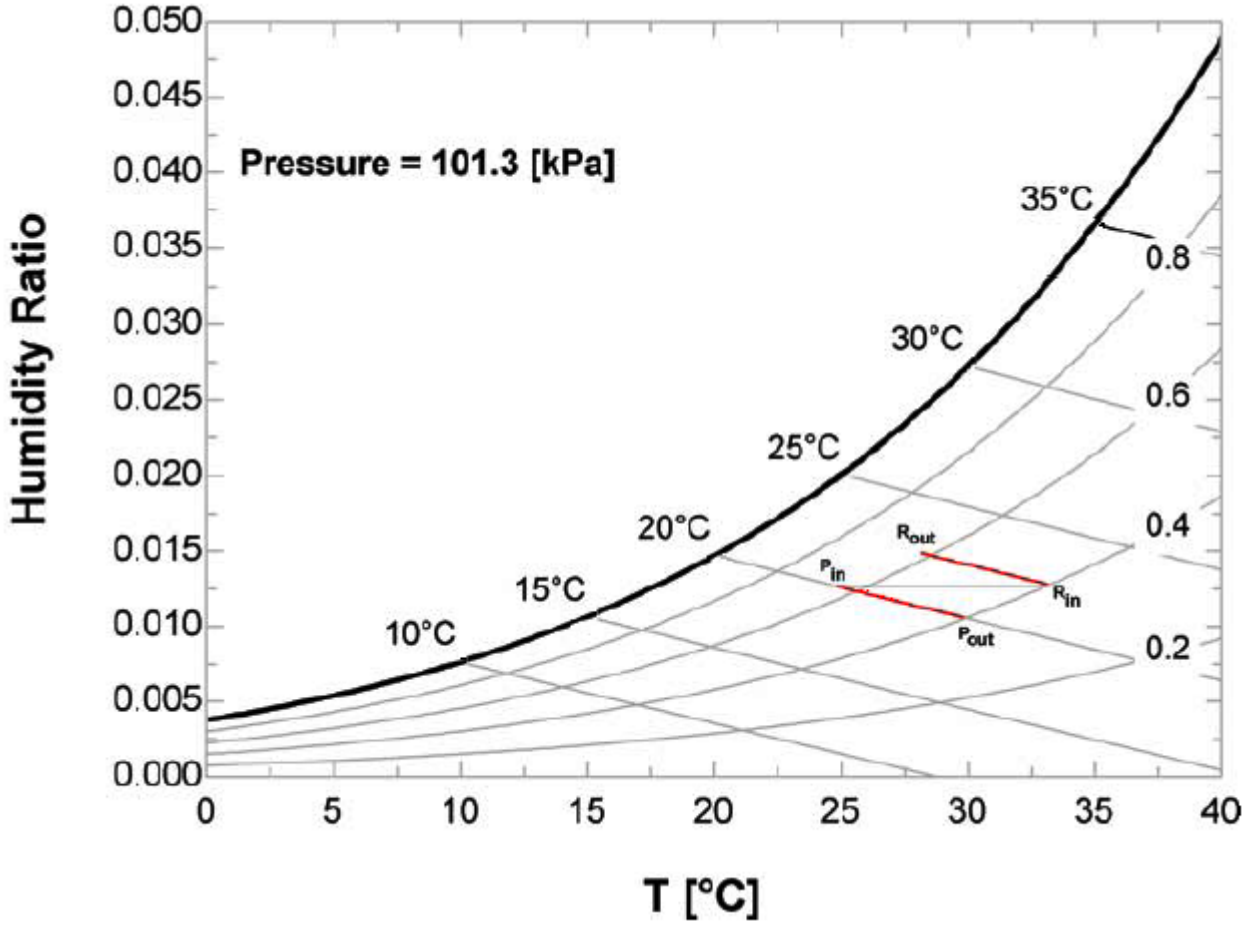

Fig. 4-5 Ideal desiccant dehumidification process.

The process air enters the dehumidifier at a certain state (usually relatively cool and moist.) As water adsorbs onto the desiccant, it gives up its heat of sorption, warming the surrounding air. The process air leaves the dehumidifier drier and warmer than it entered. The above figure also shows the ideal regeneration process from R_{in} (regeneration air inlet) to R_{out} (regeneration air outlet). It is assumed in the figure that the air source for the regeneration stream and the process stream is the same and that the regeneration stream has been sensibly heated. The regeneration stream goes through an opposite process to the process stream. Moisture on the desiccant is subjected to low relative humidity warm air and consequently desorbs, taking the heat of sorption out of the surrounding air. The regeneration stream exits the dehumidifier cooler and more moist than it entered.

As can be seen in Fig. 4-5, the ideal dehumidifier dries the process stream and adds moisture to the regeneration stream isenthalpically. In reality, the sorption and desorption processes are not isenthalpic because "waves" of moisture, temperature and enthalpy travel through the desiccant matrix contained in the wheel. Suppose the desiccant matrix is initially dry but is not being regenerated. Moist air flows over the matrix during which time, the desiccant heats up and increases in moisture content. Eventually the entire desiccant matrix becomes saturated with moisture and the outlet process air state tends towards the inlet state. The desiccant, however, does not saturate all at once. Instead, the desiccant nearest the moist air inlet becomes saturated first. Thus, a wave front travels (fairly slowly) through the desiccant behind which is saturated matrix and in front of which is unsaturated matrix. A second, much faster moving wave front moves through the desiccant just as the process air and regeneration air streams begin to flow. When the process stream is not flowing, the air in the dehumidifier comes to an equilibrium; no moisture is being added to the desiccant by the process stream and the regeneration stream, while hot does not completely dry the desiccant. When the process air begins to flow again, the hot humid air, that was trapped in the dehumidifier, is purged. The speed at which the wheel is designed to turn in a rotary system is adjusted in order to maintain the outlet conditions somewhere between the two wave fronts. The fast moving wave must be purged when the humidifier comes on (requiring a lower wheel rotation speed) but the desiccant must not be allowed to saturate (requiring a high wheel speed).

To account for the wave front propagation through the desiccant matrix, Howe and Jurinak developed a set of two potential functions that are in essence curve fits of the derived wave

front propagation characteristics for a given desiccant. Fig. 4-6 shows an example of these isopotential lines (F_1 and F_2) for silica gel.

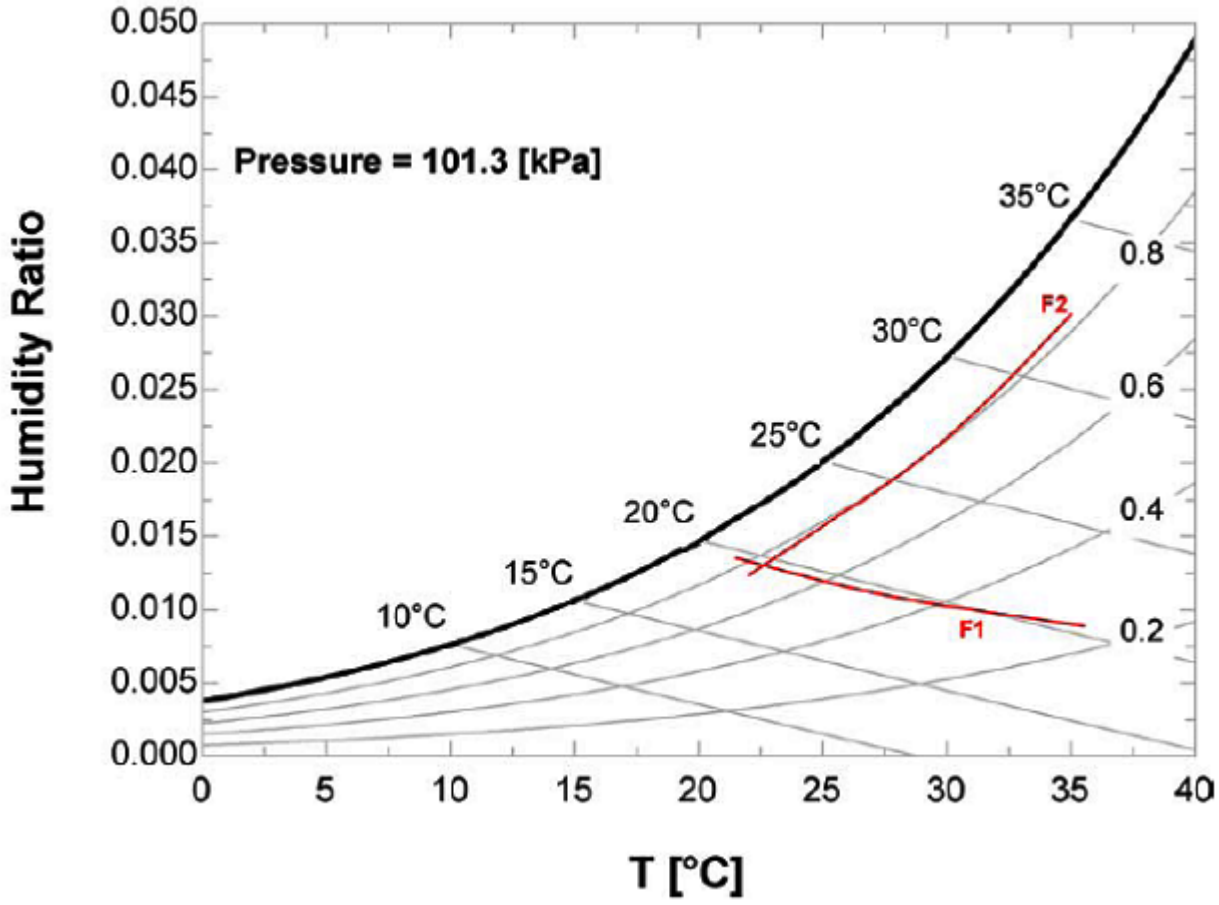

Fig. 4-6 F_1 and F_2 potential lines.

The curvature of the F_1 and F_2 isopotential lines is exaggerated over the range shown in Fig. 4-6 above to illustrate the difference in their shape as compared to that of the lines of constant relative humidity and enthalpy. The F_1 and F_2 equations derived by Jurinak for a silica gel desiccant are:

$$F_1 = \frac{-2865}{T^{1.490}} + 4.344 \cdot \omega^{0.8624} \qquad F_2 = \frac{T^{1.490}}{6360} - 1.127 \cdot \omega^{0.07969}$$

where T is measured in [K] and ω is measured in [kgH20/kgAir]. Using the F_1 and F_2 lines of isopotential the desiccant dehumidification process is shown in Fig. 4-7 below. Process air enters the dehumidifier at a state designated by point P, is warmed and dehumidified along the F_{1P} potential line, exiting the humidifier at the air state labelled D^*. On the regeneration

side, air enters the dehumidifier at state R and is cooled and humidified along the potential line F_{1R}, exiting the dehumidifier at the state corresponding to the intersection of the isopotential lines labelled F_{2P} and F_{1R}.

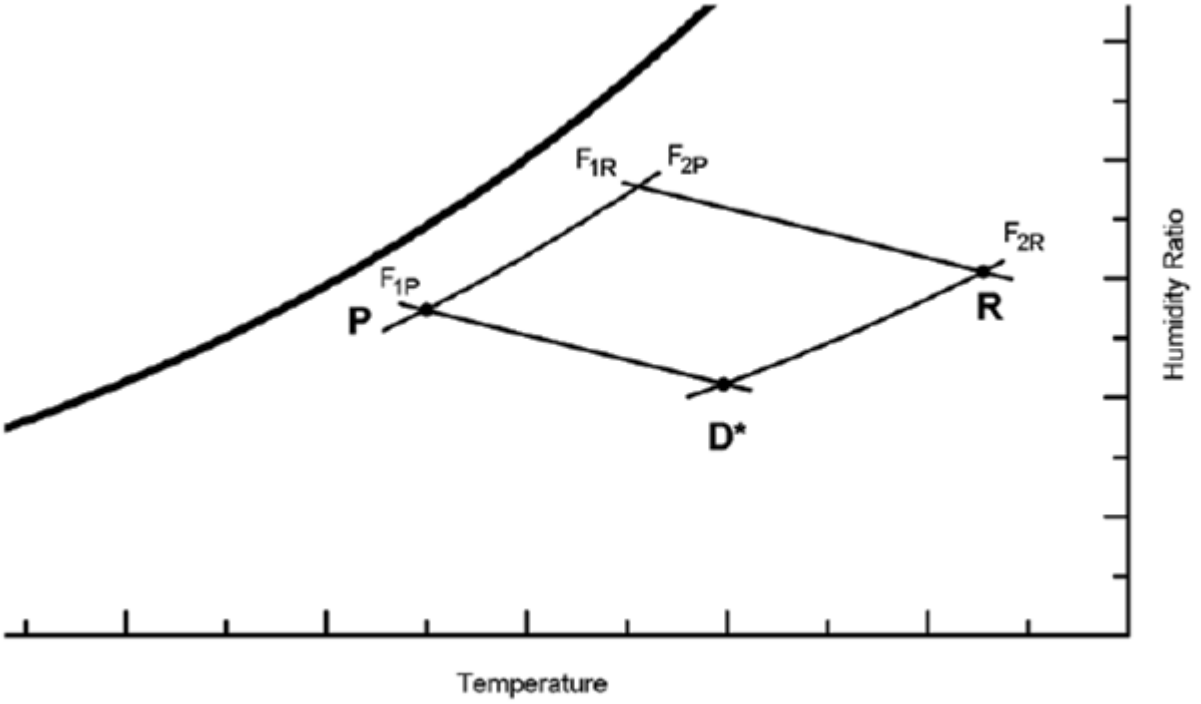

Fig. 4-7 Dehumidifier process paths using isopotential lines.

The F_1 and F_2 isopotential lines are further modified for non idealities in the system by the use of two effectiveness values ε_1 and ε_2 as defined by:

$$\varepsilon_1 = \frac{F_{1D} - F_{1P}}{F_{1R} - F_{1P}} \quad \varepsilon_2 = \frac{F_{2D} - F_{2P}}{F_{2R} - F_{2P}}$$

where D is the actual outlet state. The actual process can then be drawn as shown in Fig. 4-8 where D^* is the ideal outlet state and D is the actual outlet state.

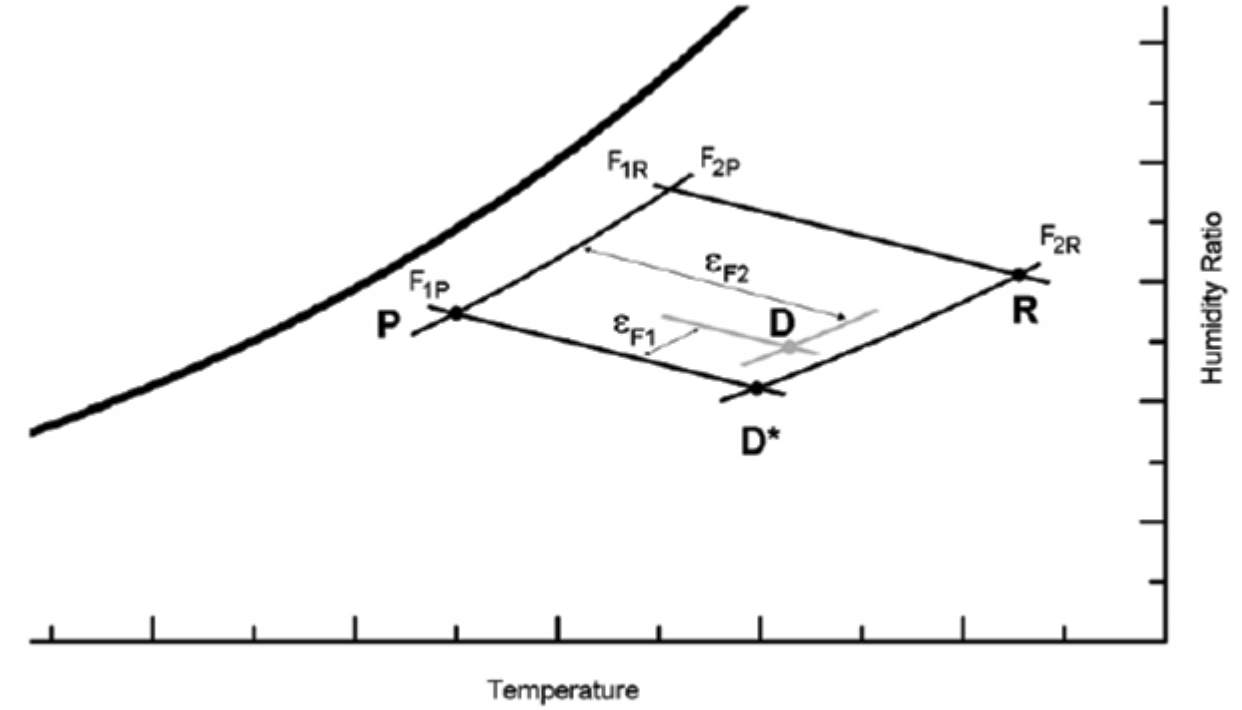

Fig. 4-8 F1 and F2 effectiveness for actual dehumidifier paths.

It appears obvious that the wheel is characterized by the two effectiveness values ε_1 and ε_2. On the basis of these two values it will be possible two build up a mathematical model that MathCAD would easily handle. So the wheel characterization aims to know ε_1 and ε_2 for any combination of regeneration air temperature and process air moisture content. The regeneration air moisture content is constant and equal to 14 g/kg because it is the result of the adiabatic cooling A-L (see Fig. 4-3).

A number of wheel performance charts have been studied to create a map of different combinations of inlet and outlet air conditions with different regeneration air stream temperature.
The following table (4-1) shows the data collected from the performance chart which refers to a 200 mm deep wheel, rotating at 15 rotations per hour (RPH). The regeneration temperature (t_{ri}) is equal to 60 °C and the regeneration air moisture content (x_{ri}) is equal to 14 g/kg.

Changes in the t_{pi} (process inlet air temperature) and the x_{pi} (process inlet air moisture content) modify the t_{po} (process outlet air temperature) and the x_{po} (process outlet air moisture content).

210 mm 2,5 m/s RPH = 15 xri = 14 g/kg Tri = 60 °C								
tpi = 10 °C			tpi = 15 °C			tpi = 20 °C		
xpi [g/kg]	xpo [°C]	tpo [°C]	xpi [g/kg]	xpo [°C]	tpo [°C]	xpi [g/kg]	xpo [°C]	tpo [°C]
2	1.6	17.3	2	1.9	21	3	2.35	26.5
3	1.8	19.5	3	2.05	23	4	2.7	28.3
4	2.05	21.2	4	2.35	25	6	3.5	31.3
5	2.4	23	6	3.15	28	8	4.45	33.7
6	2.8	24.5	8	4.1	30.5	10	5.7	35.8
7	3.25	26	10	5.25	32.5	12	7.1	37.5
						14	8.55	38.7
tpi = 25 °C						tpi = 30 °C		
xpi [g/kg]	xpo [°C]	tpo [°C]				xpi [g/kg]	xpo [°C]	tpo [°C]
3	2.75	30				3		33
4	3.1	31.7				4	3.6	34.8
6	3.9	34.5				5	4	36.1
8	4.95	37				6	4.45	37.4
10	6.2	38.9				8	5.45	39.5
12	7.65	40.5				10	6.75	41.2
14	9.05	41.8				12	8.2	43
16	10.65	43.2				14	9.65	44.3
18	12.25	44.2				16	11.25	45.6
20	13.9	44.9				18	12.8	46.8
						20	14.4	47.6
						22	16	48.2
						23	16.8	48.6

Table 4-1 Wheel performance data.

Additional data have also been collected from performance charts referring to other regeneration air temperature (T_{ri} = 80 °C, 85 °C, 90 °C, 100 °C, 110 °C)

Knowing the inlet and outlet air condition, the isopotential functions *F1* and *F2* were calculated for the *P*, *R* and *D* point (Process inlet, Regeneration air and Dehumidified air stream).

The isopotential function values allowed to calculate the two effectiveness values ε_1 and ε_2, as shown in the following table, which refers to the data acquired from the performance chart given for regeneration temperature (T_{ri}) equal to 373,15 K (= 100 °C) and regeneration air moisture content (x_{ri}) equal to 14 g/kg. T_{po} and x_{po} stand for dehumidified air stream conditions (point D)

Tri	xri	F1R	F2R	Temperatures in [K]			Moisture content in [g/kg]		
373.15	14	-0.31229	0.266165						
Tpi	**xpi**	**F1P**	**F2P**	**Tpo**	**xpo**	**F1D**	**F2D**	**□1**	**□2**
283.15	1	-0.625	0.058112	295.15	0.55	-0.59137	0.133519	0.107541	0.362442
283.15	2	-0.61581	0.021203	297.85	0.6	-0.58279	0.139497	0.108788	0.482907
283.15	3	-0.60725	-0.00135	300.15	0.7	-0.57504	0.140586	0.10923	0.530573
283.15	4	-0.59909	-0.0178	302.55	0.8	-0.56715	0.143047	0.111389	0.566434
283.15	5	-0.59121	-0.03082	304.65	0.95	-0.55976	0.142339	0.112776	0.583063
283.15	6	-0.58354	-0.04164	306.85	1.1	-0.55222	0.143244	0.11547	0.60065
283.15	7	-0.57605	-0.0509	309.35	1.3	-0.54355	0.144176	0.123229	0.615259
288.15	1	-0.60862	0.076822	300.15	0.6	-0.57606	0.148298	0.109866	0.377497
288.15	2	-0.59943	0.039912	302.35	0.65	-0.56923	0.152755	0.105152	0.498744
288.15	4	-0.58271	0.000907	306.95	0.9	-0.55389	0.154021	0.106597	0.577225
288.15	6	-0.56716	-0.02293	311.15	1.2	-0.53969	0.155409	0.107801	0.616885
288.15	8	-0.55233	-0.04031	315.15	1.6	-0.52556	0.155774	0.111497	0.639807
288.15	10	-0.538	-0.05407	318.95	2.2	-0.51064	0.153397	0.121222	0.647863
293.15	1	-0.59293	0.095691	304.85	0.7	-0.56169	0.158673	0.111341	0.369455
293.15	2	-0.58374	0.058782	306.95	0.8	-0.55488	0.160041	0.106327	0.488274
293.15	4	-0.56703	0.019776	311.15	1.05	-0.54112	0.162389	0.101703	0.578811
293.15	6	-0.55148	-0.00406	315.55	1.35	-0.52684	0.166418	0.103022	0.630875
293.15	8	-0.53664	-0.02144	319.45	1.8	-0.51292	0.166351	0.105735	0.652953
293.15	10	-0.52231	-0.03521	322.95	2.4	-0.4991	0.164428	0.110492	0.66242
293.15	12	-0.50837	-0.04663	325.85	3.2	-0.48545	0.159817	0.116889	0.66001
298.15	1	-0.5779	0.114718	308.75	0.75	-0.55049	0.170304	0.103208	0.36703
298.15	2	-0.56871	0.077809	310.85	0.9	-0.54337	0.169184	0.098796	0.48512
298.15	4	-0.55199	0.038804	315.15	1.2	-0.52927	0.171066	0.094809	0.581727
298.15	6	-0.53644	0.014968	319.15	1.6	-0.51546	0.171528	0.093589	0.623257
298.15	8	-0.5216	-0.00242	322.85	2.2	-0.50107	0.168846	0.098089	0.637656
298.15	10	-0.50727	-0.01618	326.15	2.85	-0.48766	0.167566	0.100613	0.650783
298.15	12	-0.49334	-0.02761	328.95	3.7	-0.47413	0.163921	0.106064	0.65196
298.15	14	-0.47971	-0.0374	331.65	4.7	-0.46001	0.160886	0.117662	0.653188
298.15	16	-0.46636	-0.04598	333.95	5.75	-0.44676	0.158252	0.127228	0.654283
298.15	18	-0.45323	-0.05362	335.95	7	-0.43296	0.154539	0.143842	0.650936
303.15	1	-0.56348	0.133902	312.95	0.85	-0.53834	0.180317	0.100081	0.350927
303.15	2	-0.55429	0.096993	314.95	1	-0.53169	0.179792	0.093364	0.489438
303.15	4	-0.53757	0.057988	319.15	1.4	-0.5173	0.17867	0.089996	0.579709
303.15	6	-0.52202	0.034153	322.95	1.9	-0.50347	0.177282	0.088479	0.616903
303.15	8	-0.50719	0.016768	326.05	2.6	-0.49	0.172317	0.088164	0.623699
303.15	10	-0.49285	0.003006	329.35	3.35	-0.47606	0.171215	0.092985	0.639192
303.15	12	-0.47892	-0.00842	331.95	4.3	-0.46249	0.167287	0.098579	0.639901
303.15	14	-0.46529	-0.01821	334.45	5.3	-0.4491	0.165109	0.105866	0.644641
303.15	16	-0.45194	-0.02679	336.35	6.4	-0.43656	0.16156	0.110119	0.642936
303.15	18	-0.43881	-0.03444	338.65	7.65	-0.42232	0.16011	0.130338	0.647191
303.15	20	-0.42589	-0.04134	340.35	9	-0.40892	0.15707	0.149317	0.64522
303.15	22	-0.41314	-0.04763	341.95	10.3	-0.39633	0.155231	0.16663	0.646474
303.15	23	-0.40682	-0.05058	342.65	11.05	-0.38962	0.153697	0.181934	0.644924

Fig. 4-9 and 4-10 show how the two effectiveness values ε_1 and ε_2 react to the different inlet air condition:

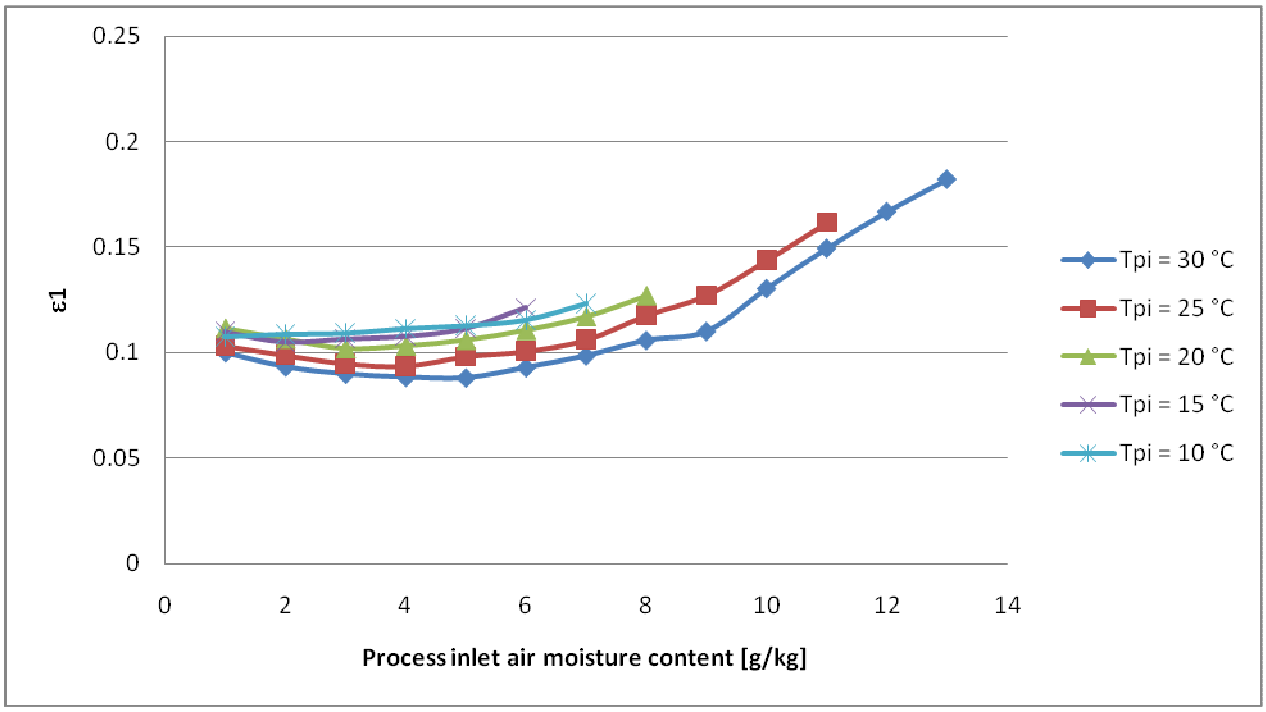

Fig. 4-9 ε_1 vs. x_{pi} for different process inlet air temperature

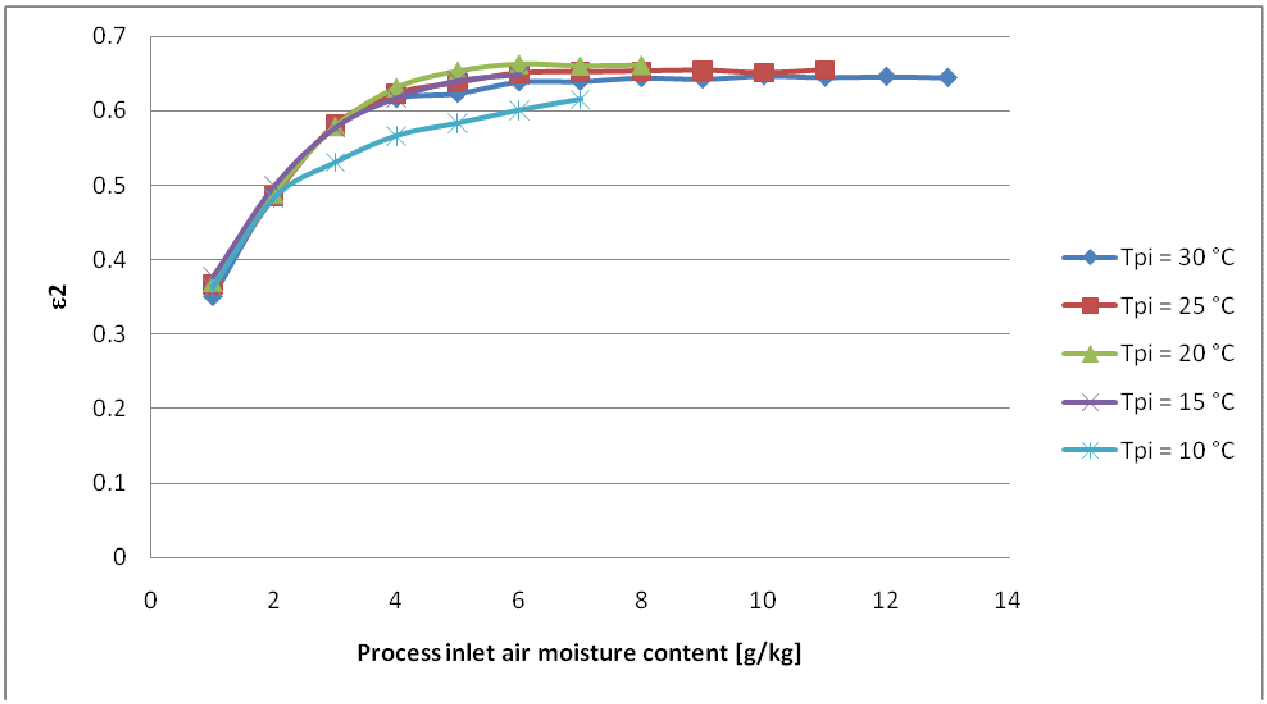

Fig. 4-10 ε_2 vs. x_{pi} for different process inlet air temperature.

Both ε_1 and ε_2 are less affected by variations in T_{pi} than variations in x_{pi}, so, to continue with the wheel characterization, only the regeneration air stream temperature and the process inlet

air moisture content were taken into account. All the collected data which will be used in the following step are shown in Fig. 4-11 and 4-12.

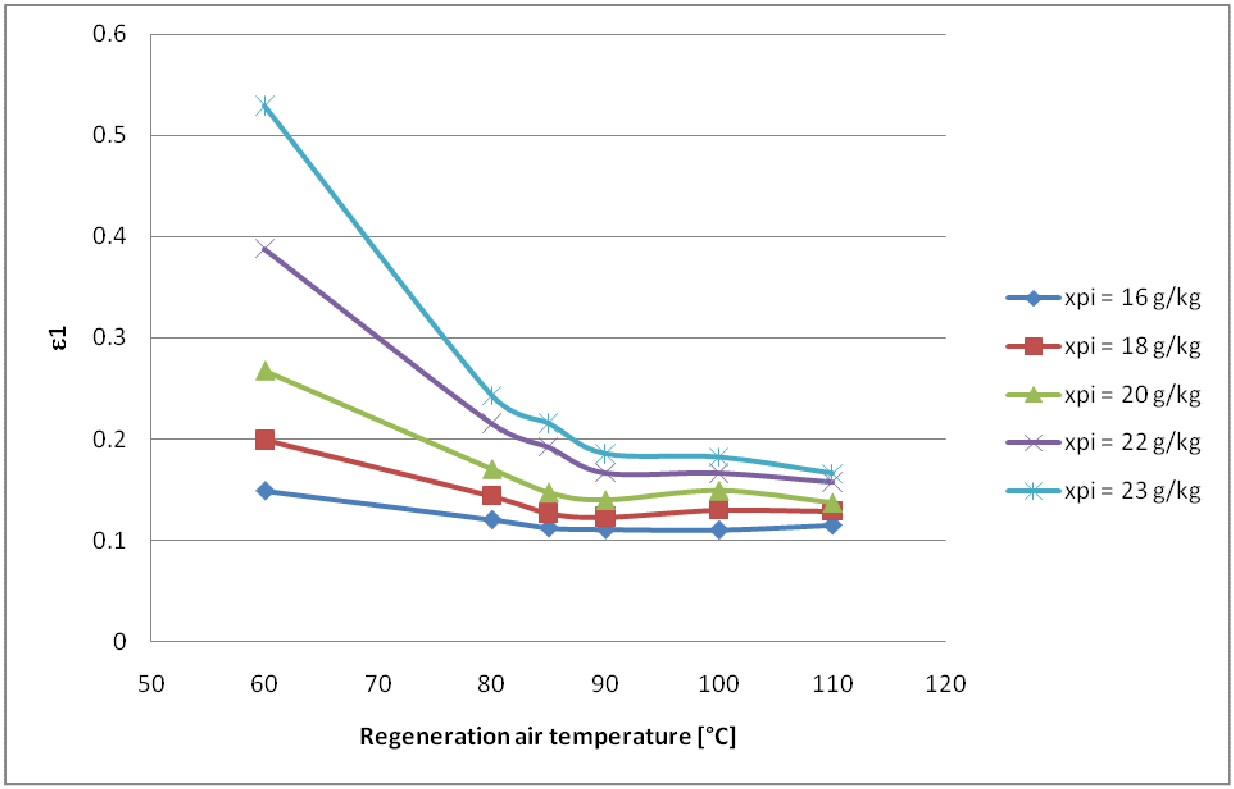

Fig. 4-11 ε_1 vs. t_{ri} for different process inlet air moisture content.

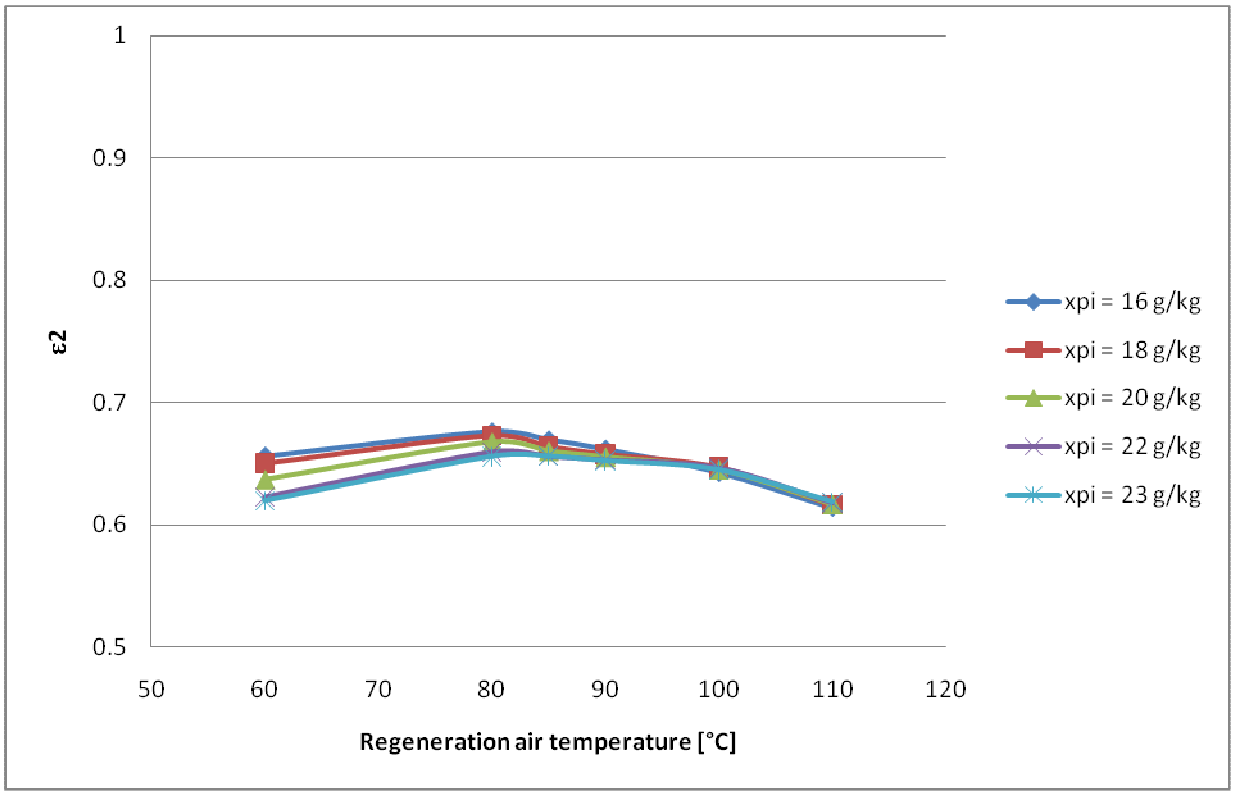

Fig. 4-12 ε_2 vs. t_{ri} for different process inlet air moisture content

The two effectiveness values depend on x_{pi} and t_{ri}. A double interpolation made on the curves shown in Fig. 4-11 and 4-12 would result in two matrices of coefficient, one for each effectiveness values, which can be used in a MathCAD routine.

The first interpolation on ε_1 starts with the following values, which refer to the curves in figure

$$t_{ri} := \begin{pmatrix} 60 \\ 80 \\ 85 \\ 90 \\ 100 \\ 110 \end{pmatrix} \qquad \varepsilon_{F1\_16} := \begin{pmatrix} 0.148965 \\ 0.120273 \\ 0.112134 \\ 0.110634 \\ 0.110119 \\ 0.114832 \end{pmatrix} \qquad \varepsilon_{F1\_18} := \begin{pmatrix} 0.199599 \\ 0.144023 \\ 0.127136 \\ 0.123217 \\ 0.130338 \\ 0.129068 \end{pmatrix}$$

$$\varepsilon_{F1\_20} := \begin{pmatrix} 0.267748 \\ 0.1706 \\ 0.147393 \\ 0.139939 \\ 0.149317 \\ 0.137355 \end{pmatrix} \qquad \varepsilon_{F1\_22} := \begin{pmatrix} 0.388185 \\ 0.215656 \\ 0.192358 \\ 0.166764 \\ 0.16663 \\ 0.157747 \end{pmatrix} \qquad \varepsilon_{F1\_23} := \begin{pmatrix} 0.529444 \\ 0.243066 \\ 0.215536 \\ 0.185341 \\ 0.181934 \\ 0.165927 \end{pmatrix}$$

All the six curves will now be interpolated with six third degree polynomial equation, one for each moisture content value:

$$\varepsilon_{1\_k}(t_{ri}) = a_{1\_k} + b_{1\_k} \cdot t_{ri} + c_{1\_k} \cdot t_{ri}^2 + d_{1\_k} \cdot t_{ri}^3 \qquad k = (16, 18, 20, 22, 23)$$

The command lines used in MathCAD for the initial interpolation are given below:

$$r_{16F1} := \text{regress}\left(t_{ri}, \varepsilon_{F1\_16}, 3\right)$$

$$\text{fit}\left(x_{16F1}\right) := \text{interp}\left(r_{16F1}, t_{ri}, \varepsilon_{F1\_16}, x_{16F1}\right)$$

$$\text{coeffs}_{16F1} := \text{submatrix}\left(r_{16F1}, 3, 7-1, 0, 0\right)$$

$$\text{coeffs}_{16F1}^{T} = \left(0.278 \quad -1.732\times 10^{-3} \quad -1.784\times 10^{-5} \quad 1.832\times 10^{-7}\right)$$

The last line shows a_{1_16}, b_{1_16}, c_{1_16}, d_{1_16} coefficients. The remaining k-coefficients were found similarly. Now it is possible to calculate the ε_1 effectiveness value for any regeneration temperature of interest, but not yet for any process air inlet moisture content.

To complete the characterization we can arrange the results in a matrix, as shown below:

$$M_{1\_F1} = \begin{pmatrix} a_{1\_16} & b_{1\_16} & c_{1\_16} & d_{1\_16} \\ a_{1\_18} & b_{1\_18} & c_{1\_18} & d_{1\_18} \\ a_{1\_20} & b_{1\_20} & c_{1\_20} & d_{1\_20} \\ a_{1\_22} & b_{1\_22} & c_{1\_22} & d_{1\_22} \\ a_{1\_23} & b_{1\_23} & c_{1\_23} & d_{1\_23} \end{pmatrix} \quad M_{1\_F1} = \begin{pmatrix} 0.278 & -1.732\times 10^{-3} & -1.784\times 10^{-5} & 1.832\times 10^{-7} \\ 0.893 & -0.02 & 1.694\times 10^{-4} & -4.531\times 10^{-7} \\ 1.858 & -0.05 & 4.889\times 10^{-4} & -1.597\times 10^{-6} \\ 2.366 & -0.058 & 5.076\times 10^{-4} & -1.469\times 10^{-6} \\ 4.702 & -0.131 & 1.263\times 10^{-3} & -4.097\times 10^{-6} \end{pmatrix}$$

Similarly the moisture content values can be written as a vector:

$$x_{pi} = \begin{pmatrix} 0.016 \\ 0.018 \\ 0.020 \\ 0.022 \\ 0.023 \end{pmatrix}$$

Considering each M_{1_F1} column as a function of x_{pi} the second interpolation would result in a set of coefficients which allow to calculate the ε_l value for any regeneration temperature and moisture content values.

MathCAD can easily extract each column of interest using the following command lines:

$$\alpha_{cF1} := \text{submatrix}(M_{1\_F1}, 0, 4, 0, 0)$$

$$\beta_{cF1} := \text{submatrix}(M_{1\_F1}, 0, 4, 1, 1)$$

$$\gamma_{cF1} := \text{submatrix}(M_{1\_F1}, 0, 4, 2, 2)$$

$$\delta_{cF1} := \text{submatrix}(M_{1\_F1}, 0, 4, 3, 3)$$

The resulting vector are reported below:

$$\alpha_{cF1} = \begin{pmatrix} 0.278 \\ 0.893 \\ 1.858 \\ 2.366 \\ 4.702 \end{pmatrix} \quad \beta_{cF1} = \begin{pmatrix} -1.732\times 10^{-3} \\ -0.02 \\ -0.05 \\ -0.058 \\ -0.131 \end{pmatrix} \quad \gamma_{cF1} = \begin{pmatrix} -1.784\times 10^{-5} \\ 1.694\times 10^{-4} \\ 4.889\times 10^{-4} \\ 5.076\times 10^{-4} \\ 1.263\times 10^{-3} \end{pmatrix} \quad \delta_{cF1} = \begin{pmatrix} 1.832\times 10^{-7} \\ -4.531\times 10^{-7} \\ -1.597\times 10^{-6} \\ -1.469\times 10^{-6} \\ -4.097\times 10^{-6} \end{pmatrix}$$

The second interpolation can now begin. The command lines which refer to the α function are reported below, command for β, γ and δ are analogous:

$r_{\alpha F1} := \text{regress}\left(x_{pi}, \alpha_{cF1}, 3\right)$

$\text{fit}\left(x_{\alpha F1}\right) := \text{interp}\left(r_{\alpha F1}, x_{pi}, \alpha_{cF1}, x_{\alpha F1}\right)$

$\text{coeffs}_{\alpha F1} := \text{submatrix}\left(r_{\alpha F1}, 3, 7-1, 0, 0\right)$

$\text{coeffs}_{\alpha F1}{}^{T} = \left(-250.755 \;\; 4.014\times 10^{4} \;\; -2.136\times 10^{6} \;\; 3.797\times 10^{7}\right)$

The second matrix of coefficients can now be written:

$$M_{2\_F1} = \begin{pmatrix} \alpha_1 & \beta_1 & \gamma_1 & \delta_1 \\ \alpha_2 & \beta_2 & \gamma_2 & \delta_2 \\ \alpha_3 & \beta_3 & \gamma_3 & \delta_3 \\ \alpha_4 & \beta_4 & \gamma_4 & \delta_4 \end{pmatrix} \qquad M_{2\_F1} = \begin{pmatrix} -250.755 & 4.014\times 10^{4} & -2.136\times 10^{6} & 3.797\times 10^{7} \\ 8.057 & -1.285\times 10^{3} & 6.811\times 10^{4} & -1.205\times 10^{6} \\ -0.086 & 13.642 & -720.917 & 1.27\times 10^{4} \\ 3.02\times 10^{-4} & -0.048 & 2.525 & -44.368 \end{pmatrix}$$

Now it is possible to calculate the effectiveness value ε_1 for any combination of t_{ri} and x_{pi} by using the following equation:

$$\varepsilon_1\left(t_{ri}, x_{pi}\right) = \left[M_{2\_F1} \cdot \begin{pmatrix} 1 \\ x_{pi} \\ x_{pi}^2 \\ x_{pi}^3 \end{pmatrix} \right]^T \cdot \begin{pmatrix} 1 \\ t_{ri} \\ t_{ri}^2 \\ t_{ri}^3 \end{pmatrix}$$

The two set of interpolation can also be used to find the matrix of coefficients which allows to calculate ε_2:

$$M_{2\_F2} = \begin{pmatrix} -33.909 & 5.24\times 10^{3} & -2.677\times 10^{5} & 4.543\times 10^{6} \\ 1.115 & -168.429 & 8.589\times 10^{3} & -1.46\times 10^{5} \\ -0.012 & 1.789 & -91.109 & 1.551\times 10^{3} \\ 4.125\times 10^{-5} & -6.236\times 10^{-3} & 0.318 & -5.415 \end{pmatrix}$$

$$\varepsilon_2\left(t_{ri}, x_{pi}\right) = \left[M_{2\_F2} \cdot \begin{pmatrix} 1 \\ x_{pi} \\ x_{pi}^2 \\ x_{pi}^3 \end{pmatrix} \right]^T \cdot \begin{pmatrix} 1 \\ t_{ri} \\ t_{ri}^2 \\ t_{ri}^3 \end{pmatrix}$$

Fig. 4-13 andFig. 4-14 below show the comparison between the effectiveness values calculated with the interpolation method and the same values taken from the performance charts:

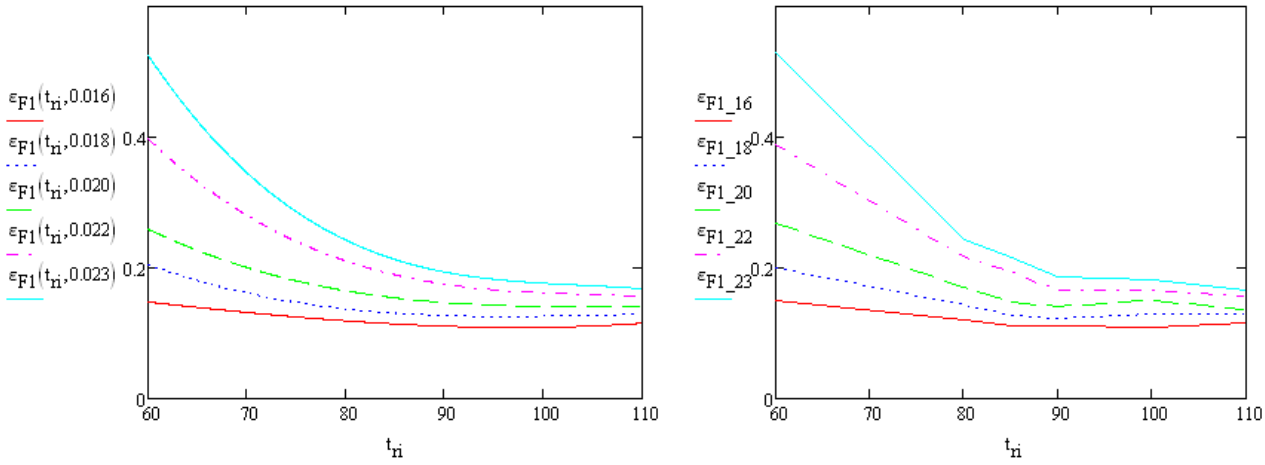

Fig. 4-13 Comparison between calculated and original ε_1 curves

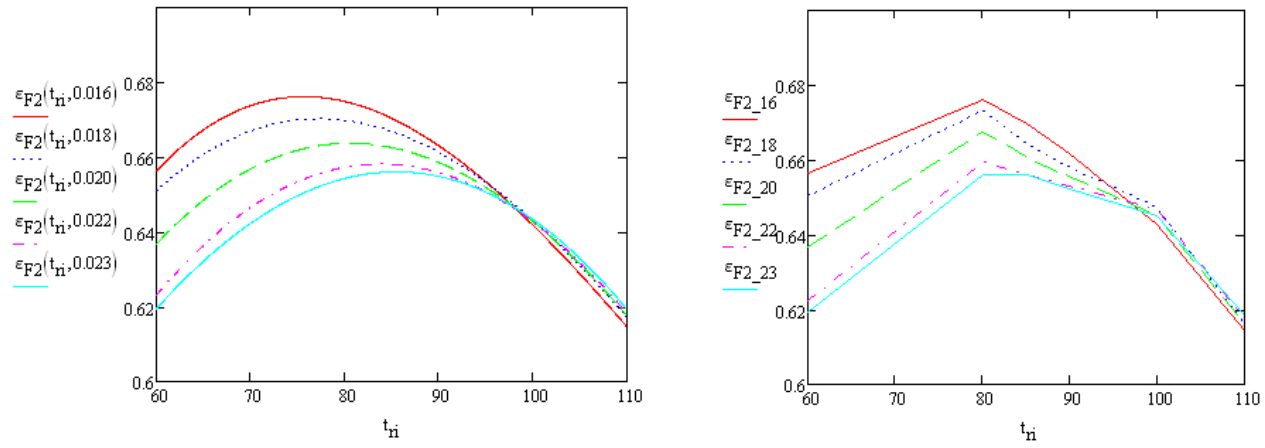

Fig. 4-14 Comparison between calculated and original ε_2 curves.

The wheel characterization is now complete and MathCAD would easy handle this component.

4.4.System analysis

A mathematical model of the system shown in Fig. 4-2 was built using MathCAD to perform the energy and exergy analysis to point out the main inefficiency. The sensitivity analysis was also carried out. The independent variables chosen for the sensitivity analysis are the slope of

the room line R (see Fig. 4-3) defined as $\left(R = \frac{Q_{sens}}{Q_{sens} + Q_{lat}} \right)$ being Q_{sens} the overall sensible and Q_{lat} the overall building latent load, and the regeneration temperature ($t_{reg} = t_G$) of the desiccant wheel, connected to the boiler. Once these two variables and the outside temperature and humidity (t_E, x_E) are known, it will be possible to proceed with the calculation of the other points of the thermal cycle; the analysis was aimed at calculating the Exergy Efficiency (ζ) of the whole system.

The system operates in steady state condition. The air mass flow rate is assumed to be $m_a = 1$ kg/s.
Outside air and room air temperature and humidity condition are known and are reported in the table below.

	Temperature [°C]	**Moisture content [g/kg]**
Outside (E)	*35*	*23*
Room (A)	*26*	*11*

Table 4-2 Outside air and room air condition.

The inlet air temperature is a constant of the analysis and has been chosen according to indoor comfort condition. It has been set 8 °C below room air temperature:

$$t_I = t_A - 8\,°C = 18\,°C$$

The inlet air moisture content (x_I) and the total cooling load depend on the slope of room air, which is the independent variable, and can be calculated by using the following equation:

$$x_I(R_{am}) := \frac{\left[c_{pa}\cdot(T_A - T_I)\cdot(R_{am} - 1)\right] + R_{am}\cdot r\cdot x_A}{R_{am}\cdot r}$$

$$Q_{cool}(R_{am}) := m_a\cdot\left[c_{pa}\cdot(T_A - T_I) + r\cdot(x_A - x_I(R_{am}))\right]$$

where:

- c_{pa} stands for air specific heat capacity $\quad c_{pa} := \frac{1kJ}{kg\cdot K}$

- *r* stands for latent heat of water $r := 2500\frac{kJ}{kg}$

Fig. 4-15 shows how the slope of room line impacts on x_I and Q_{cold}

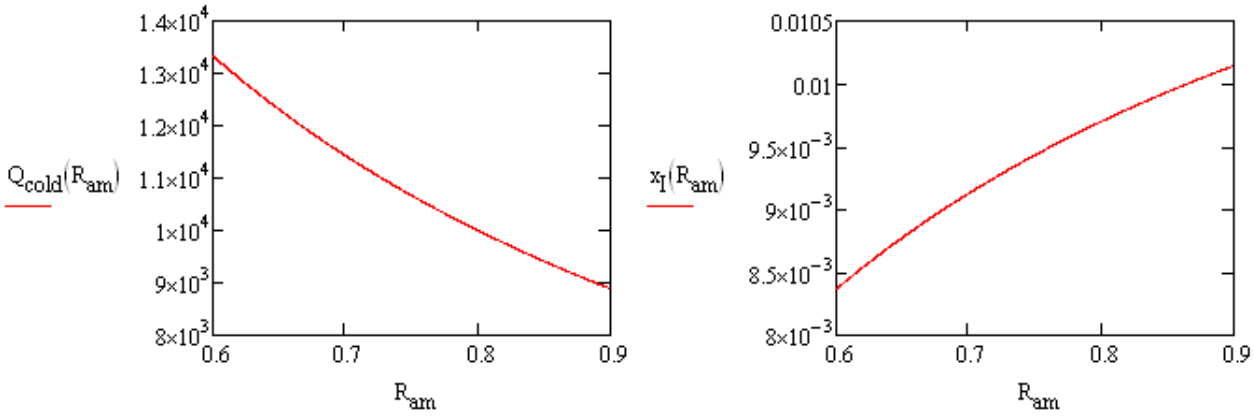

Fig. 4-15 Q_{cold} (in kW) and x_I (in kg/kg) values vs. slope of room line.

The more R rises to its maximum (= 1), the lower the latent loads are. Decreasing latent loads implies the reduction of the total cooling power needed and dehumidification processes.

The moisture content x_I is equal to the moisture content x_C, which is related to the DEC process air outlet. The DEC process air outlet temperature (t_C) will be assessed further.
Air condition at point L are known as they came from the adiabatic saturation of room air, after a sensible heating the air is ready to regenerate the desiccant wheel (G). As the sensible heating process does not change the air moisture content, it is possible to state that $x_L = x_G$

$$t_L = 18{,}7\ °C \qquad x_L = x_G = 14{,}5\ \frac{g}{kg}$$

The regeneration air temperature (t_G) is the other independent variable of the analysis.

DEC process inlet air conditions (t_B and x_B) are still not known; they will be found by using the effectiveness values method.
The model finds the process air inlet conditions which allow the wheel to obtain the needed dehumidification ($x_B - x_C$), as shown in Fig. 4-3. As the point B is located on the saturation curve (RU = *100 %), x_B* and t_B are related by the following equation

$$x_t(t) := 0.622\frac{RU \cdot p_{VS}(t)}{101325 - RU \cdot p_{VS}(t)} \qquad \text{where RU} = 1$$

The graph in the following figure, which has been calculated under the hypothesis of regeneration temperature t_G equal to 90 °C and slope of room air R_{am} equal to 0,75, shows how process air inlet temperature impacts on the total dehumidification ($\Delta x = x_B - x_C$) and on the process air outlet temperature x_C.

Figure comes from the MathCAD worksheet, the following notation has been used:

$$t_{in\_DEC} = t_B \qquad \Delta x(t_{in\_DEC}) = \Delta x \qquad X_C(t_{in\_DEC}) = x_C$$
$$x_t(t_{in\_DEC}) = x_B \qquad x_I(R_{amb}) = x_I \qquad TT_C(t_{in\_DEC}) = t_C$$

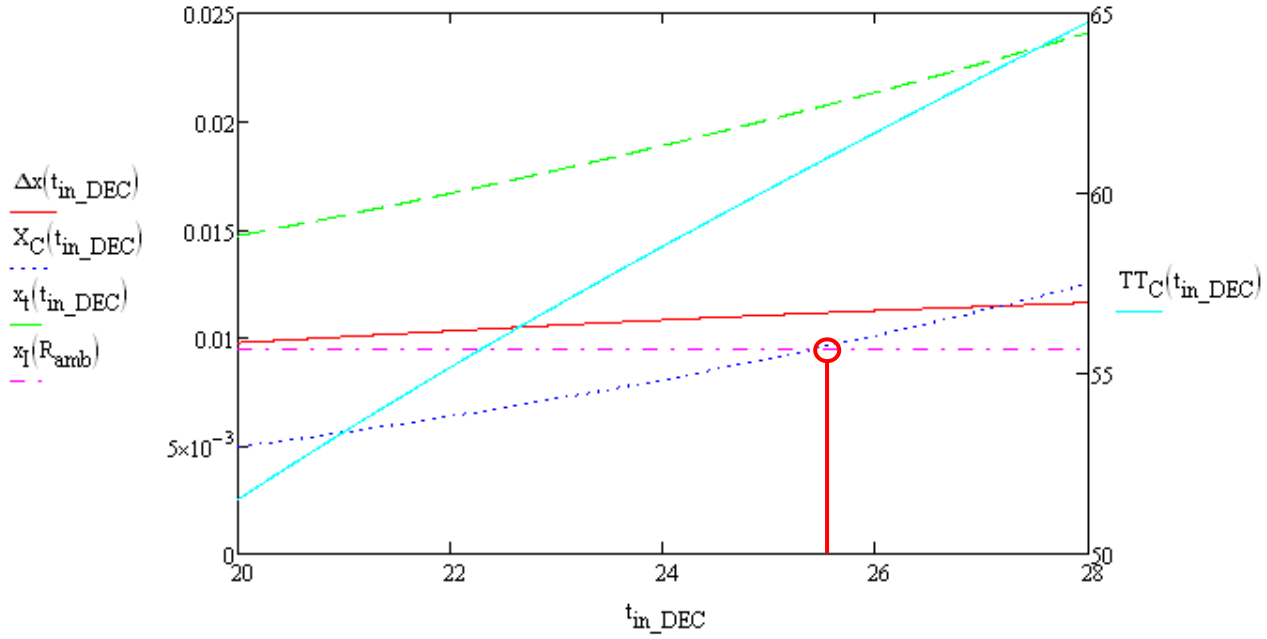

Fig. 4-16 Wheel dehumidification and process air outlet temperature vs. process air inlet temperature.

The required process air outlet moisture content (x_I) has also been shown.

The total dehumidification operated by the wheel (red line) seems not to be much affected by the process air inlet condition, it is quite constant and ranges from 9,7 to 11,5 g/kg. Process air outlet temperature ranges from 51,5 to 64,7 °C. It rises more than process air inlet temperature because of the water vapour latent heat transferred to the air stream during the condensation process.

To continue with the analysis the process air inlet temperature value matching the required outlet air moisture content has to be known. It is shown in the graph by vertical line passing through the red circle, which is located on the intercept between x_C and required x_I. At the same time the precooling load, which refers to the E – B transformation (see Fig. 4-3), will also be known.

The subroutine finds the point using the successive approximations method.

$$t_{in3}(t_{reg}, x_{reg}, x_I) := \left| \begin{array}{l} t_{in3} \leftarrow 22 \\ \text{for } i \in 0..800 \\ \quad \left| \begin{array}{l} t_{in3} \leftarrow (t_{in3} + 0.5) \\ \text{break if } xval(t_{reg}, x_{reg}, t_{in3}, x_t(t_{in3})) > x_I \end{array} \right. \\ t_{in3} \end{array} \right.$$

$$t_{in2}(t_{reg}, x_{reg}, x_I) := \left| \begin{array}{l} t_{in2} \leftarrow t_{in3}(t_{reg}, x_{reg}, x_I) \\ \text{for } i \in 0..800 \\ \quad \left| \begin{array}{l} t_{in2} \leftarrow (t_{in2} - 0.1) \\ \text{break if } xval(t_{reg}, x_{reg}, t_{in2}, x_t(t_{in2})) < x_I \end{array} \right. \\ t_{in2} \end{array} \right.$$

$$t_{in}(t_{reg}, x_{reg}, x_I) := \left| \begin{array}{l} t_{in} \leftarrow t_{in2}(t_{reg}, x_{reg}, x_I) \\ \text{for } i \in 0..800 \\ \quad \left| \begin{array}{l} t_{in} \leftarrow t_{in} + 0.01 \\ \text{break if } xval(t_{reg}, x_{reg}, t_{in}, x_t(t_{in})) > x_I \end{array} \right. \\ t_{in} \end{array} \right.$$

At this step of the analysis the last two points of the thermal cycle that have to be calculated are the point F and the point D: the former is related to the exhaust air stream exiting from the rotary heat exchanger (HEX), while the latter indicates the conditions of the process air exiting from the same component. Both of them can be calculated starting from conditions of air in L and C and knowing the rotary exchanger efficiency (η_{ex} = 0,7) by using the following equations. Remember that the regeneration air flow rate is supposed to be equal to the process air flow rate.

$$t_F = t_L + \eta_{ex} \cdot (t_C - t_L)$$
$$t_D = t_C - t_F + t_L$$

$x_D = x_C$ and $x_F = x_L$ because the heat exchanger does not operate any latent transformation.

MathCAD is able to handle all of these relationship taking into account the two independent variables t_G (t_{reg}) and R (R_{am}) as shown below:

Rotating heat exchanger outlet exhaust air temperature and moisture content

$$T_F(\eta, t_{reg}, x_{reg}, t_{proc}, x_{proc}) := T_L + \eta \cdot (T_C(t_{reg}, x_{reg}, t_{proc}, x_{proc}) - T_L)$$

$$x_F := x_t(t_L)$$

Rotating heat exchanger outlet process air temperature and moisture content

$$T_D(\eta, t_{reg}, x_{reg}, t_{proc}, x_{proc}) := T_C(t_{reg}, x_{reg}, t_{proc}, x_{proc}) - T_F(\eta, t_{reg}, x_{reg}, t_{proc}, x_{proc}) + T_L$$

$$x_D := x_C$$

MathCAD is now able to calculate the psychrometric conditions of all the points of the thermal cycle and it is possible to proceed with the energy and exergy analysis.

The specific exergy content of humid air and water are calculated by using the following MathCAD equations:

Humid air specific exergy content (T in K and x in kg/kg)

$$ex(T, x) := (c_{pa} + x \cdot c_{pv}) \cdot \left(T - T_0 - T_0 \cdot \ln\left(\frac{T}{T_0}\right) \right) + (1 + X(x)) \cdot R_a \cdot T_0 \cdot \ln\left(\frac{p}{p_0}\right) + R_a \cdot T_0 \cdot \left[(1 + X(x)) \cdot \ln\left(\frac{1 + X_0}{1 + X(x)}\right) + X(x) \cdot \ln\left(\frac{X(x)}{X_0}\right) \right]$$

Water specif exergy content (T in in K)

$$ex_w(T) := c_{pw} \cdot (T - T_0) - T_0 \cdot c_{pw} \cdot \ln\left(\frac{T}{T_0}\right) - R_v \cdot T_0 \cdot \ln(RH_0)$$

Table 4-3 shows the psychrometric conditions for the desiccant system cycle calculated for t_G = 90°C and R = 0,75:

Point	t [°C]	x [g/kg]	h [kJ/kg]	e [kJ/kg]
A	*26*	*11*	*54,09*	*0,675*
B	*25,4*	*20,5*	*77,69*	*0,178*
C	*60,7*	*9,4*	*85,49*	*1,752*
D	*31,3*	*9,4*	*44,43*	*0,742*
E	*35*	*23*	*94,11*	*0*
F	*48,1*	*14*	*84,52*	*0.561*
G	*90*	*14*	*127,72*	*4,791*
H	*54,7*	*25,1*	*120,22*	*0,645*
I	*18*	*9,4*	*41,84*	*1,214*
L	*18,7*	*14*	*39,16*	*0,742*

Table 4-3 Psychrometric condition for the desiccant system cycle.

Now it is possible to proceed with energy and exergy balances. The precooling coil energy and exergy balance equations are:

Enthalpy difference between cooling coil inlet and outlet

$$\Delta h_{cc\_1}(t_{reg}, x_{reg}, x_I) := c_{pa}\cdot\left[T_E - \left[\left(t_B(t_{reg}, x_{reg}, x_I)\right) + 273.15\right]\cdot K\right] + r\cdot\left(x_E - x_t\left(t_B(t_{reg}, x_{reg}, x_I)\right)\right)$$

Water flow rate circulating inside the precooling coil

$$m_{cc\_1}(t_{reg}, x_{reg}, x_I) := m_a\cdot\frac{\Delta h_{cc\_1}(t_{reg}, x_{reg}, x_I)}{c_{pw}\cdot\Delta T_{cc}}$$

Precooilng power needed to operate the air cooling and dehumidification

$$Q_{cc\_1}(t_{reg}, x_{reg}, x_I) := m_a\cdot\Delta h_{cc\_1}(t_{reg}, x_{reg}, x_I)$$

Exergy needed to operate the air cooling and dehumidification

$$E_{cc\_1}(t_{reg}, x_{reg}, x_I) := m_{cc\_1}(t_{reg}, x_{reg}, x_I)\cdot\left(ex_{in\_cc} - ex_{out\_cc}\right)$$

The condensate mass flow rate leaving the precooling coil and its exergy content are calculated as follows:

Condensate mass flow rate

$$m_c(t_{reg}, x_{reg}, x_I) := m_a\cdot\left(x_E - x_t\left(t_B(t_{reg}, x_{reg}, x_I)\right)\right)$$

Condensate mass exergy content

$$E_c(t_{reg}, x_{reg}, x_I) := m_c(t_{reg}, x_{reg}, x_I) \cdot ex_w\left[\left(t_B(t_{reg}, x_{reg}, x_I)\right) + 273.15\right] \cdot K$$

The cooling coil energy and exergy balance is made by using the following equations:

Water flow rate circulating inside the cooling coil

$$m_{cc\_2}(\eta, t_{reg}, x_{reg}, t_{proc}, x_{proc}) := m_a \cdot \frac{c_{pa} \cdot \left(T_C(t_{reg}, x_{reg}, t_{proc}, x_{proc}) - T_F(\eta, t_{reg}, x_{reg}, t_{proc}, x_{proc}) + T_L - T_I\right)}{c_{pw} \cdot \Delta T_{cc}}$$

Cooilng power needed to operate the process

$$Q_{cc\_2}(\eta, t_{reg}, x_{reg}, t_{proc}, x_{proc}) := m_{cc\_2}(\eta, t_{reg}, x_{reg}, t_{proc}, x_{proc}) \cdot \left(c_{pw} \cdot \Delta T_{cc}\right)$$

Exergy needed to operate the air cooling

$$E_{cc\_2}(\eta, t_{reg}, x_{reg}, t_{proc}, x_{proc}) := m_{cc\_2}(\eta, t_{reg}, x_{reg}, t_{proc}, x_{proc}) \cdot \left(ex_{in\_cc} - ex_{out\_cc}\right)$$

The heating coil equations are as follows:

Water flow rate circulating inside the heating coil

$$m_{hc}(\eta, t_{reg}, x_{reg}, t_{proc}, x_{proc}) := m_a \cdot \frac{c_{pa} \cdot \left(T_G - T_F(\eta, t_{reg}, x_{reg}, t_{proc}, x_{proc})\right)}{c_{pw} \cdot \Delta T_{hc}}$$

Heating power needed to operate the process

$$Q_{hc}(\eta, t_{reg}, x_{reg}, t_{proc}, x_{proc}) := m_{hc}(\eta, t_{reg}, x_{reg}, t_{proc}, x_{proc}) \cdot \left(c_{pw} \cdot \Delta T_{hc}\right)$$

Exergy needed to operate the air heating

$$E_{hc}(\eta, t_{reg}, x_{reg}, t_{proc}, x_{proc}) := m_{hc}(\eta, t_{reg}, x_{reg}, t_{proc}, x_{proc}) \cdot \left(ex_{in\_hc} - ex_{out\_hc}\right)$$

For the evaporative cooler the calculation proceeds as follows:

Feedwater temperature

$$T_w := 288K$$

Water comsumption

$$m_{ev} := m_a \cdot \left(x_L - x_A\right)$$

Feedwater exergy

$$e_{fw} := ex_w(T_w)$$

Inlet exergy

$$E_{in\_ec} := m_{reg} \cdot ex(T_A, x_A) + m_{ev} \cdot e_{fw}$$

Outlet exergy

$$E_{out\_ec} := m_{reg} \cdot ex(T_L, x_L)$$

The system useful exergy (E_u) depends on inlet air temperature (constant) and moisture content x_I, which changes with R:

$$E_u(R_{am}) := m_a \cdot e_I(R_{am})$$

To evaluate the irreversibility production, calculations proceed as follows:

Rotary heat exchangen

$$I_{rot}(\eta, t_{reg}, x_{reg}, t_{proc}, x_{proc}) := m_a \cdot (ex(T_C, x_C) - ex(T_D, x_C) - m_a \cdot (ex(T_F, x_F) - ex(T_L, x_L))$$

Precooling coil

$$I_{cc\_1}(t_{reg}, x_{reg}, x_I) := m_{cc\_1} \cdot (ex_{in\_cc} - ex_{out\_cc}) - m_a \cdot (ex(T_B, x_B) - ex(T_E, x_E)) - E_c(t_{reg}, x_{reg}, x_I)$$

Cooling coil

$$I_{cc\_2}(\eta, t_{reg}, x_{reg}, t_{proc}, x_{proc}, R_{am}) := E_{cc\_2} - m_a \cdot (ex(T_I, x_I) - ex(T_D, x_D)$$

Heating coil

$$I_{hc}(\eta, t_{reg}, x_{reg}, t_{proc}, x_{proc}) := E_{hc} - m_a \cdot (ex(T_G, x_G) - ex(T_F, x_F))$$

Evaporative cooler

$$I_{ec} := E_{in\_ec} - E_{out\_ec}$$

DEC

$$I_{DEC}(t_{reg}, x_{reg}, t_{proc}, x_{proc}, x_I) := m_a \cdot (ex(T_B, x_B)) + m_a \cdot (ex(T_G, x_G)) - [m_a \cdot (ex(T_C, x_C)) + m_{reg} \cdot (ex(T_H, x_H))]$$

Wasted exergy

$$I_{wst}(t_{reg}, x_{reg}, t_{proc}, x_{proc}, x_I) := E_c + m_a \cdot (ex(T_H, x_H))$$

Total Irreveribility production

$$I_{tot}(\eta, t_{reg}, x_{reg}, t_{proc}, x_{proc}, x_I, R_{am}) := I_{rot} + I_{cc\_1} + I_{cc\_2} + I_{hc} + I_{ec} + I_{DEC} + I_{wst}$$

The following table (Table 4-4) shows the exergy balance for the desiccant system cycle calculated for t_G = 90°C and R = 0,75:

Component	E_{in} [kJ/kg]	E_{out} [kJ/kg]	Exergy Efficiency [%]	Irreversibility [kW]	Irreversibility [%]
Precooling coil	*0,949*	*0,335*	*35,3*	*0,164*	*2,5*
Cooling coil	*0,802*	*0,472*	*58,8*	*0,33*	*5,1*
Heating coil	*5,84*	*4,23*	*72*	*1,61*	*25*
HEX	*1,01*	*0,211*	*20,9*	*0,799*	*12,4*
Evap. cooler	*0,93*	*0,77*	*82,8*	*0,16*	*2,5*
DEC	*4,146*	*1,574*	*37,9*	*2,572*	*40*
Wasted ex.				*0,802*	*12,5*
Total				*6,437*	*100*

Table 4-4 Exergy balance for the desiccant system cycle.

Table 4-4 shows that the heating coil and the DEC are responsible for over the 60 % of the total irreversibility production. There is a wide gap between the exergy content of the two air streams (the regeneration and the process air), which are forced to interact inside the DEC: the exergy content of the inlet process air is equal to 0,178 kJ/kg, while for the regeneration air inlet is equal to 4,791 kJ/kg, and this gap leads to high irreversibility production and low exergy efficiency.

The heating coil is characterized by a high exergy efficiency level (72 %), but as it operates with high exergy content streams (hot water and regeneration air at high temperature) its losses are relevant for the global exergy balance.

4.5.Final results

The following figures are given by the investigation made on the energy and exergy performance of the described system. Two different set of simulation have been made in order to make a comparison between the conventional production of hot water, heated by a boiler, and the production of hot water exploiting a solar panel collectors field able to give an *SF* equal to 0,5.

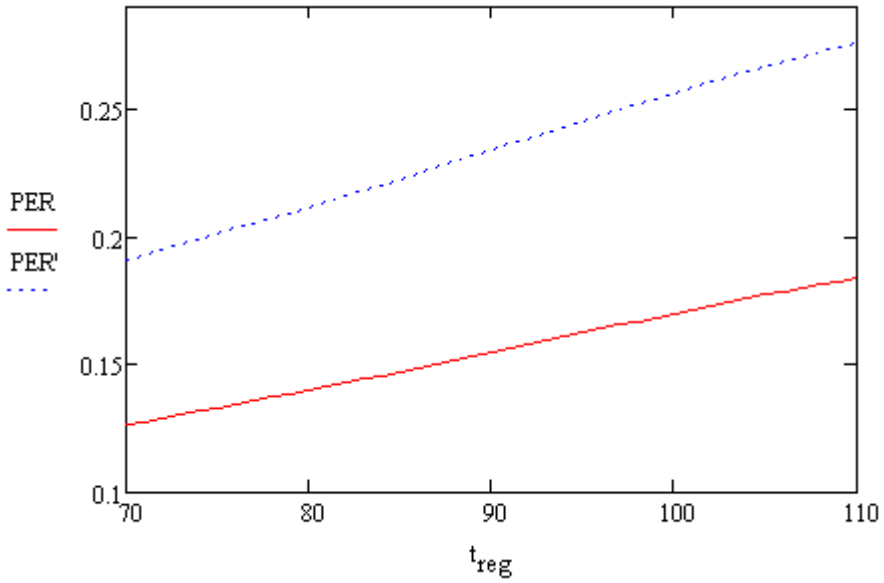

Fig. 4-17 Conventional system (*PER*) and solar cooling system (*PER'*) energy performance vs. regeneration temperature.

Fig. 4-17 shows that the solar cooling system needs less amount of energy to operate and give the same final effect of the conventional system. Performance rises with regeneration temperature and this means that when the desiccant wheel works at its best (high temperature) the other components which require energy to operate (cooling coils) reduce their consumptions.

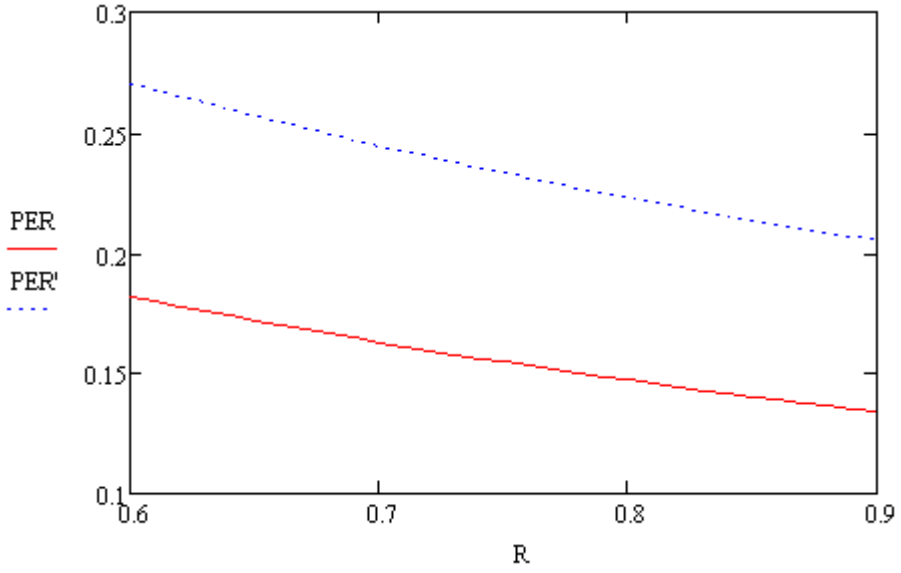

Fig. 4-18 Conventional system (*PER*) and solar cooling system (*PER'*) performance vs. Room line

Fig. 4-18 shows that the system works at its best for lower R values, which means higher latent load. The REP decreases when the sensible load becomes higher and the desiccant

wheel is less effective in the air handling process. The result of the simulation indicates that the optimal field of application for the system is building with relevant latent load.

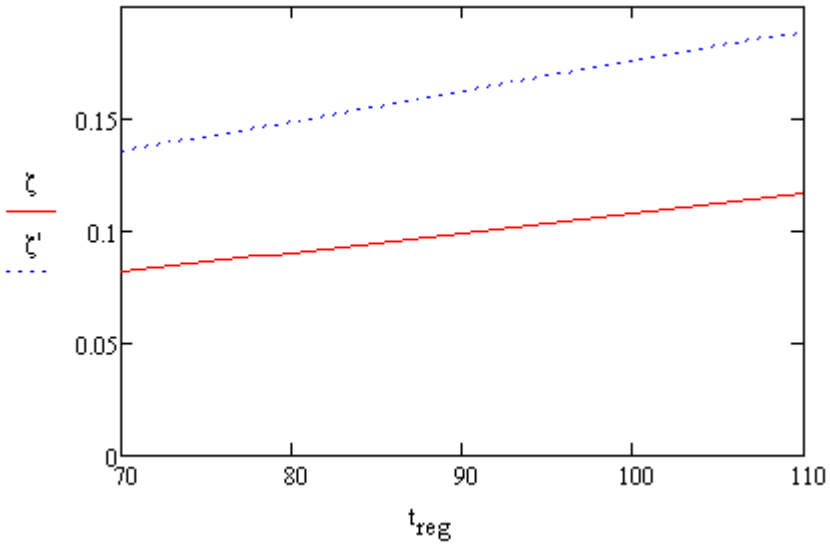

Fig. 4-19 Conventional system (ζ) and solar cooling system (ζ') exergy efficiency vs. regeneration temperature.

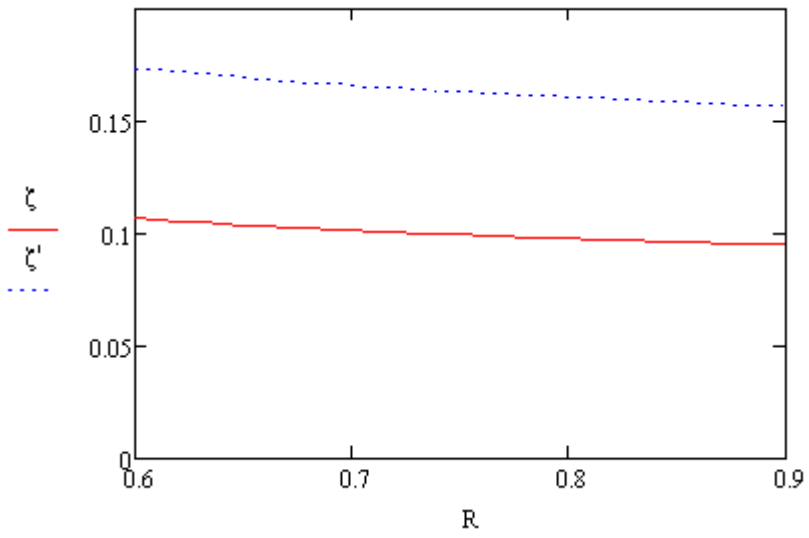

Fig. 4-20 Conventional system (ζ) and solar cooling system (ζ') exergy efficiency vs. Room line.

Fig. 4-19 andFig. 4-20, which refer to the exergy analysis, confirm results of the energy analysis. Higher regeneration temperatures allow better energy utilization and system performance rises when the latent loads are relevant.

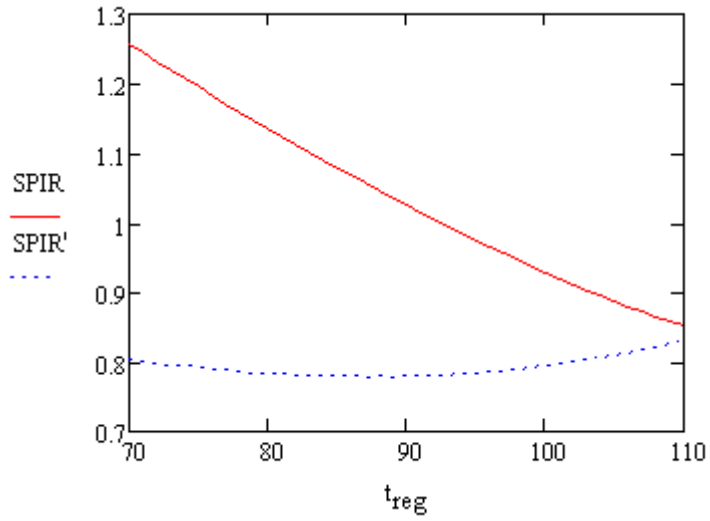

Fig. 4-21 Conventional system (*SPIR*) and solar cooling system (*SPIR'*) specific irreversibility production vs. regeneration temperature.

As shown in Fig. 4-21, the conventional system *SPIR* lowers when higher regeneration temperature are used, while for the solar cooling system the *SPIR'* is stable in a wide range of temperature. This happens because conventional system *SPIR* is strictly related with the hot water production while the solar cooling system *SPIR'* is less affected from this relationship.

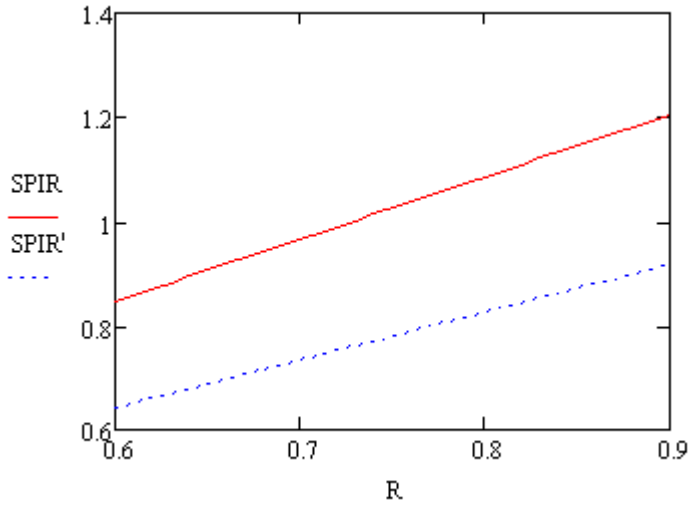

Fig. 4-22 Conventional system (*SPIR*) and solar cooling system (*SPIR'*) specific irreversibility production vs. Room line.

Once again the exergy analysis, and more specifically the SPIR parameter, shows that the solar cooling system is capable of best performance and that the DEC system works at its best with high latent loads.

Finally the sensitivity analysis was carried out to point out how changes in the regeneration temperature and room line values impact on mentioned figures of merit (*PER*, ζ and *SPIR*). Results are shown in the following figures.

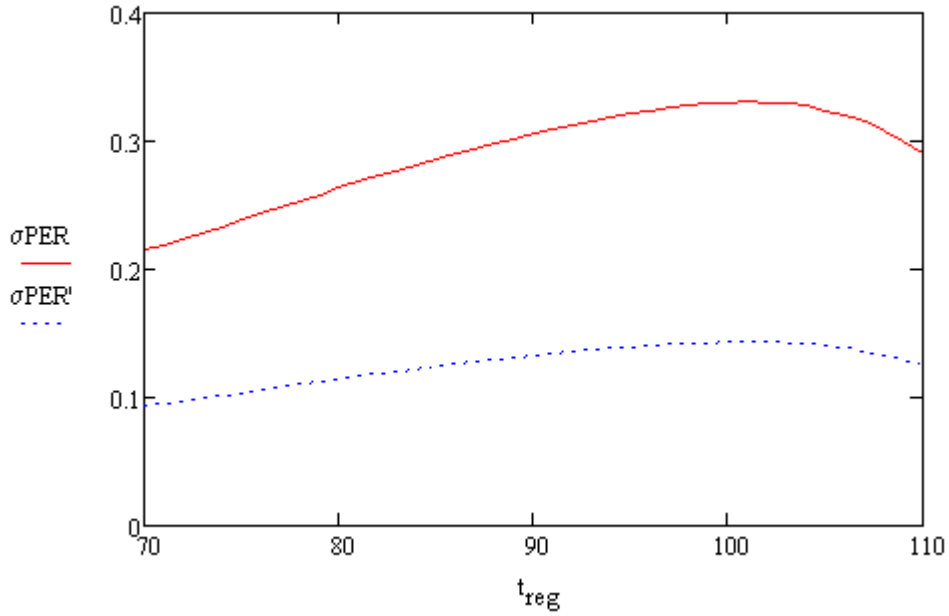

Fig. 4-23 Sensitivity analysis of t_{reg} impact on conventional system (σPER) and solar cooling system ($\sigma PER'$) energy performance.

Fig. 4-23 shows that changing the regeneration temperature has a greater impact on conventional system performance than solar cooling system. This happens because rising with t_{reg} leads to greater gas consumption, but solar cooling system takes advantage of evacuated solar collectors which cover 50 % of the required energy to produce hot water.

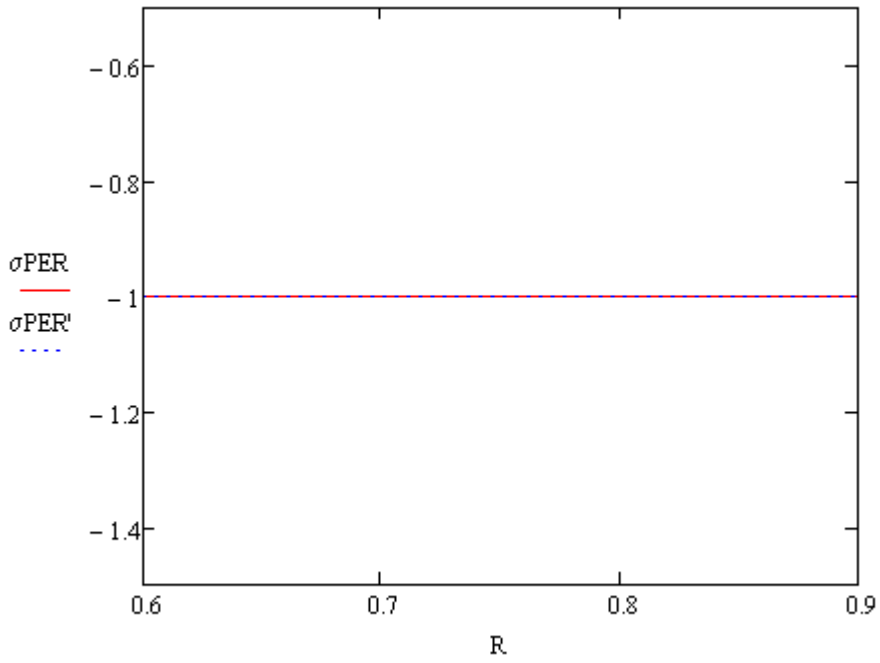

Fig. 4-24 Sensitivity analysis of *R* impact on conventional system (*σPER*) and solar cooling system (*σPER'*) energy performance.

Fig. 4-24 Shows that there is no difference between *R* impact on conventional or solar cooling systems. For both of them rising with R (lowering the latent loads) leads to the same energy performance decrease.

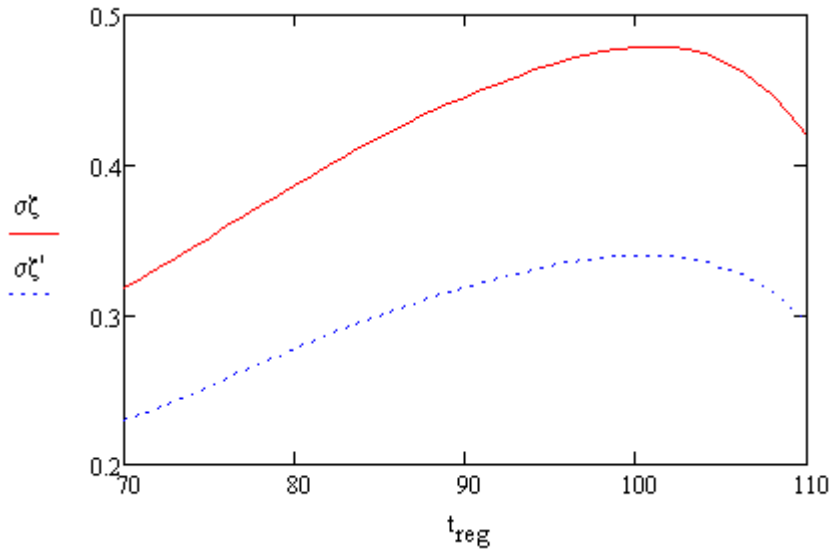

Fig. 4-25 Sensitivity analysis of t_{reg} impact on conventional system (*σζ*) and solar cooling system (*σζ'*) exergy performance.

Fig. 4-25 shows the sensitivity of the exergy efficiency to the regeneration air temperature. It has a maximum for t_{reg} = 100 °C, and after that sensitivity decreases but it continues to assume positive values. This means that growing with air temperature would lead to an increase of the plant performance but the growth would be smaller and smaller. Once again t_{reg} variation has a greater impact on conventional system (where water is heated by the conventional boiler only) than solar cooling system, taking advantage of the solar collectors.

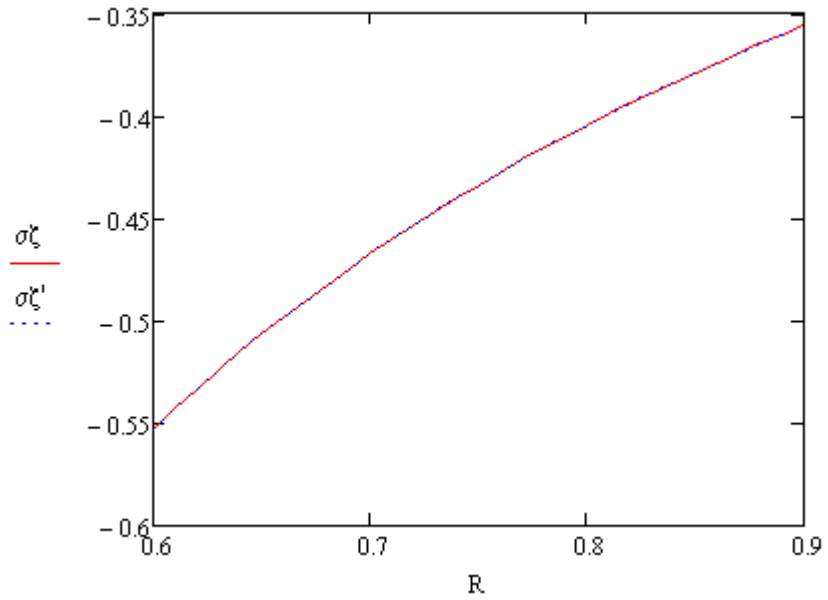

Fig. 4-26 Sensitivity analysis of *R* impact on conventional system ($\sigma\zeta$) and solar cooling system ($\sigma\zeta'$) exergy performance.

Fig. 4-26 shows the sensitivity of the exergy efficiency to the *R* factor. As stated before, DEC systems work at their best when the Q_{lat} is high and comparable with the Q_{sens}. The curve shows that an even little change of the loads (and of the *R* factor) would lead to a great variation of the efficiency.

The graph also shows that there is no difference between conventional system and solar cooling system behaviour.

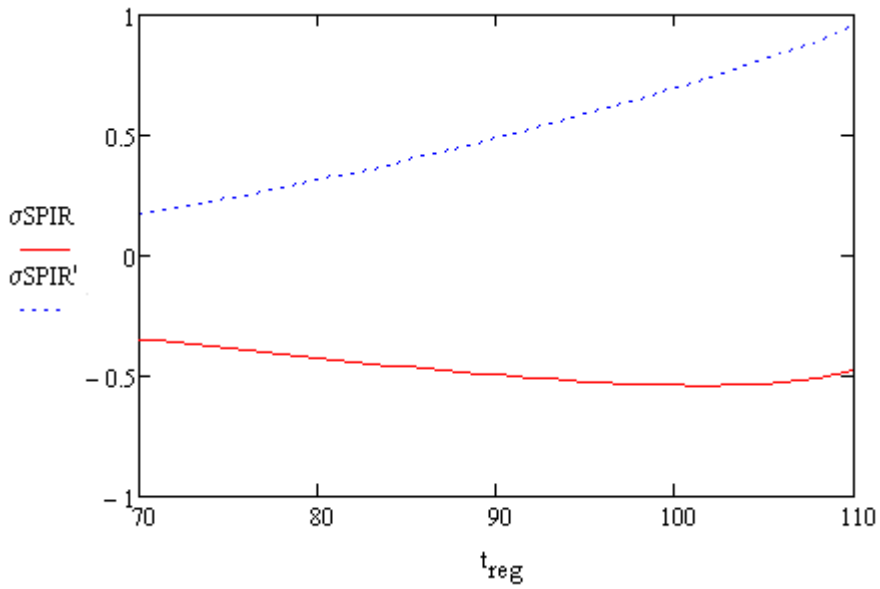

Fig. 4-27 Sensitivity analysis of t_{reg} impact on conventional system ($\sigma SPIR$) and solar cooling system ($\sigma SPIR'$) irreversibility production.

As seen before while performing the exergy analysis, solar cooling system *SPIR* increases with t_{reg} and, for high temperature (t_{reg} > 100 °C), even little variations have a great impact (see Fig. 4-27). On the other hand, for the conventional system, being the sensitivity curve always negative, higher regeneration temperature always leads to lower *SPIR*.

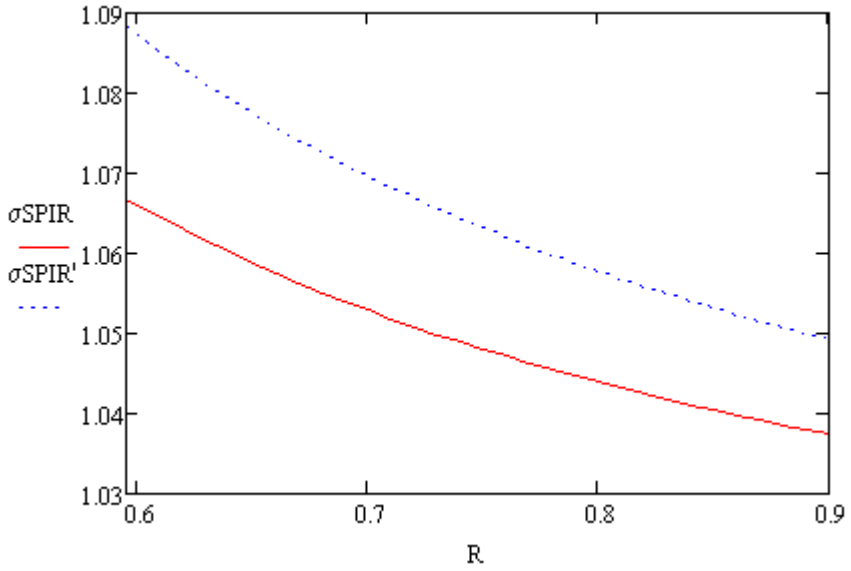

Fig. 4-28 Sensitivity analysis of *R* impact on conventional system ($\sigma SPIR$) and solar cooling system ($\sigma SPIR'$) irreversibility production.

Once again the slope of the room line variation have the same impact on solar cooling and conventional systems (see Fig. 4-28): for both of them increasing *R* leads to the same performance reduction. Even the sensitivity analysis of *SPIR* to the *R* factor sates that *DEC* systems work at their best when the Q_{lat} is high and comparable with the Q_{sens}.

5. CONCLUSIONS

This work investigated about differences in how a solar cooling system works from a First and a Second Law point of view.

For what concerns the first system layout (see Fig. 3-1) referred to an adsorption machine powered by a solar collectors field, it mainly results that components that assume high energy efficiency index (such as the gas boiler) are responsible for great irreversibility production leading to low exergy efficiency. To rise the global system efficiency their contribution has to be reduced and improving the solar collector panel area can be the solution, as shown in Fig. 3-38 Fig. 3-39. For system with low SF and equipped whit a low COP chiller the first, and maybe easiest, improvement to do is about the chiller itself, especially if the aim is to reduce the SPIR, as shown in Fig. 3-40 and Fig. 3-41. To rise the PER index both solution can work but the best is once again to raise the solar energy contribution (see figure Fig. 3-42 and Fig. 3-43).

There are two main information coming from the study about the DEC system. The first is that DEC systems are able to achieve higher results than conventional system in terms of exergy efficiency (ζ) like shown in Fig. 4-19 and Fig. 4-20, taking advantage of both the adsorption wheel and the rotary heat exchanger; Fig. 4-25 states that increasing the wheel regeneration temperature leads to an high system performance improvement. The second main result of the analysis is that this kind of systems works at their best while latent load are relevant (see Fig. 4-18, Fig. 4-20 and Fig. 4-22), exploiting desiccant wheel capabilities.

A substantial benefit, from both the First and Second Law point of view, is procured by solar energy. In a First Law perspective the advantage is obviously due to the primary energy savings (only); in a Second Law perspective is attributable not only to the reduced primary energy needs, but also to that unique feature of solar energy such as its relatively low energy

potential, i.e. much closer than the conventional power sources to the exergy levels required by the final uses occurring in this kind of applications (heating fluids at moderate temperatures).

To complete the study and to have an in depth analysis of the proposed system performance a cost accounting study should be done, in particular the Life Cycle Analysis (LCA) and the Life and Cost Cycle Analysis (LCCA).

6. BIBLIOGRAPHY

[1] Henning, H.M.; Erpenbeck, T.; Hindenburg, C.; Santamaria, I.S., "*The potential of solar energy use in desiccant cooling cycles*". Int. J. Refrig. 2001, 24, 220–229

[2] Wepfer W.J., Gaggioli R.A. , Obert E.F., "*Proper evaluation of available energy for HVAC*", ASHRAE Trans. Vol. 85, Part 1, 1979, p.667-677.

[3] A. Sapienza, S. Vasta, A. Freni, G. Restuccia, "*Design and Operation of a new adsorption chiller prototype driven by low grade thermal energy"*, 3rd International Conference Solar Air-Conditioning Conference, 30 Settembre-2 Ottobre 2009, Palermo, Italia. CD-Proceedings ISBN 978-3-941785-06-9, Paper ID 024, 2009

[4] Henning H.M. (Ed.), *Solar assisted air-conditioning in buildings – a handbook for planners*; Springer, 2004, ISBN: 3-211-00647-8.

[5] Jurinak, J.J., "*Open Cycle Desiccant Cooling – Component Models and System Simulations*," PhD Thesis, University of Wisconsin – Madison, 1982

[6] "*ROCOCO: Reduction Of COsts of solar COoling systems, Final Report 2008*", Anita Preisler coordinator, Sixth Framework Programme.

[7] Marletta L.**, "***Exergy analysis of solar cooling, a worked example*", Report for the IEA-Task 38, 2008. Available online: www.iea-shc-task38.org).

[8] Marletta L., "*A comparison of methods to optimize air conditioning systems according to the exergonomic approach*", ASME J. Ener. Res. Technol. 2001, 123, 304–310

[9] Marletta L., Evola G., Dipasquale C., "*Solar-assisted Desiccant Systems in hot and humid Climates: Limitations and Solutions*", Proceedings of the 3rd International Conference Solar Air Conditioning OTTI, Palermo (I), September 30th – October 2nd., 2009

[10] Pons M., Kodama A., "*Entropic Analysis of adsorption open cycles for air conditioning*", International J. of Energy Research, 2000, 24, Part I. First and second Law analysis , pp-. 251-262 ; Part 2. Interpretation of experimental data , pp- 263-278.

[11] Sisò M. L.; Gurruchaga G. I., Proville M. C., Carrera M. A., "*Design, Control Strategy and Installation of a Solar Cooling Plant with two hot Storage Tanks and two different Temperature Levels*", Proceedings of the II International onference Solar Air Conditioning OTTI, Tarragona (E), October 18th -19th., 2007, pp 265-270, ISBN 978-3-934681-61-3

[12] Beccali M., Finocchiaro P., Nocke B., Gioria S., "*Solar desiccant cooling AHU coupled with chilled ceiling: description of a new installation at DREAM in Palermo*",

Proceedings of the II International onference Solar Air Conditioning OTTI, Tarragona (E), October 18th -19th., 2007, pp 389-394, ISBN 978-3-934681-61-3

[13] Wurtz E., Maalouf C., "*Analysis of the operation of a solar desiccant cooling system",* Proceedings of the 61st ATI National Congress - International Session "Solar Heating and Cooling" Perugia (I), September 14th, 2006, pp 57-62, ISBN 88-6074-050-9

[14] W.-S. Chang , C.-C. Wang, C.-C. Shieh, "*Design and performance of a solar-powered heating and cooling system using silica gel/water adsorption chiller*" Applied Thermal Engineering 29 (2009), pp 2100–2105

[15] X.Q. Zhai, R.Z. Wang, "*Experimental investigation and performance analysis on a solar adsorption cooling system with/without heat storage*" Applied Energy 87 (2010) pp. 824–835

[16] A. Kodama, M. Ohkura, T. Hirose, "*An Energy Flow Analysis of a Solar Desiccant Cooling Equipped with a Honeycomb Adsorber*" Adsorption 11: pp. 597–602, 2005

[17] Halliday, S.P., C.B. Beggs, and P.A. Sleigh, "*The Use of Solar Desiccant Cooling in the UK: A Feasibility Study*" Applied Thermal Engineering, 22, 1327–1338 (2002).

[18] Hildbrand C, Dind P, Pons M, Buchter F., "*A new solar powered adsorption refrigerator with high performance*" Sol Energy 2004;77:311–8

[19] Henning H.M. "*Solar assisted air conditioning of buildings – an overview*" Applied Thermal Engineering 27 (2007) pp. 1734–1749

[20] Henning H.M., "*Design and performance of a new thermally driven air conditioning system for Mediterranean climates*", in: VII Euro - Mediterranean Conference, Local Utilities and Sustainable Development in the Mediterranean Area, Palermo, 3–5 June 2004.

[21] Solair Project, *Survey of Available Technical Solutions and Successful Running Systems*, Cross-Country Analysis; 2008.

[22] Adnot, J. Energy efficiency of room air conditioners (EERAC). Study of the Directorate General for Energy (DGXVII) of the Commission of the EC, Final report, 1999. Available online: http://www.coolregion.fr/doc-/CLIM_RA/doc_ref/5_Ecole_Mines_Paris _EERACGB.pdf

[23] Adnot, J. "*Energy Efficiency and Certification of Central Air Conditioners (EECCAC)"*. Final Report Volume 2, 2003.Available online: http://www.energyagency.at/(de)/publ/pdf/aircondbig_v2.pdf

[24] EN 15603:2008: "*Energy performance of buildings–Overall energy use and definition of energy ratings*". European Standard, Jan. 2008, European Commettee for Standardization, Ref. No. 15603.2008 E.

[24] Bejan, A. "*Advanced Engineering Thermodynamics*"; Wiley: New York, NY, USA,1998.

[25] Wark, K. "*Advanced Engineering Thermodynamics for Engineers*"; McGraw Hill: New York, NY, USA,1995

[26] Dincer, I.; Rosen M. "*Exergy. Energy, Environment and Sustainable Development*"; Elsevier: Oxford, UK, 2007.

[27] Ren, C.Q.; Li, N.P. "*Principles of exergy analysis in HVAC and evaluation of evaporative cooling schemes*". Build. Environ. 2002, 37, 1045–1055.

[28] Cammarata, G.; Fichera A.; Mammino, L.; Marletta, L. "*Exergonomic optimization of an air conditioning system*". ASME J. Ener. Res. Technol. 1997, 119, 12–19

[29] Tozer R.; Valero A.; Lozano M. "*Thermoeconomics applied to HVAC*". ASHRAE Trans. 1999, 105, 1247–55

[30] Baehr, H.D. "*Thermodynamik*"; Springer: Berlin, Germany, 2000

[31] Brzustowsy, T.A.; Brena, A., "*Second Law analysis of energy processes*". Trans. Can. Soc. Mech. Eng. 1980, 10, 20–29

[32] Mei, V.C; Chen, F.C.; Lavan, Z., "*An assessment of desiccant cooling and dehumidification technology*". Report for the Oak Ridge Nat. Lab. USA, Contract No. DE, ac05-840r21400, 1992

[33] Eicker, U., "*Solar Technologies for Buildings*"; J. Wiley: London, UK, 2003.

[34] Henning, H.M. "*Industry Newsletter: IEA-SHC Solar Air-Conditioning and Refrigeration*", January2009, Available online: www.iea-shc.org/publications/downloads/task38-enewsletter-2009-01.pdf

ACKNOWLEDGEMENTS

I am heartily thankful to my tutor, Prof. Luigi Marletta, for his guidance, encouragement and good advice, in spite of having a lot of other work to do. I also thank Prof. Alfio Consoli, who maintains this PhD course at a high quality level. This thesis would not have been possible unless the contribution of Andrea Frazzica, Salvo Vasta and all of the research group of Thermally Driven Heat Pumps of the CNR-ITAE of Messina: thank you for your support and the stimulus to run my TRNSYS simulations.

I want to thank Gianpiero Evola, who has made available his support in a number of ways and helped me to do my research work when needed. I would like to show my gratitude to Bice, who helped me fighting against the bureaucracy. Thanks to all of my PhD colleagues for standing by me in good and bad times.

A special thank goes to my parents and to Monica for their unconditional support throughout my PhD course, in particular for their patience and understanding. I know, at times, my temper is particularly trying.